The Dissertation Committee for Martha M. Gross Certifies that this is the approved version of the following dissertation:

Development of Polysulfide Battery Systems with Low-cost Active Materials and Solid Electrolytes

Committee:

Arumugam Manthiram, Supervisor

John B. Goodenough

Guihua Yu

Gyeong S. Hwang

Development of Polysulfide Battery Systems with Low-cost Active Materials and Solid Electrolytes

by

Martha M. Gross

Dissertation

Presented to the Faculty of the Graduate School of

The University of Texas at Austin

in Partial Fulfillment

of the Requirements

for the Degree of

Doctor of Philosophy

The University of Texas at Austin

May 2019

Acknowledgements

I would first like to express my gratitude to my supervisor, Professor Arumugam Manthiram, for giving me this opportunity and offering his guidance and support throughout my doctoral studies. I also wish to thank my committee members, Professors John B. Goodenough, Guihua Yu, and Gyeong S. Hwang, for their keen insight into my work and helpful suggestions. I would like to thank Dr. Xingwen Yu for this thoughtful ideas and Dr. Longjun Li for teaching me about his own work. Without either of them I would not have had a firm foundation on which to build my work.

Additionally, I would like to express my gratitude towards current and former members of Professor Manthiram's group, particularly Robert Pipes, Dr. Ke-Yu Lai, Sanjay Nanda, Dr. Chi-Hao Chang, Dr. Pauline Han, Min-Je 'Daniel' Park, and Dr. Sheng-Heng Chung for their advice, help, encouragement, and friendship. I would also like to acknowledge Texas Materials Institute staff members Dr. Steve Swinnea, Dr. Karalee Jarvis, and Dr. Hugo Celio for helping me achieve quality data and results, and CNC machinist Daniel Smith without whom I would still be milling parts.

I would like to thank the National Science Foundation Integrated Graduate Education and Research Traineeship, the Cockrell School of Engineering, and the U. S. Department of Energy for their financial support of my studies and research. I would also like to thank Mr. Timothy Grant, who was a valuable early mentor and the inspiration for my career path. Finally, I would like to thank my friends and my family for their unconditional love and support. It is largely due to them that some crumbs of my sanity have remained intact.

Development of Polysulfide Battery Systems with Low-cost Active Materials and Solid Electrolytes

Martha M. Gross, Ph.D.

The University of Texas at Austin, 2019

Supervisor: Arumugam Manthiram

Effective utilization of renewable, intermittent energy sources will require cost-effective, long-life energy storage systems. Sulfur is a low-cost, benign, and widely abundant material that has attracted substantial attention as a battery material due to its promise of a high energy density (1,675 mA h g^{-1}). Dissolved sulfur in the form of aqueous polysulfide promises to overcome the limitations associated with solid sulfur, such as its low conductivity and poor electrochemical utilization. However, batteries with aqueous polysulfide as a redox material often suffer from degradation due to chemical crossover of the polysulfide. Aqueous polysulfide also suffers from sluggish redox kinetics, requiring the use of a catalyst. This work aims to demonstrate novel aqueous polysulfide battery couples and improve the lifetime and performance of aqueous polysulfide batteries enabled by the development of novel catalysts and the use of a solid electrolyte separator to confine the aqueous polysulfide.

First, a zinc-aqueous polysulfide battery with a mediator-ion solid electrolyte is demonstrated with both a Li^+ and Na^+ mediator ion. The CoS electrocatalyst developed for improved aqueous polysulfide redox kinetics presents improved stability when synthesized on a stable stainless-steel substrate. Overall, the battery exhibits good energy density and

capacity retention, and the choice of mediator ion is determined to have substantial impact on the battery performance.

A long-life polysulfide-air battery is developed with a highly active CuS polysulfide catalyst, mediator-ion solid electrolyte, and decoupled air electrodes for oxygen reduction and evolution reactions. The redox activity of the CuS in the absence of polysulfide at the intermediate voltages of a polysulfide-air battery are shown to have minimal effect on its long-term cycling stability.

Next two polysulfide-polyhalide battery systems, polysulfide-polybromide and polysulfide-polyiodide, are demonstrated with a mediator-ion solid electrolyte to eliminate chemical crossover of the redox-active materials and enable excellent long-term cyclability. The polyiodide catholyte proves to be substantially less corrosive to the Na^+-conducting solid electrolyte than the polybromide catholyte, and a Li^+-conducting solid electrolyte is shown to have remarkable stability in both the polybromide and polyiodide catholytes.

Lastly, a novel sodium-aqueous polysulfide hybrid battery is developed in which a sodium metal anode and nonaqueous anolyte are protected from the aqueous polysulfide catholyte with a solid electrolyte. The hybrid system is shown to have remarkable long-term cycling performance compared to fully nonaqueous room-temperature sodium-sulfur batteries. A novel freestanding CuS-CNT electrode is developed and it demonstrates excellent catalytic activity towards polysulfide redox.

Table of Contents

List of Tables

List of Figures

Chapter 1: Introduction

1.1 Motivation

The world energy mix is seeing a shift from nonrenewable fossil fuel energy sources to renewable energy sources with wind and solar in the lead. Costs continue to fall, but the intermittency of renewable sources is increasingly becoming a bottleneck to their further penetration into the energy market. Large-scale energy storage will be necessary for the transition to the full potential of renewable generation. However, current battery technologies use expensive, scarce, or geographically constrained materials that will not be scalable to the level needed. New battery chemistries are necessary that use widespread and abundant materials that are economical to extract on a large scale.

1.2 Aqueous Polysulfide

1.2.1 Sulfur as a Battery Material

Sulfur has attracted a substantial amount of interest as a battery material. It is extremely cheap, being a byproduct of the oil and gas refining process and highly abundant.[1-2] Its light weight and two-electron transfer per sulfur atom translates into a very high gravimetric energy density of 1,675 mA h g^{-1}_S. There are, however, a number of challenges in developing sulfur as a battery material. In addition to being very insulating ($\sigma \approx 1 \times 10^{-30}$ S cm^{-1}), the intermediate discharge products of sulfur (*i.e.*, polysulfides) are highly soluble in a wide variety of standard electrolytes, including both aqueous and organic electrolytes.[3-5] Licht et al. pioneered work starting in the early 1990s that turned the high solubility of polysulfides into an advantage by utilizing highly concentrated solutions of aqueous polysulfide as an energy dense catholyte. The aqueous polysulfide was coupled to high activity metal anodes to produce very high energy density aqueous

zinc- and aluminum-sulfur batteries.[6-7] However, their work also showed that at high concentrations, the dissolved polysulfides reacted with the metal anodes, forming a passivating layer and preventing the battery from being recharged.[8] Initial attempts to develop rechargeable polysulfide batteries were ultimately unsuccessful, in large part due to the fact that the types of separators used to block polysulfide shuttling proved insufficient.[9-12] Interest in polysulfide as a battery material was revived when the PolyPlus Battery Company, later verified by Li et al., demonstrated a rechargeable lithium metal-aqueous polysulfide hybrid battery, in which the lithium metal was protected from the aqueous catholyte by a Li^+-conducting solid electrolyte.[13-14] Following this work, Demir-Cakan et al. used a solid electrolyte separator to demonstrate lithium-ion-aqueous polysulfide batteries.[15] The use of a solid electrolyte to contain the aqueous polysulfide and the development of the mediator-ion system, as discussed in Section 1.5, has opened up the opportunity to develop battery systems based on aqueous polysulfide with a wide variety of couples not limited to Li or Li-ion anodes, as this work will show.

1.2.2 Characteristics of Aqueous Polysulfide

Elemental sulfur (S_8) is minimally soluble in deionized water, but its solubility begins to increase on the addition of sodium hydroxide.[16] In the presence of sulfide S^{2-}, however, sulfur becomes highly soluble, reacting with the sulfide to form polysulfide chains of composition S_x^{2-}.[4, 17] In aqueous solutions, it is generally accepted that medium- and short-chain polysulfides preferentially form with $1 < x \leq 5$.[18-20] Some authors have argued that higher order polysulfides ($5 < x \leq 9$) are present in aqueous solutions, but if so, they are present in minute quantities compared to the lower order polysulfides.[21-22] In aqueous solution, sulfide and polysulfide undergo a series of disproportionation reactions at equilibrium such that if equimolar amounts of sulfur (S) and sulfide salt (M_2S) are mixed

together, the product is not M_2S_2 but rather a series of products as per the following reactions:

$$S^{2-} + H^+ \leftrightarrow HS^- \quad (1.1)$$

$$HS^- + H^+ \leftrightarrow H_2S \quad (1.2)$$

$$(x-1){S_{x+1}}^{2-} + HS^- + OH^- \leftrightarrow x{S_x}^{2-} + H_2O \qquad x = 2-4 \quad (1.3)$$

where H^+ and OH^- are naturally present in the aqueous environment. Which products form and their concentrations are highly dependent on the pH and concentration of the initial materials.[23] At low pH (< 7), HS^- is the dominant specie, but a significant amount of H_2S is also formed, a per reaction 1.2. At mild alkaline pH (7 – 9), S_5^{2-} dominates while at intermediate pH, (9 – 14), the tetrasulfide S_4^{2-} ion dominates. As pH increases, the lower order polysulfide species S_3^{2-} and S_2^{2-} dominate in turn, as shown in Figure 1.1.

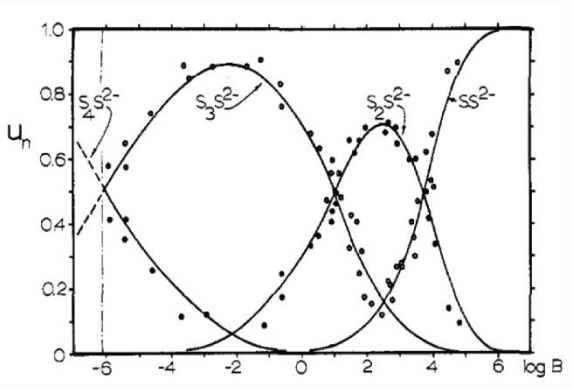

Figure 1.1 Polysulfide specie distribution. u_n is defined as the fraction of zerovalent sulfur present in S_nS^{2-}.* $B = [HS^-][OH^-]/S^0$ where $[HS^-]$ and $[OH^-]$ correspond to their respective species concentration, and S^0 denotes the total amount of zerovalent sulfur. logB of -6 corresponds to a pH of 6, while logB of 6 corresponds to a pH of 18. Reprinted from Ref. 18.

*Polysulfide is generally accepted to contain a sulfide ion S^{2-} with all remaining sulfur considered to be nonvalent (S^0). For this reason, some literature uses the notation S_nS^{2-} to refer to polysulfide ions.

Because the disproportionation of aqueous polysulfide makes exact description of solution composition difficult, authors typically define a solution to contain M_2S_x based on the concentration of precursor materials. For example, a solution with 1 M Na_2S + 3 M S + 0.1 M NaOH mixed together would be said to contain 1M Na_2S_4 + 0.1 M NaOH based on the initial concentrations of Na_2S and S. This definition will be used for the remainder of this dissertation.

The solubility of polysulfide is highly dependent on the cation of the sulfide salt. Li_2S, Na_2S, and K_2S have solubility limits of, respectively, 2.2, 2.3, and 8.8 m,* or 9.5, 17, and 49 % w/w.[4] The solubility limit of K_2S_4 has been determined to be 8.5 m at room temperature.[24] Definitive measurement of Li_2S_x and Na_2S_x polysulfide solubility limits are not available, though in the course of this work we have achieved a full dissolution of 2.4 M Na_2S_4 at room temperature.

The theoretical redox reaction and its voltage for each of the polysulfide species are as follows:

$$3{S_4}^{2-} + 2e^- \rightarrow 4{S_3}^{2-} \qquad -0.48 \text{ V vs SHE} \qquad (1.4)$$

$$2{S_3}^{2-} + 2e^- \rightarrow 3{S_2}^{2-} \qquad -0.50 \text{ V vs SHE} \qquad (1.5)$$

$${S_2}^{2-} + 2e^- \rightarrow 2S^{2-} \qquad -0.52 \text{ V vs SHE} \qquad (1.6)$$

The mixture of polysulfide species present at equilibrium, each with their own associated redox potential, can mean that the measured voltage of a polysulfide solution at equilibrium does not correspond to the theoretical voltage of an individual specie. The concentrations and distribution of the polysulfide species can be calculated based on the solution temperature and starting concentrations of hydroxide, sulfide, and nonvalent sulfur, using equilibrium constants measured by Giggenbach and Teder.[18, 25] The species concentrations

*In the work before the mid-2000s, concentration of aqueous polysulfide was reported in terms of molality (m). Modern work, however, references concentration in molarity (M).

can then be used in equation 1.7 developed by Lessner et al. to determine the equilibrium potential of the polysulfide solution.[26]

$$E = E^0 - \frac{RT}{6F} ln\left(\frac{[HS^-]^4[OH^-]^4}{[S_4^{2-}]}\right) - \frac{RT}{6F} ln\left(\frac{\gamma_{HS^-}{}^4\ \gamma_{OH^-}{}^4}{\gamma_{S_4^{2-}}}\right) \quad (1.7)$$

where R is the gas constant, T is temperature (K), and F is Faraday's constant. The equations rely on equilibrium constants measured at dilute concentrations (≤ 0.1 M), and as the activity coefficients (γ) are unknown, the activity coefficient term is usually neglected in the calculation. These assumptions introduce error and as a result, they are not reliable for exact quantification of solution voltage at higher concentrations. The open circuit voltage of different concentrations of Na_2S_4 + 0.1 M NaOH was measured over the course of this work, and it was found that the voltage approached the theoretical potential of S_4^{2-} as the concentration of nominal Na_2S_4 approached the solubility limit, as shown in Figure 1.2.

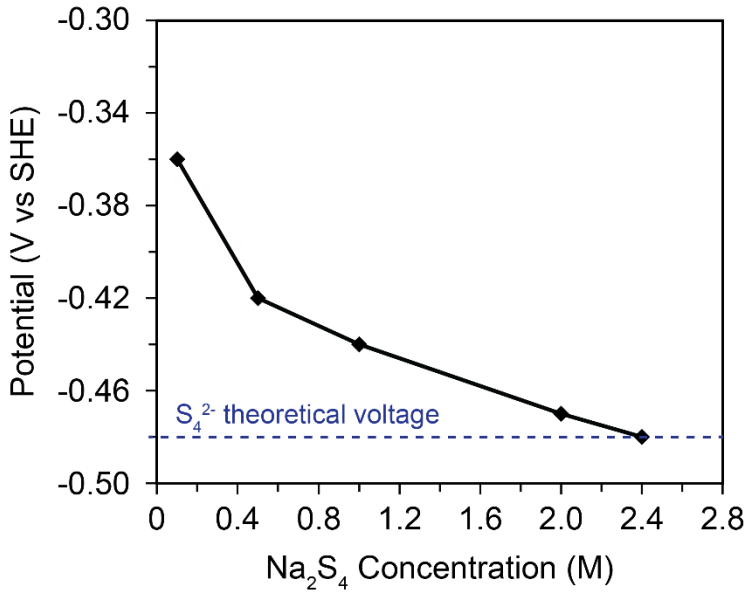

Figure 1.2 Variation in the measured potential of Na_2S_4 + 0.1 M NaOH solution with changes in concentration.

Aqueous polysulfide species are thermodynamically unstable, degrading to thiosulfate ($S_2O_3^-$) by the general reaction:

$$S^0 + OH^- \rightarrow {}^1/_4\, {S_2O_3}^{2-} + {}^1/_2\, HS^- + {}^1/_4\, H_2O \qquad (1.8)$$

where S^0 is the nonvalent sulfur present in the polysulfide species. This is of some concern to would-be battery developers, as it raises the possibility of irreversible battery degradation. The kinetics of polysulfide degradation was studied for conditions relevant to aqueous battery operation under ambient pressure and moderate temperatures, 25 – 85 °C, by Licht and Davis in a potassium-based system.[23] They confirmed the polysulfide specie responsible for degradation to be S_5^{2-} by a two step mechanism:

$${S_5}^{2-} + OH^- \rightarrow S_4O^{2-} + HS^- \qquad \text{(slow)} \qquad (1.9)$$

$$S_4O^{2-} + 2OH^- \rightarrow {S_2O_3}^{2-} + 2HS^- \qquad \text{(fast)} \qquad (1.10)$$

Licht and Davis determined in their work that at this temperature range, the conversion of polysulfide to thiosulfate was irreversible. They also found that under conditions of high concentrations of polysulfides and low concentrations of potassium hydroxide (KOH), polysulfide was stable on the order of years, even at temperatures of 85 °C. Therefore, with proper tailoring of electrolyte composition, batteries that utilize aqueous polysulfide as a redox-active material should suffer from only minor degradation during their lifetimes. The effect of the cation on polysulfide degradation has not been studied, and it is unknown at this time if the lower solubility of polysulfide in Li^+ or Na^+ solutions or the lower dissociation behavior of polysulfide in the presence of Li^+ or Na^+ compared to K^+ have any effect on its long-term stability.

1.2.3 Challenges

Aqueous polysulfide as a battery material faces a few challenges. First, aqueous polysulfide is reactive with air. Polysulfide reacts with oxygen to produce thiosulfate and

sulfur.[27] Furthermore, to maintain its kinetic stability, polysulfide catholytes always contain added hydroxide to maintain a pH of 9 - 14. Hydroxide readily reacts with carbon dioxide in the air to form carbonates. This reaction reduces the pH of the system and accelerates degradation of polysulfide.[25, 28-29] In the case of flow battery systems, the carbonate precipitates may clog the channels and electrodes. Another challenge is the generation of hydrogen sulfide (H_2S) gas. As equation 1.2 describes, H_2S is a natural product of polysulfide disproportionation. It is also readily generated during cycling of polysulfide, particularly during reduction of the lower order polysulfides.[15] Dissolution of H_2S gas causes a loss of active material and capacity fade in a battery. Furthermore, H_2S is both toxic and flammable and its generation creates a safety hazard. A final challenge for using aqueous polysulfide as a battery material is the sluggish redox kinetics of polysulfide. For adequate power performance, it therefore requires a catalyst, as will be discussed in the next section.

1.2.4 Catalyst for Aqueous Polysulfide Redox

The need for a catalyst when electrochemically cycling polysulfide was first identified by Hodes et al. in their work on photoelectrochemical cells (PECs).[30] They were also the first to explore potential catalysts for polysulfide redox. They compared carbon to a traditional catalyst, Pt-black, along with CoS, PbS, RuS_2, and two compositions of sulfided brass (70% Cu and 95% Cu). Catalytic activity of the transition-metal sulfides greatly exceeded that of carbon and Pt-black, with the 95% Cu sulfided brass displaying the highest catalytic activity. CoS, PbS, and 70% Cu sulfided brass performed equally well and had the second highest catalytic activity. Their work also showed that both compositions of sulfided brass contained Cu_2S phase, which proved to be unstable in long-

term cycling. PbS also proved to be unstable. They, therefore, suggested CoS as the ideal catalyst due to its high activity and robust stability.[31]

Since Hodes et al.'s pioneering work, other transition-metal sulfides have been identified as catalysts for polysulfide redox. Pyrite-phase transition-metal sulfides, such as FeS_2, CoS_2, and NiS_2, have been studied for their catalytic activity towards polysulfide reduction.[32] Layered transition-metal sulfides like MoS_2 and WS_2 have also been studied.[33-34] The catalytic activity of ferrites MFe_2O_4 (M = Fe, Cu, Co) and surface-modified mesoporous carbons towards oxidation of sulfide to form polysulfides has also been studied.[35-36] However, the bulk of studies on polysulfide catalysts have been undertaken with regards to enhanced activity in dye-sensitized solar cells (DSSCs), quantum dot sensitized solar cells (QDSSCs), and water treatment for sulfide removal.[37-41] Studies in which polysulfide and its catalyst are cycled under conditions relevant to a battery are typically limited to using CoS or Ni boiled in polysulfide to form a NiS_x surface layer, as these have shown the most promise in terms of stability.[33, 42] The NiS_x, though it is less expensive and less toxic than the CoS, has a substantially lower catalytic activity as well.[33, 43] Batteries that use aqueous polysulfide will require the use of a low-cost and environmentally benign catalytic electrode to achieve good power performance.

1.3 ANODE MATERIALS

Aqueous polysulfide has an intermediate voltage, as discussed in equations 1.4 – 1.6. This offers the possibility for it to function as an anolyte or a catholyte in high energy density batteries. High activity metal anodes, when paired with aqueous polysulfide catholytes, can be used in both static and hybrid flow battery configurations. Two different metal anodes were tested in this work: zinc and sodium.

1.3.1 Zinc

Zinc (Zn) is a widely used anode material in batteries, due to its low cost, low toxicity, high energy density, and wide availability.[1, 44] Zn is also the most electropositive metal that demonstrates reasonable stability in aqueous solutions. Zn undergoes different redox reactions depending on the pH of the electrolyte. In acidic and neutral media, Zn undergoes the reaction 1.11, while in alkaline media, it undergoes the simplified reaction 1.12.[45]

$$Zn \rightarrow Zn^{2+} + 2e^{-} \qquad 0.76 \text{ V vs SHE} \qquad (1.11)$$

$$Zn + 4OH^{-} \rightarrow [Zn(OH)_4]^{2-} + 2e^{-} \qquad 1.22 \text{ V vs SHE} \qquad (1.12)$$

Due to its higher voltage, alkaline electrolyte is generally preferred when using Zn as an anode whenever it is possible. Alkaline electrolyte is also preferred as Zn in acidic media undergoes a strong hydrogen evolution reaction, which corrodes the metal over time, limiting its capacity and shelf life. However, the use of alkaline electrolyte complicates the behavior of Zn. Reaction 1.12 can be expanded as follows:[46]

$$Zn \rightarrow Zn^{2+} + 2e^{-} \qquad (1.13)$$

$$Zn^{2+} + 4OH^{-} \rightarrow [Zn(OH)_4]^{2-} \qquad (1.14)$$

$$[Zn(OH)_4]^{2-} \rightarrow ZnO + H_2O + 2OH^{-} \qquad (1.15)$$

As reactions 1.13 – 1.15 show, in alkaline media, the Zn surface is oxidized during discharge and the resulting Zn^{2+} ion is solvated with hydroxide to form the zincate ion. When the solubility limit is reached, the zincate ion precipitates into insulating ZnO which results in a loss of active material.[45, 47] Furthermore, the preferred Zn species is pH-dependent, as shown in Figure 1.3.

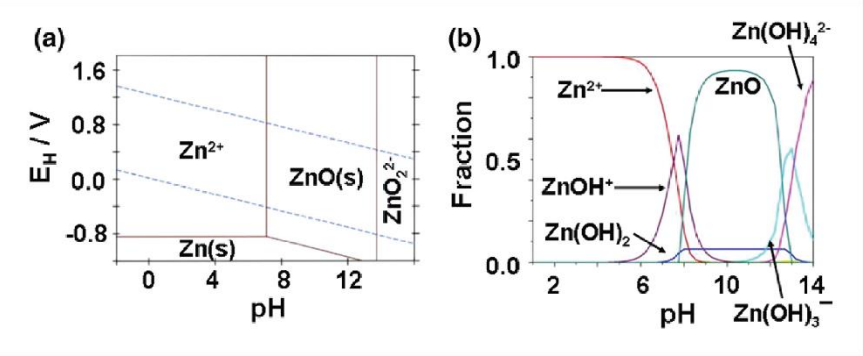

Figure 1.3 (a) Pourbaix diagram of Zn and (b) speciation of Zn^{2+} as a function of pH. Reprinted from Ref. 45.

Below a pH of 13, a ZnO passivation layer forms on the Zn anode surface. Maintenance of the electrolyte pH is particularly important for Zn batteries that use a solid electrolyte, as common solid electrolyte materials are unstable in strongly alkaline or acidic environments. Therefore, pH must be balanced between optimal Zn performance and long-term stability of the solid electrolyte.

A further challenge to the development of a rechargeable Zn anode is uneven deposition of Zn^{2+} on charge and the resulting dendrite formation. An image of a cycled Zn anode showing ZnO deposition and dendrite formation is shown in Figure 1.4. A variety of methods have been tested to prevent dendrite formation during cycling. Alloying agents like mercury and lead have been tested, as have a wide variety of additives for the electrolyte such as citric acid, sodium dodecyl sulfate (SDS), thiourea, and cetyltrimethylammonium bromide (CTAB).[47-51] Dendrite formation is often slowed by these methods, but not fully suppressed, and it remains a challenge for the long-term development of rechargeable Zn anodes.

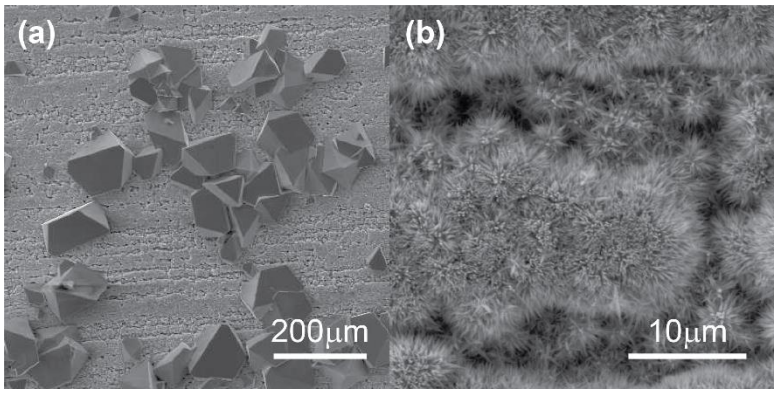

Figure 1.4 SEM images of Zn anode after cycling, showing (a) ZnO deposition on Zn surface and (b) formation of Zn dendrites.

1.3.2 Sodium

Sodium (Na) has attracted substantial attention as an anode material in recent years due to its wide abundancy, low cost, high capacity (1166 mA h g^{-1}), and low reduction potential (–2.71 versus SHE).[2, 52-53] It has traditionally been used in high temperature molten sodium-sulfur batteries, but there has been a strong interest recently in developing new room-temperature sodium-sulfur batteries to eliminate the safety hazards and maintenance costs associated with high temperature battery operation.[54-56] The development of sodium-metal anodes has been hampered by is great reactivity. Like lithium and other high activity metals, sodium readily forms dendrites during cycling.[57] Early research treated metallic sodium in a similar fashion to metallic lithium with regards to electrolyte selection and dendrite formation. However, recent research has begun to elucidate differences between lithium and sodium, with particular regard to the formation of the solid electrolyte interface (SEI).[58-59] This body of work has begun to identify that simply migrating the electrolytes and additives used in lithium-based systems to their sodium-based counterparts is not guaranteed to produce a stable SEI layer on the sodium

anode, or to allow for good cyclability.[58, 60-61] A comparison of the performance of Li symmetric cells and their Na-based counterparts is shown in Figure 1.5.

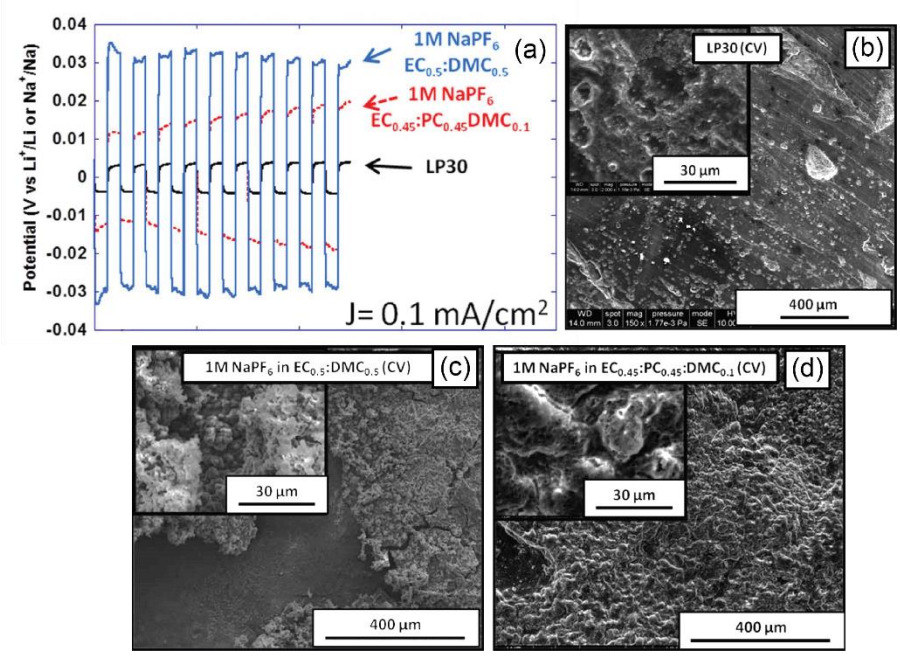

Figure 1.5 Characterization of Li and Na symmetric cells with different electrolytes. (a) galvanostatic cycling performance of Li and Na metal symmetric cells. (b) SEM image of Li after plating/stripping by cyclic voltammetry. (c – d) SEM image of Na after plating/stripping by cyclic voltammetry in different electrolytes. LP30 electrolyte consists of 1 M $LiPF_6$ in $EC_{0.5}$: $DMC_{0.5}$. Modified from Ref. 58.

To achieve good cyclability with sodium-metal anode, a variety of systems have been tested. Work on new electrolytes, such as the glyme-based electrolytes with $NaPF_6$ salts studied by Seh et al., and ultra-concentrated NaSFI salts in ether- and hydrofluoroether-based electrolytes studied by, respectively, Cao et al. and Zheng et al., have proved promising for long-term cycling of Na-metal anodes.[62-64] Other approaches to improving sodium-metal cycling efficiency include the deposition of an artificial SEI layer, such as Al_2O_3 or polymeric alucone by atomic layer deposition or molecular layer deposition, as demonstrated by Luo et al. and Zhao et al.[65-67] Novel approaches also include

the use of porous current collectors and doped interlayers to suppress dendrite formation.[68-69] There has been substantial progress in developing of high cycling-efficiency sodium-metal anodes, and this remains an active area of research.

1.4 CATHODE MATERIALS

Typically, when polysulfide is used as an anolyte, it is coupled with low-cost catholytes in flow battery systems. The use of a liquid anolyte and catholyte allows for the decoupling of energy and power density, which is a major advantage of these types of systems.[44, 70-71] This work demonstrates three catholyte couples for aqueous polysulfide, enabled by means of a mediator-ion solid electrolyte as further described in Section 1.5.

1.4.1 Air

Oxygen (O_2) is considered a great candidate for batteries due to its high theoretical capacity and energy density. Ideally, the use of oxygen directly from the air further increases the energy density of the system as oxygen does not have to be contained within the battery electrode. In practice, however, rechargeable air cathodes have proven to be difficult to achieve.

The redox reactions of O_2 are highly dependent on the electrolyte. In aqueous electrolyte, reactions are dependent on pH:

$$O_2 + 4H^+ + 4e^- \rightarrow 2H_2O \qquad \text{pH} < 7 \qquad 1.23 \text{ V vs SHE} \qquad (1.16)$$

$$O_2 + 2H_2O + 4e^- \rightarrow 4OH^- \qquad \text{pH} \geq 7 \qquad 0.40 \text{ V vs SHE} \qquad (1.17)$$

Acidic catholytes have a clear advantage in terms of voltage compared to alkaline catholytes. Acidic catholytes also have an advantage in that they do not have a problem of CO_2 ingression.[47, 72] As previously discussed in Section 1.2.3, alkaline catholytes suffer from reaction between the OH^- and CO_2 in air to form carbonates (CO_3^{2-}), which are largely

insoluble in the catholyte and block pores in the gas diffusion layer (GDL), preventing O_2 from entering the cell.[73]

The primary challenge associated with air cathodes is the necessity of catalysts for oxygen reduction (ORR) and oxygen evolution (OER) reactions. Catalysts must be stable in the catholyte and demonstrate high catalytic activity. However, even the best performing catalysts typically suffer degradation over time. IrO_2 catalyst for OER and Pt/C catalyst for ORR are considered the reference standards by which novel catalysts are developed, and there have been extensive reviews written on the wide variety of catalysts developed, from transition-metal oxides to highly doped amorphous carbons with novel morphologies.[74-78] Most catalysts rely on a carbon substrate due to carbon's high conductivity and low cost, and the ease of tailoring carbon properties. However under the highly oxidative voltages associated with OER, even when the overpotential is lowered by a catalyst, carbon substrates are prone to severe degradation owing to the oxidation of carbon to form CO_2.[79] There has been development of carbon-free substrates to alleviate this issue.[75] There has also been the development of a decoupled electrode system, in which current is passed through separate electrodes during charge and discharge. The decoupled electrode system allows for independent optimization of the ORR and OER catalysts as well.[80] The stabilizing effect of the use of a decoupled air electrode is shown in Figure 1.6.

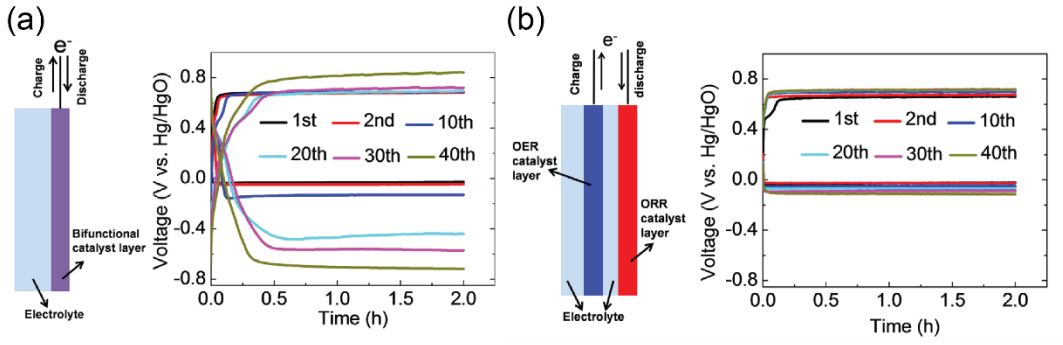

Figure 1.6 Cycling performance of hybrid Li-Air battery with (a) bifunctional and (b) decoupled electrode with Pt/C ORR and $NiCo_2O_4$ OER catalysts. Reprinted from Ref. 80.

1.4.2 Polyhalides

Halides have been considered for a wide variety of battery systems, from solid-state lithium-iodide batteries to seawater batteries.[81-82] This work focuses on the use of polybromide and polyiodide in aqueous electrolyte as redox-active materials for large-scale batteries.

1.4.2.1 Polybromide

Polybromide is considered a good candidate for batteries due to the low cost, wide abundancy, and high voltage of bromine (1.05 versus SHE).[2, 83] Bromine (Br_2) is sparingly soluble in water, but highly soluble in bromide (Br^-) solutions, due to its ability to complex with the Br^- ion to form polybromide ions as per the reaction:[84]

$$Br_2 + Br_{n-2}^{\ -} \rightarrow Br_n^{\ -} \qquad \text{n = 3, 5, 7} \qquad (1.18)$$

While the higher order polybromides form in aqueous solutions, with regard to batteries it is generally the Br_3^- polybromide ion that is discussed. There are two battery systems that make use of polybromide that have reached a commercial stage: (i) polysulfide-polybromide (PSB) flow batteries and (ii) zinc-bromine hybrid flow batteries (ZBBs).[83, 85] PSB flow batteries use a concentrated aqueous polybromide catholyte consisting of NaBr

+ Br_2 in which Br_2 is fully dissolved as Br_3^- polybromide ion. The ZBB, in contrast, utilizes a dilute electrolyte in which quaternary ammonium salts are added to complex with Br_2, forming a conductive liquid salt that phase separates from the aqueous electrolyte due to differences in density and its immiscibility with water during charge.[70] The ZBB has been targeted for applications that require low to moderate power densities and small installation sizes (< 2 MW), while the PSB battery applications are targeted for larger installations (> 10 MW) due to differences in cost and battery performance metrics.[86] Due to its application for large-scale energy storage, this work focuses on the PSB battery as discussed further in Chapter 5.

1.4.2.2 Polyiodide

Iodine (I_2) behaves similarly to bromine in aqueous solutions, in that it complexes with the iodide ion to form polyiodide and is capable of high solubilities in aqueous solutions as a result.[87] Only recently has aqueous polyiodide been explored as a redox flow catholyte, with Li et al. presenting the first zinc-polyiodide redox flow battery in 2015.[88] Polyiodide has elicited interest as it has faster redox kinetics than polybromide, and a higher solubility.[87, 89] Furthermore, it is less corrosive. However, polyiodide has a lower redox voltage (0.54 V versus SHE) than polybromide, so the use of polyiodide potentially comes at a cost of reduced energy density.

1.4.2.3 Challenges

Bromine and iodine are both highly corrosive and toxic materials.[90-91] The complexation of Br_2 and I_2 is a dynamic equilibrium, in which free Br_2 and I_2 can be found in aqueous solution. Both Br_2 and I_2 fume at room temperature, though the vapor pressure of I_2 is substantially lower than that of Br_2 as shown in Figure 1.7. As a result, great care

must be taken to not release the toxic fumes.[92] Polyiodide is considered to be safer and less corrosive than polybromide, but controls must still be placed to prevent its release.[93] Vapor management systems and corrosion-resistant materials necessary to manage these materials can increase the system-level costs of these aqueous polyhalide batteries.

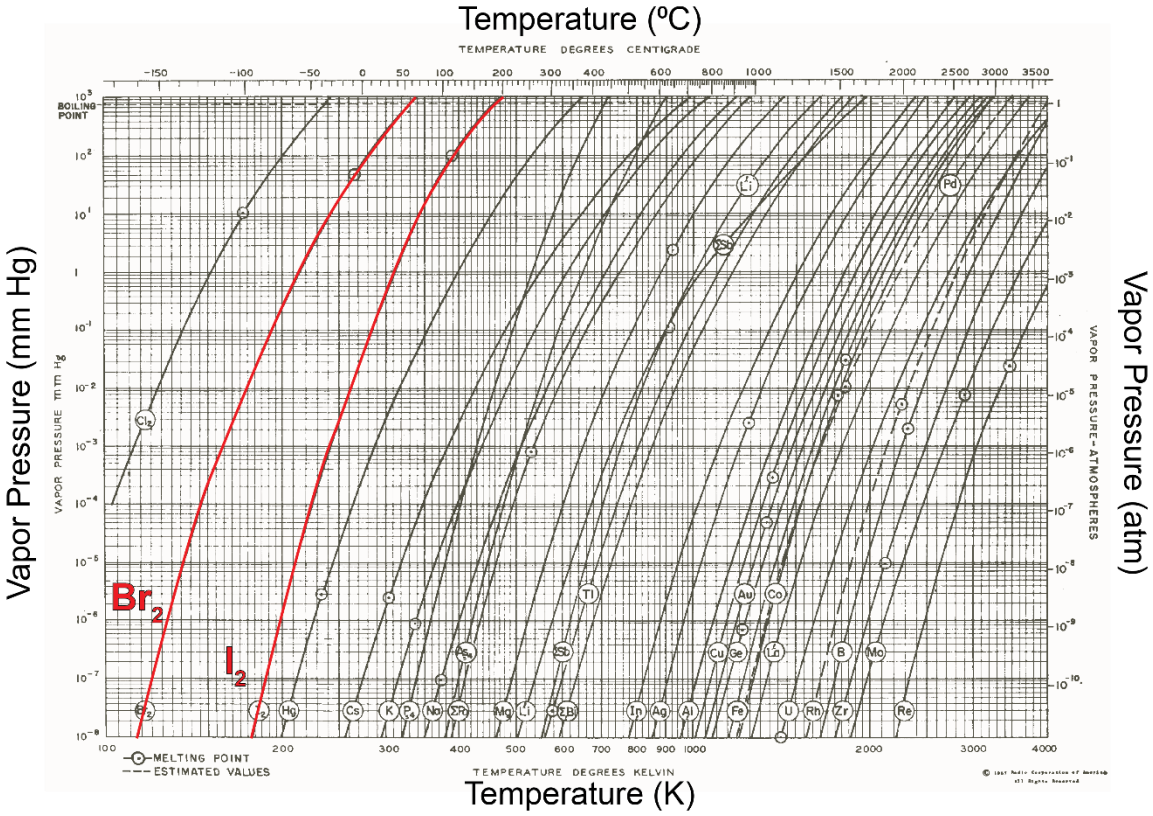

Figure 1.7 Vapor pressure differences of common elements. Br_2 and I_2 are highlighted. Reprinted from Ref. 94.

1.5 Solid Electrolyte Separators

1.5.1 Types of Separator Materials

There are a wide variety of separators that are used in batteries, each tailored to optimize desirable characteristics. They can be loosely defined by their primary purpose: physical barriers, ionic transport membranes, and functional separators.[95] Physical barrier

separators, such as glass fiber and Celgard separators, serve the primary purpose of providing a physical barrier between the anode and cathode materials during cycling with the goal of preventing short circuits in the battery, while still maintaining ionic contact between the electrodes. Ionic transport membranes, such as Nafion, anion exchange membranes, and porous membranes, exhibit some degree of ionic selectivity, allowing preferential transport of the desired ionic specie and blocking other ionic species from moving across the membrane. These types of membranes are typically deployed in flow battery configurations.[96-97] Functional separators have been functionalized in some regard to produce a desired characteristic, such as in the case of coated separators for polysulfide trapping in lithium-sulfur batteries.[98] Solid electrolytes demonstrate superior performance as both physical barriers and highly selective ionic transport membranes by these definitions. They have been extensively researched in this regard for high-temperature batteries, such as molten sodium-sulfur batteries.[99] Improvements in ionic conductivities and improved costs have made them increasingly attractive for use in room-temperature batteries.

1.5.2 Solid Electrolyte

Solid electrolytes that are used as a separator must exhibit good mechanical strength, high ionic conductivity, good chemical stability with the other electrolyte materials, low cost, and in the case of batteries with proton-containing electrolytes such as aqueous systems, low H^+ conduction. There is extensive research being performed on solid electrolytes, but as of this writing, solid electrolytes that are commercially available are generally limited to Li^+- and Na^+-conducting NASICON-type ceramics. Briefly, NASICON consists of a rhombohedral R-3c $A_xB_2P_3O_{12}$ unit cell comprised of a corner-sharing BO_6 octahedra and PO_4 tetrahedra skeleton with A^+ cations occupying two sites:

six-coordinated M1, labeled in Figure 1.8 as a green sphere, and eight-coordinated M2, labeled in Figure 1.8 as a yellow sphere.[100] Substitution of the B^{4+} ion with di-, tri-, and pentavalent ions, and substitution of PO_4^{3-} with SiO_2^{4-} with charge balance restored by A^+ cations can be used to improve ionic conductivity.

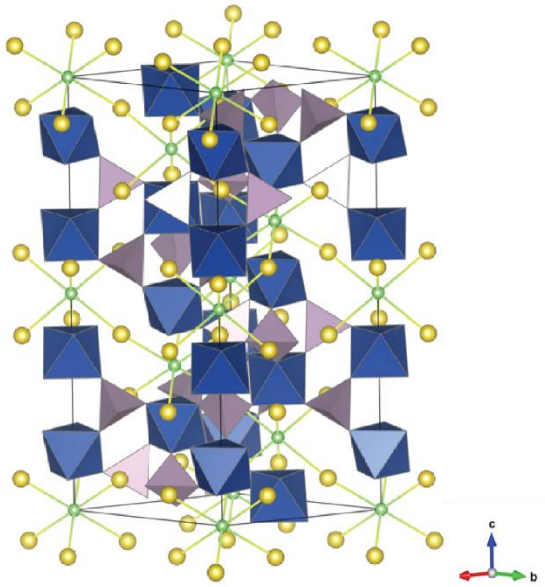

Figure 1.8 NASICON unit cell. MO_6 units are represented as blue octahedra, and PO_4 units are represented as purple tetrahedra. M1 and M2 sites are represented by, respectively, green and yellow spheres. Conduction pathways of A^+ cations are represented by yellow/green lines between M1 and M2 sites. Reprinted from Ref. 100.

Synthesis methods can also have a profound impact on the ceramic properties. Li^+-ion solid electrolytes have found good success with glass-ceramic synthesis methods, in which first a glass of the desired composition is formed, and then heat treated to precipitate a crystalline phase.[101] Na^+-ion NASICON structure ceramics have not achieved the same room-temperature ionic conductivities with glass-ceramic synthesis methods yet, and so for these materials sintering is the preferred method of synthesis.

Ohara, Inc. of Japan is currently the industry leader in the production of Li^+-ion conducting glass-ceramics (LICGC) for use in batteries. They produce a NASICON-type glass-ceramic of composition $Li_{1+x+y}Al_xTi_{2-x}Si_yP_{3-y}O_{12}$ (LATP). This ceramic demonstrates low permeability to water and good mechanical strength, chemical stability, and room-temperature conductivity (~1 x 10^{-4} S cm^{-1}), as shown in Figure 1.9.

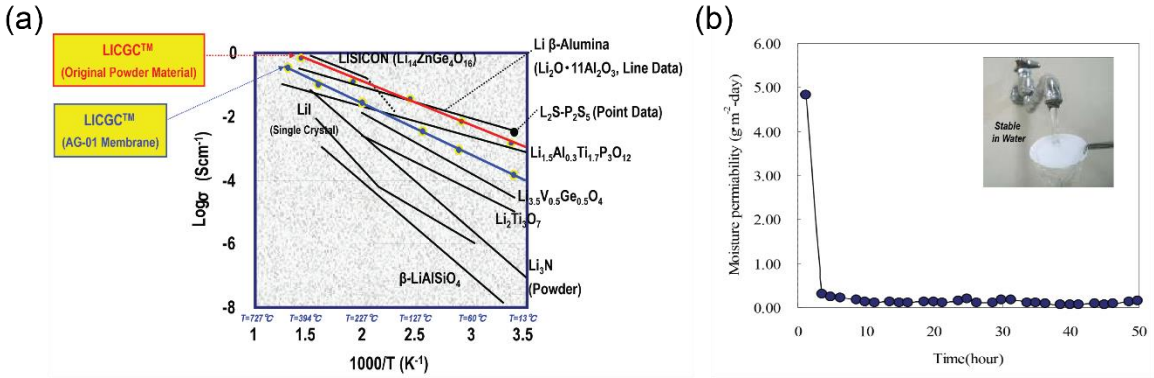

Figure 1.9 Properties of LATP membrane from Ohara, Inc.: (a) ionic conductivity of LICGC material and membrane and (b) water permeability of the ceramic. Inset: ceramic stability in water. Reprinted from Ref. 102.

Development of sodium-based batteries was initially supplanted by lithium-based batteries due to their promise of better performance, but the low cost and wide availability of sodium coupled with the concern about the long-term availability of lithium has led to a renewed interest in sodium-based batteries. However, development of ceramic electrolytes for room-temperature sodium-based batteries has lagged behind that of their lithium conducting counterparts. As a result, offerings of Na^+-ion conducting solid electrolytes with high room-temperature ionic conductivity are limited. For this work, we used NASICON obtained from 4 to One Energy (transferred to Ce&Chem Co. Ltd (South Korea) in 2015). The NASICON has a purity of > 95 %, with ZrO_2 being the main impurity

phase, and a density of 3.21 g cm^{-3} compared to a reference density of 3.27 g cm^{-3}.[103] Properties of the NASICON are shown in Figure 1.10.

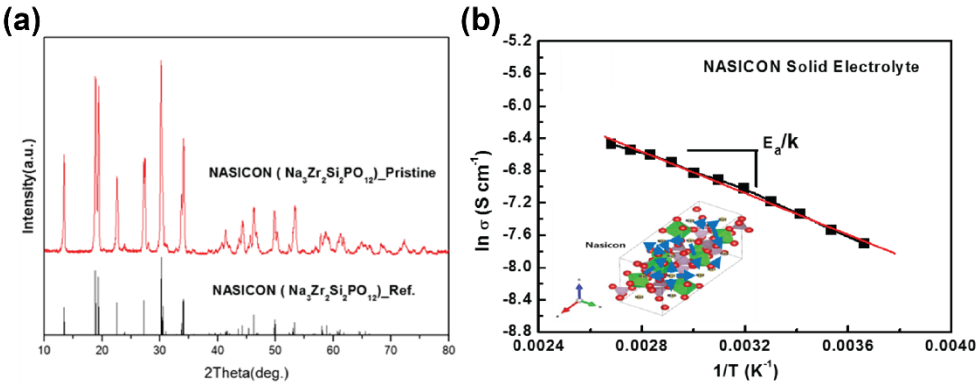

Figure 1.10 Properties of NASICON from 4 to One Energy, showing the (a) XRD analysis of phase composition and (b) ionic conductivity; inset: NASICON crystal structure. Reprinted from Ref. 103.

1.5.3 Mediator-Ion System

The use of Li^+ and Na^+ solid electrolytes have traditionally been restricted to battery systems that use Li or Na metal anodes. There are, however, a vast number of battery systems that would benefit from the use of a solid electrolyte whose active materials do not contain either Li^+ or Na^+. The concept of a "mediator-ion" system was developed to overcome this obstacle.[74] In a mediator-ion system, a Li^+ or Na^+ solid-state electrolyte (SSE) is used as a separator. The corresponding cation acts as an ionic mediator, in that it does not actively participate in the reactions at the anode or cathode, but rather passively migrates through the solid electrolyte to balance charge during cycling.[104-105] A schematic of the mediator-ion system is shown in Figure 1.11. The use of a mediator-ion system allows for the development of a wide variety of battery couples that are not possible with traditional battery separators. The solid electrolyte also allows for optimization of anolytes and catholytes separately. For example, anolytes and catholytes of different pHs can be

coupled together, as has been demonstrated for alkaline Zn and Fe anodes with acidic air cathodes.[74, 105-106] This work will make extensive use of the mediator-ion system to demonstrate long-life, low-cost active material battery couples.

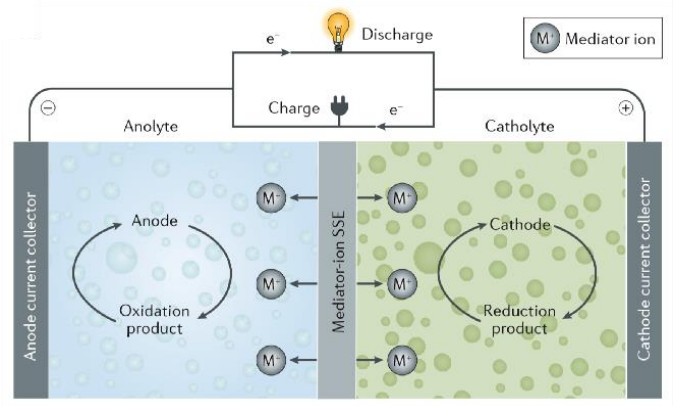

Figure 1.11 Schematic of the mediator-ion system. Reprinted from Ref. 104.

1.6 OBJECTIVES

The primary objective of this dissertation is to demonstrate low-cost, high energy density battery systems with fully liquid aqueous polysulfide as one of the redox-active electrodes as enabled by the use of a solid electrolyte. This dissertation also works to improve polysulfide battery performance by the development of efficient and inexpensive catalysts for polysulfide redox. This work establishes that aqueous polysulfide makes an excellent battery material, and the use of a solid electrolyte allows its broad application to a variety of battery systems.

Chapter 1 introduces the characteristics of aqueous polysulfide, its promise as a battery material and its challenges. Additionally, it provides a brief introduction of polysulfide catalysts, as well as the different anodes and catholytes that can be paired with aqueous polysulfide when protected by a solid electrolyte in this dissertation. Chapter 2

provides an overview of the general experimental methods used in this work to successfully demonstrate the aqueous polysulfide battery systems and their catalysts.

In Chapter 3, a rechargeable zinc-aqueous polysulfide (ZAPS) battery with a mediator-ion solid-state electrolyte is demonstrated. The differences between lithium- and sodium-based mediator-ion systems is shown, as are improvements to the traditional CoS catalyst used for polysulfide redox. However, the ZAPS battery exhibits a low theoretical cell voltage of 0.74 V and utilizes an expensive Co-based catalyst which is detrimental to the goal of developing low-cost, high energy density battery systems. Subsequent chapters focus on battery systems with increased voltage and low-cost polysulfide catalysts.

Chapter 4 introduces the development of a long-cycle life polysulfide-air battery and a low-cost covellite phase CuS catalyst. A mediator-ion solid electrolyte is used to separate the alkaline polysulfide anolyte from the acidic air catholyte. Some insight is presented into the redox behavior of CuS at intermediate voltages and pH relevant to polysulfide catholytes, and its long-term stability as a catalyst is demonstrated. The polysulfide-air battery is proven to achieve a long-cycle life, as enabled by the use of decoupled ORR and OER electrodes with an acidic catholyte.

The effectiveness of the solid electrolyte separator at blocking chemical crossover and the subsequent enhancement of battery cycle life is further demonstrated in polysulfide-polyhalide batteries in Chapter 5. Polysulfide-polybromide batteries are shown to have a high power density and high coulombic efficiency, but corrosion of the solid electrolyte by the polybromide catholyte is proven to be an issue. Polysulfide-polyiodide batteries have a lower voltage and are thus shown to have a lower power density than polysulfide-polybromide batteries, but are demonstrated to have substantially fewer issues of corrosion between the solid electrolyte and the polyiodide catholyte. The tradeoffs between stability and performance are discussed.

Chapter 6 demonstrates a high energy, room temperature sodium-aqueous polysulfide hybrid battery with long-cycle life. The rational design of a CuS-CNT electrode is presented for improved catalysis of aqueous polysulfide redox. The differences in electrochemical behavior between the hybrid sodium-aqueous polysulfide battery and traditional nonaqueous sodium-sulfur room temperature batteries is demonstrated. Electrochemical participation of the nonaqueous anolyte at the sodium anode is also discussed. Finally, a summary of this work on long-life, low-cost battery systems is given in Chapter 7.

Chapter 2: General Experimental Methods

2.1 Materials & Synthesis

Aqueous polysulfide was prepared using N_2-purged deionized water under N_2 flow in a Schlenk line. Sodium or lithium hydroxide (NaOH, $LiOH \cdot H_2O$), anhydrous sodium or lithium sulfide (Na_2S, Li_2S), and sulfur (S) were dissolved in deionized water at the desired concentrations. Synthesis procedures for all remaining materials are reported in each individual chapter. All batteries used either a Li^+ -conducting glass-ceramic obtained from Ohara, Inc, LATP ($Li_{1+x+y}Al_xTi_{2-x}Si_yP_{3-y}O_{12}$, 150 μm thickness, $\sigma = \sim 1 \times 10^{-4}$ S cm^{-1}) or a Na^+-conducting sintered ceramic obtained from 4 to One Energy Corporation ($Na_3Zr_2Si_2PO_{12}$ (NASICON), hand polished to 0.5 mm thickness, $\sigma = \sim 1 \times 10^{-3}$ S cm^{-1}) as specified in each chapter.

2.2 Materials Characterization

General characterization techniques are presented in the following section. Specific characterization procedures will be described in each individual chapter.

2.2.1 Scanning Electron Microscopy (SEM) and Energy Dispersive Spectroscopy (EDS)

Morphology analysis of electrodes and solid electrolytes was performed with a FEI Quanta 650 field emission SEM for high resolution images, and either a Tescan Vega3 SEM or a JEOL JSM-5610 SEM for low resolution images. Elemental composition analysis of EDS spectra or maps of the analyzed materials was obtained with the SEM-attached spectrometer.

2.2.2 Transmission Electron Microscopy (TEM) and Select Area Electron Diffraction (SAED)

High resolution morphology and SAED phase identification of CoS and CuS catalysts were obtained with a JEOL 2010F TEM equipped with scanning transmission electron microscopy (STEM) and corresponding EDS.

2.2.3 X-ray Diffraction (XRD)

Phase information was collected by XRD with a Rigaku MiniFlex 600 equipped with Cu Kα radiation, at a voltage of 40 kV and current of 15 mA. Crystalline phases were determined by comparing the obtained XRD patterns with JCPDS cards.

2.2.4 UV-Visible Spectroscopy (UV-Vis)

UV-Vis was performed to identify polysulfide speciation in dilute solutions of 1mM Na_2S_4 with a Cary 5000 UV-Vis NIR Spectrometer from 800 to 200 nm at a scan rate of 600 nm min^{-1}.

2.2.5 X-ray Photoelectron Spectroscopy (XPS)

Surface and bonding characterization of CoS catalyst was performed with a Kratos Axis Ultra DLD XPS.

2.2.6 Wide-Angle X-ray Scattering (WAXS)

WAXS analysis was performed on CuS electrodes with a Ganesha SAXSLAB SAXS/WAXS laboratory beamline. WAXS was performed when low mass loading of the catalyst and catalyst nanostructure prevented the obtainment of clear, quantitative data by XRD.

2.2.7 Raman Spectroscopy

Raman spectroscopy materials characterization was performed with a Witec Micro-Raman Spectrometer Alpha 300 using a 488 nm laser and a 600 g mm^{-1} grating (blaze wavelength: 500 nm).

2.3 ELECTROCHEMICAL CHARACTERIZATION

2.3.1 Cell Assembly

Cells were assembled with custom-built housing, designed for each battery system tested. Schematics for each type of cell assembly can be found in Appendix A. Sodium anodes were assembled in an argon-filled glovebox, while cell components containing polysulfide electrolytes were assembled in a nitrogen-purged glovebag. All other cell components were assembled in air unless otherwise specified.

2.3.2 Cyclic voltammetry (CV)

Cyclic voltammetry was performed with an Arbin BT 2000 battery cycler, an Autolab PGSTAT302N potentiostat (Eco Chemie B.V.), or a CH Instruments 1040A potentiostat as specified in each chapter. CVs of polysulfide-containing electrolyte were performed either in full cells or in half-cells in which the polysulfide was separated from the reference and counter electrodes by a solid electrolyte. CVs were performed at variable scan rates ($mV\ s^{-1}$).

2.3.3 Electrochemical Impedance Spectroscopy (EIS)

EIS measurements to obtain data on impedance of cells and catholytes were performed with an integrated Solartron 1287 and 1260 platform from 0.01 Hz to 1 MHz. Measurements of polysulfide were with either CoS@SS catalyst working electrode and Pt wire counter electrode, or planar stainless steel electrodes polished to a mirror finish.

Custom chambers were assembled in in an N_2-purged glovebag to prevent exposure of the polysulfide electrolyte to air.

2.3.4 Galvanostatic cycling and rate-performance testing

Galvanostatic cycling and rate-performance testing was performed with an Arbin BT 2000 battery cycler. Charge-discharge curves were primarily performed at a current density of 0.5 mA cm^{-2}. Other current densities used are detailed as necessary in individual chapters. Rate testing was performed by discharging and charging cells or half-cells for 5 cycles at the specified current density. Power density information was collected from the end of discharge of the fifth cycle.

Chapter 3: A Rechargeable Zinc-Aqueous Polysulfide Battery with a Mediator-Ion Solid Electrolyte*

3.1 INTRODUCTION

Dissolved sulfur in the form of polysulfide has attracted attention as a candidate energy storage media due it the high energy density (1,675 mA h g^{-1}_S) and its large solubility in both aqueous and organic solvents.[5, 24, 107] Batteries containing a high density of dissolved redox active sulfur in the form of polysulfides allows for a high system-wide energy density, as these batteries do not require inactive materials such as binders or conductive additives, or excess electrolyte typically needed for solid sulfur cathodes.[108] Polysulfide in aqueous solvent has a particularly high solubility, achieving up to 8.5 molal concentrations in the case of K_2S_4.[24] Initial work with aqueous polysulfide focused on static primary batteries, and only recently have static secondary batteries with polysulfide active material been explored.[6-7, 14-15, 109-111] A summary of prior work on static batteries with aqueous polysulfide active material can be found in Table 3.1. A summary of the vanadium redox flow battery is provided for a comparison as a standard battery technology for grid-level energy storage in the table.

Zinc is an attractive anode material due to its low cost and widespread use as an industrial metal. It offers a voltage of -1.22 V (versus standard hydrogen electrode (SHE)) and reasonable stability and cyclability in alkaline electrolytes.[112] When used in a zinc-sulfur battery, however, zinc rapidly reacts with polysulfides to form a passivating zinc sulfide (ZnS) film on the anode surface, which prevents discharge of the anode. Bendikov et al. successfully demonstrated a single compartment (no separator) zinc-aqueous

*M. M. Gross and A. Manthiram "Rechargeable Zinc-Aqueous Polysulfide Battery with a Mediator-Ion Solid Electrolyte," *ACS Appl. Mater. Interfaces*, 2018, **10**, 10612-10617.
M. M. Gross carried out the experimental work. A. Manthiram supervised the project. All participated in the preparation of the manuscript.

polysulfide battery with a strongly alkaline electrolyte (pH ≥ 15), which prevented passivation of the anode, allowing the battery to discharge.[7] However, the cell was not rechargeable.[8] Complete separation of the zinc anode and polysulfide catholyte is necessary for the battery to be rechargeable.

Cell Chemistry	Polysulfide Composition	OCV (V)	System Specific Capacity (mA h g^{-1})	Gravimetric Energy Density (W h kg^{-1})	Limiting Electrode	Separator	Battery Type	# Cycles	Ref.
Al-K_2S_4	K_2S_4 $S + K_2S_x$	1.79[a]	361.7[a] 505[a]	647[a] 910[a]	K_2S_4 $S + K_2S_x$	Nafion, Raipore	Primary	–	6, 113
Zn-K_2S_4	K_2S_4, $S + K_2S_4$	1.04[a]	550[a]	572[a]	K_2S_4	Permion, none	Primary	–	7-8
Li-Li_2S_4	Li_2S_4	~2.6[b]	[d]	[d]	Li_2S_x	LIC-GC	Secondary	100	13
K_2S_x-$LiMn_2O_4$	K_2S_x	1.5[b]	110[b,c]	165[c]	$LiMn_2O_4$	LIC-GC	Secondary	>100	110
Li-Li_2S_4	Li_2S_4, $S + Li_2S_4$	2.67[b]	1030[b,c], 1202[b,c]	654[a]	Li_2S_4	LATP	Secondary, Primary	20 -	14
K_2S_x-$LiMn_2O_4$	K_2S_x	1.5[b]	90[b,c]	135[c]	$LiMn_2O_4$	Nafion	Secondary	200	15
$Na_{0.44}MnO_2$ -Na_2S_5	Na_2S_5	0.80[b]	40[b]	32[c]	$Na_{0.44}MnO_2$	Nafion	Secondary	200	111
Zn-Li_2S_4, Zn-Na_2S_4	Li_2S_4, Na_2S_4	0.89[b]	349[a] 349[a], 318[b]	251[a] 251[a], 203[b]	Li_2S_4, Na_2S_4	LATP, NASICON	Secondary, Secondary	- 50	This Work
V^{II}/V^{III}- V^{IV}/V^{V}	–	1.25[a]	227[a]	283[a]	V^{IV}/V^{V}	Nafion	Flow	500-2000	70

Table 3.1 Summary of prior work for static secondary batteries using aqueous alkali metal polysulfide as an anolyte or catholyte. [a]theoretical value based on active materials, [b]measured value based on active materials, [c]per kilogram of active cathode material, [d]value not reported

Recently Li et al. demonstrated a lithium-aqueous polysulfide battery that used a lithium ion-conducting solid-state electrolyte (SSE) to separate a metallic lithium anode from an aqueous polysulfide catholyte.[14] Demir-Cakan et al. employed a lithium ion-conducting SSE to separate a $LiMn_2O_4$ cathode from a polysulfide anolyte.[110] The SSE, as demonstrated in these studies, is so effective at separating the reactive polysulfide catholyte that Visco et al. are working to commercialize a lithium-sulfur battery based on the use of the SSE.[109] In the case of a zinc anode, however, a Zn^{2+} ion SSE that operates at room temperature is not practically available.[114-115]

Herein we demonstrate a rechargeable zinc aqueous polysulfide (ZAPS) battery by means of a mediator-ion SSE. The ZAPS battery consists of a Zn anode, an alkaline anolyte, a mediator-ion SSE, an aqueous polysulfide catholyte, and catalytically active cobalt sulfide (CoS) electrode. We demonstrate the concept and electrochemical characteristics of our rechargeable ZAPS battery with both a lithium and sodium mediator ion.

3.2 Experimental Methods

3.2.1 Synthesis of Aqueous Polysulfide

Aqueous polysulfide catholyte solution was prepared as described in Chapter 2 by mixing NaOH with Na_2S and S in a 1 : 1 : 3 molar ratio to form a nominal 0.1 M Na_2S_4 + 0.1 M NaOH solution. 0.1 M Li_2S_4 catholyte solution was prepared in the same manner with lithium-based counterparts. 1 M Na_2S_4 pretreatment solution was prepared by mixing NaOH with Na_2S and S in a 1 : 10 : 30 molar ratio in the same manner to form a nominal 1 M Na_2S_4 + 0.1 M NaOH solution.

3.2.2 Preparation of CoS Catalyst

316 stainless steel (SS) mesh substrate was pretreated by descaling in an acidic solution consisting of 1 mL HF + 3 mL HNO_3 + 46 mL deionized water. The SS mesh was rinsed with ethanol to remove any residual oils, air-dried, and then soaked in HF/HNO_3 solution for 10 minutes to remove the oxide scale. The SS mesh was then rinsed with deionized water and air-dried.

Electrodeposition of cobalt (Co) on SS mesh as Co@SS followed a modified procedure from Premlatha et al.[116] The Co electrodeposition bath was prepared by making a solution containing 100 g L^{-1} cobalt acetate and 40 g L^{-1} boric acid. The SS mesh was placed in the Co electrodeposition bath to submerge a geometric area of 0.25 cm^2. A constant current of –3 mA was applied for 5 minutes while the bath was maintained at 35 – 40 °C. Measurement was taken with a saturated calomel electrode as the reference electrode and platinum foil as the counter electrode. Electrodeposition of Co@brass was performed in the same manner, using a brass mesh rinsed with ethanol as the working electrode.

After electrodeposition, the Co@SS and Co@brass were pretreated to convert Co to CoS by the following method: Co@SS and Co@brass were assembled in air in a ZAPS battery as described below with 1 M Na_2S_4 pretreatment solution as the catholyte. Co@SS and Co@brass were then cycled by cyclic voltammetry for 250 cycles from 0.2 V – 1.2 V vs. Zn/Zn^{2+} at a scan rate of 5 mV s^{-1}. Cyclic voltammetry was performed with an Arbin BT 2000 battery cycler.

3.2.3 Materials Characterization

Morphology and elemental analysis of the CoS@SS and CoS@brass were characterized by SEM, TEM, and EDS as described in Chapter 2. Surface and bonding

characterization was obtained by XPS, and phase identification of materials was gathered by XRD as further described in Chapter 2.

3.2.4 Electrochemical Characterization

Electrochemical impedance spectroscopy (EIS) measurements were performed as described in Chapter 2. Cyclic voltammetry of the ZAPS battery was performed with an Autolab PGSTAT302N potentiostat (Eco Chemie B.V.) from 0.3 to 1.2 V versus Zn/Zn^{2+} for 1 cycle at a scan rate of 0.5 mV s^{-1}, and 10 cycles at a scan rate of 10 mV s^{-1}, in which the last cycle is shown.

3.2.5 Zinc-Aqueous Polysulfide (ZAPS) Battery Tests

The ZAPS batteries were assembled with an in-house designed cell modified from our previous publications for the hybrid Li-air battery.[80] A schematic of the cell assembly is shown in Appendix A. For these experiments, the cathode chamber was modified to make it near-hermetic to prevent continuous H_2S evolution during battery cycling by attaching the SSE directly to the acrylic cathode chamber housing with epoxy. Cathodes were assembled by filling the cathode chamber with the catholyte solution, inserting the CoS@SS electrode (or CoS@brass), inserting a polydimethylsiloxane (PDMS) plug, and sealing the chamber with ethylene vinyl-acetate (EVA) adhesive. The assembly was performed in an N_2-purged glovebag. The cell anode was a piece of Zn sheet with a Ti wire current lead.

Final assembly of the cells consisted of the Zn anode, an alkaline anolyte, a solid-state electrolyte (SSE), catholyte solution, and CoS@SS or CoS@brass catalyst electrode. Cells with a Na^+ mediator ion (Na-ZAPS) used 0.5 M NaOH anolyte, NASICON SSE, and 0.1 M Na_2S_4 + 0.1 M NaOH catholyte. Cells with a Li^+ mediator ion (Li-ZAPS) used 0.5

M LiOH anolyte, LATP SSE, and 0.1 M Li_2S_4 + 0.1 M LiOH catholyte. The ZAPS batteries assembled for galvanostatic cycling contained 20 μL of catholyte, while the ZAPS batteries assembled for pretreatment or cyclic voltammetry were assembled with 45 μL of catholyte.

Charge-discharge curves were performed at 0.5 mA cm^{-2} current density unless otherwise specified. Rate testing of the Na-ZAPS and Li-ZAPS batteries occurred by discharging each battery for 15 min and resting for 1 h before beginning testing. Batteries were cycled as described in Chapter 2, where a cycle consisted of discharging for 30 min followed by charging for 30 min.

3.3 Results & Discussion

Figure 3.1 presents a schematic of the ZAPS battery on discharge. On discharge, Zn is oxidized to form the zincate ion by the following reaction:

$$Zn + 4OH^- \rightarrow [Zn(OH)_4]^{2-} + 2e^- \qquad 1.22 \text{ V } \textit{vs.} \text{ SHE} \qquad (3.1)$$

At the cathode, dissolved S_4^{2-} (predominant) is reduced to S^{2-} by the following simplified reaction for extremely high concentrations of polysulfide,

$$S_4^{2-} + 6e^- \rightarrow 4S^{2-} \qquad \sim -0.50 \text{ V vs SHE} \qquad (3.2)$$

and by the following simplified reaction for moderate to low concentrations of polysulfide:[24]

$$S_4^{2-} + 6e^- + 4H_2O \rightarrow 4HS^- + 4OH^- \qquad \sim -0.50 \text{ V vs SHE} \qquad (3.3)$$

Charge balance is maintained by Li^+ or Na^+ mediator ions shuttling from the anolyte, through the mediator-ion SSE to the catholyte. On charge, the reverse reactions occur. The proof-of-concept battery demonstrated in this work uses moderate concentrations of polysulfide, so the balanced reaction of this cell can be described as:

$$3Zn + 8OH^- + S_4^{2-}\,4H_2O \rightarrow 3[Zn(OH)_4]^{2-} + 4HS^- \qquad (3.4)$$

Participation of the hydroxide at the anode reduces the overall capacity of the battery from the theoretical 550 mA h g^{-1} for a ZnS reaction product to a still high capacity of 349 mA h g^{-1}.

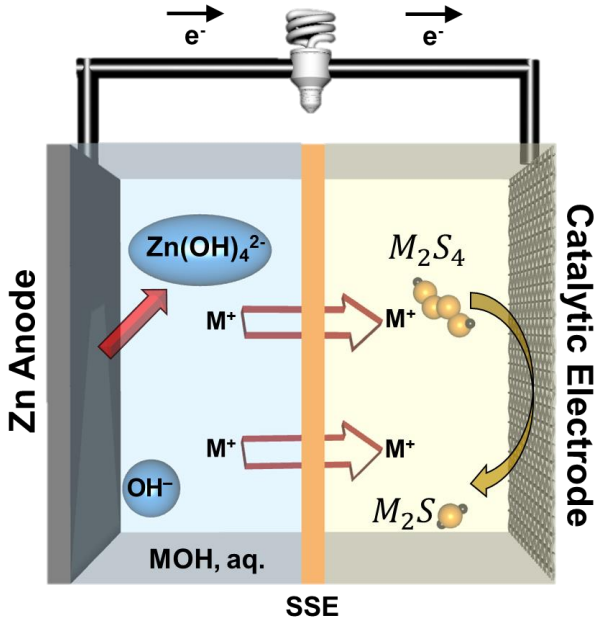

Figure 3.1 Illustration of the zinc-aqueous polysulfide battery, in which alkali metal M is either Na or Li. SSE is an alkali-metal-ion-conducting solid-state electrolyte.

It should be noted that sulfur, when dissolved in aqueous media in the presence of sulfides, forms a multitude of species including HS^-, H_2S, S^{2-} and polysulfide species S_x^{2-} (x = 2 – 5), as described in Section 1.2.2 of the introduction. This was confirmed by UV-Visible spectroscopy, as shown in Figure 3.2.[18] In our system, the catholyte is at a high pH of ~13 due to added sodium or lithium hydroxide, which shifts the specie distribution so that S_4^{2-} dominates at equilibrium. For this reason, in this report we describe our catholyte as containing Na_2S_4 or Li_2S_4 as a nominal description. Based on the high concentration of S_4^{2-} in our system, the theoretical voltage is expected to be about 0.74 V. Despite this low

voltage, due to the high capacity of the zinc and polysulfide active materials the ZAPS battery has a theoretical energy density of 251 W h kg^{-1} of total active material.

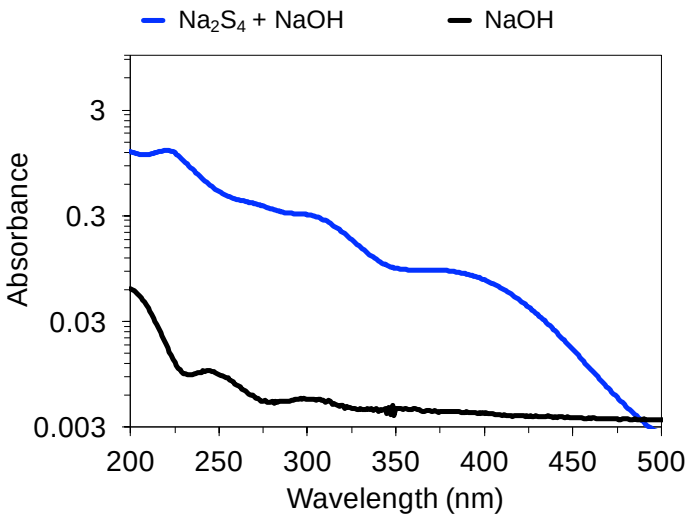

Species	Absorption peak (nm)
S_2^{2-}	354
S_3^{2-}	302
S_4^{2-}	372
S_5^{2-}	296
HS^-	221

Figure 3.2 UV-Vis spectra of the as-prepared polysulfide catholyte and a table detailing polysulfide species and their corresponding peak. The information in the Table was obtained from Ref. 18.

A CoS electrocatalyst was prepared for use in the ZAPS battery as it is a well-known catalyst for polysulfide reduction.[32-33] CoS was prepared by first electrodepositing cobalt on a stainless steel mesh substrate as Co@SS followed by pretreating the Co@SS in 1 M Na_2S_4 solution to form CoS@SS, as further detailed in Section 3.2.2. Figure 3.3 shows the scanning electron microscopy (SEM) images, transmission electron microscopy (TEM) images with selected area electron diffraction (SAED) patterns, and energy dispersive spectroscopy (EDS) composition maps of the catalyst.

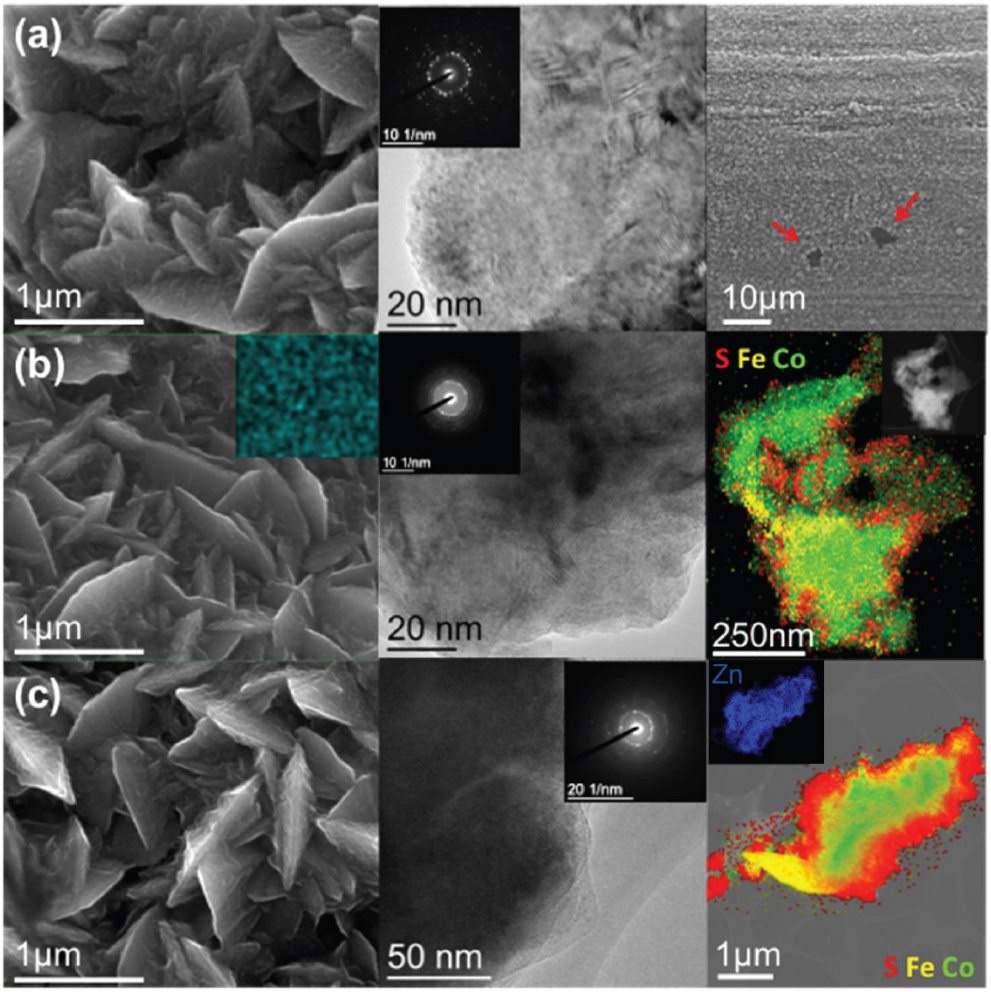

Figure 3.3 SEM images, TEM image (inset: SAED pattern), and EDS mapping of (a) Co@SS surface after deposition on SS mesh substrate, with the arrows highlighting regions of bare substrate, (b) CoS@SS surface after pretreatment in 1M Na_2S_4 (inset: EDS map of sulfur) and (c) CoS@SS surface after cycling in a ZAPS battery for 50 cycles

The Co deposited as a hierarchical nanoflake structure, fully covering the steel surface except for small patches, as shown in Figure 3.3a. The patches of bare steel are likely due to incomplete stripping of the native oxide scale before deposition.

The Co deposit is highly polycrystalline. Figure 3.3b shows that pretreatment of the Co to form CoS resulted in a uniform sulfur distribution and an unchanged surface

morphology. TEM and EDS show the CoS layer to be 40-80 nm thick, and it retains the highly polycrystalline nature of the Co deposit. X-ray photoelectron spectroscopy (XPS) shows Co 2p and S 2p peaks characteristic of mixed-phase cobalt sulfide, as shown in Figure 3.4 a – b.[117]

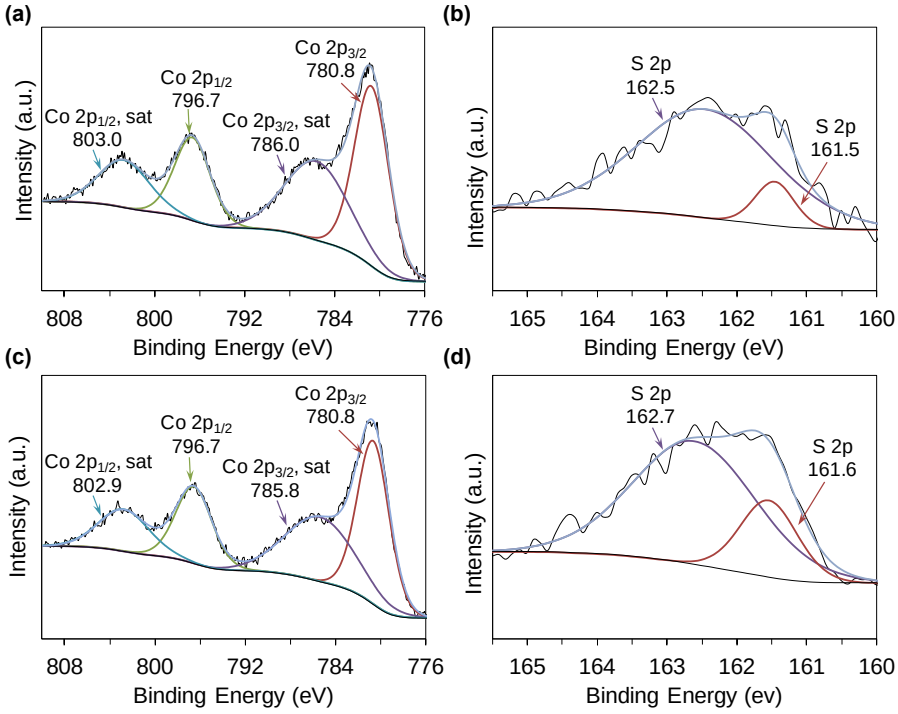

Figure 3.4 XPS spectra for CoS electrocatalyst showing the (a) Co 2p and (b) S 2p regions before cycling and the (c) Co 2p and d) S 2p regions after cycling for 50 cycles.

This is further corroborated by SAED in which peaks of multiple Co-S phases can be matched. Surface morphology and XPS spectra remained relatively unchanged after cycling in a ZAPS battery for 50 cycles, as shown in Figures 3.3c and 3.4 c – d. TEM shows that after cycling, the surface of the CoS has become more amorphous and the thickness of the sulfide layer has increased. The SAED pattern is unchanged after cycling, indicating that crystalline Co-S phases persist after cycling. Furthermore, EDS shows some

Zn signal on the catalyst surface after cycling, which may be indicative of a minor leak between the anode and cathode chambers of the battery.

Traditionally, brass has been used as a substrate for CoS.[7, 14, 24, 31] This is likely due to its reasonable stability and the ease of depositing Co onto the brass substrate. However, as has been noted by Hodes and Manassen, the brass is not fully stable and sheds Cu_2S particles very slowly over time when submerged in polysulfide solutions.[31] In our work we tested both brass and steel as substrates for the CoS catalyst. ZAPS batteries with CoS@SS and CoS@brass electrodes were assembled as described in Section 3.2.5 and the surface morphology was analyzed after 50 cycles, as shown in Figure 3.5. CoS@brass showed cracking and pitting of the CoS film surface after cycling, indicating inadequate stability. Comparison of the cycling performance shows that the ZAPS battery assembled with CoS@brass electrode had a lower initial discharge capacity compared to the ZAPS battery built with CoS@SS, and showed a greater loss of capacity during cycling. For this reason, further testing of ZAPS batteries used CoS@SS.

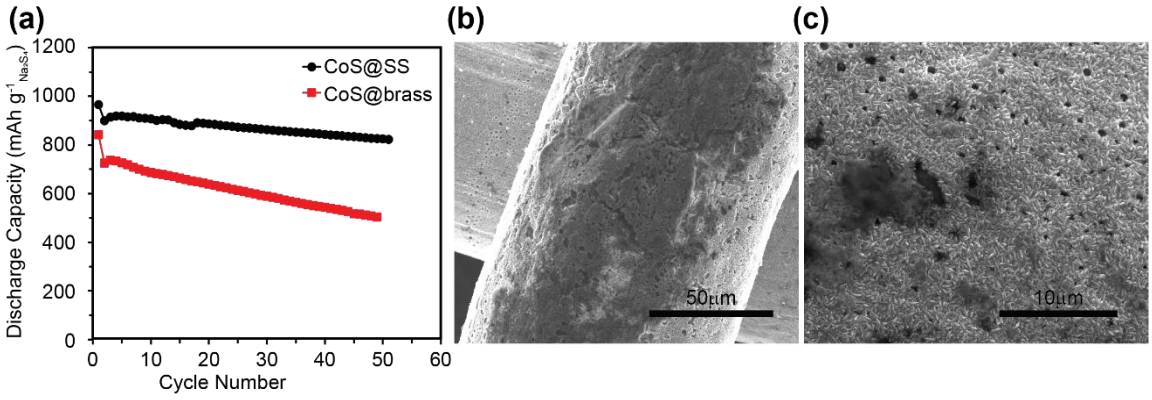

Figure 3.5 (a) Cycling discharge capacity of the ZAPS batteries with the CoS@SS and CoS@brass catalytic electrodes. SEM images of CoS@brass after cycling in a ZAPS battery for 50 cycles showing (b) cracking of the CoS film and (c) pitting of the CoS@brass surface.

The ZAPS batteries were assembled with a metallic Zn anode, 0.5 M NaOH anolyte, $Na_3Zr_2Si_2PO_{12}$ (NASICON) SSE, 0.1 M Na_2S_4 + 0.1 M NaOH catholyte, and CoS@SS catalytically active electrode. Open-circuit voltage (OCV) of the battery was 0.89 V. Numerical calculation using the methods and equilibrium constants reported by Lessner et al.[26] was used to determine the polysulfide species concentrations per equations 1.1 – 1.3 and using equation 1.7, the theoretical OCV was calculated to be 0.91 V. This value is within the expected error based on the concentration of the catholyte. Batteries were assembled with an excess of Zn and anolyte, so performance was analyzed based on the limiting polysulfide catholyte. Voltage limits of the battery during cycling were determined by first discharging the battery at 0.5 mA cm^{-2} current density to completion. The onset voltage of the hydrogen evolution reaction (HER) was determined to be 0.19 V, as shown in Figure 3.6a. To achieve a deep discharge of the battery a discharge voltage of 0.3 V was chosen. A separate battery was discharged at 0.5 mA cm^{-2} current density to 0.3 V, then charged to completion. Figure 3.6b shows two plateaus, one for the conversion of S^{2-} to S_4^{2-}, and other for the conversion from S_4^{2-} to nonvalent sulfur (S^0). These plateaus correspond to the redox peaks demonstrated by cyclic voltammetry (CV) in Figure 3.6c. An upper voltage limit of 0.9 V was chosen to ensure that no solid sulfur precipitation occurred during cycling.

Electrochemical stability of the ZAPS battery was studied by cycling the battery for 50 cycles. Figure 3.6e shows the voltage profile of the cycling ZAPS battery. The first discharge shows a relatively flat plateau, while all subsequent charge and discharge cycles display a sloped voltage profile. All reported capacities and energy densities in this chapter are per gram of Na_2S_4 unless otherwise specified. The initial discharge capacity is 966 mA h g^{-1}, which is above the theoretical capacity of Na_2S_4 (924 mA h g^{-1}). This higher-than-theoretical capacity achieved may be due to a thin film of deposited sulfur on the CoS@SS

electrode after pretreatment not visible by SEM, or due to some electrochemical participation of the catalyst. CV of the ZAPS battery with and without polysulfide shows that even without polysulfide, the CoS demonstrates a minor amount of electrochemical activity which may be attributed to the known pseudocapacitance of CoS (Figure 3.6d).[118] The electrochemical performance reveals that the ZAPS battery maintains a highly reversible discharge capacity of 822 mA h g^{-1} after 50 cycles (Figure 3.6f). The coulombic efficiency of the battery was ~100% throughout cycling. Despite the low discharge voltage of ~ 0.64V, the ZAPS battery displayed a maximum energy density of 586 W h kg^{-1}, and retained an energy density of 529 W h kg^{-1} after 50 cycles. The energy density can be improved with improved catalysts to lower the discharge overpotential. No change is observed in overpotential during cycling, or in the SSE phase as measured by x-ray diffraction, implying good stability of the SSE in alkaline and polysulfide media, as seen in Figure 3.7.

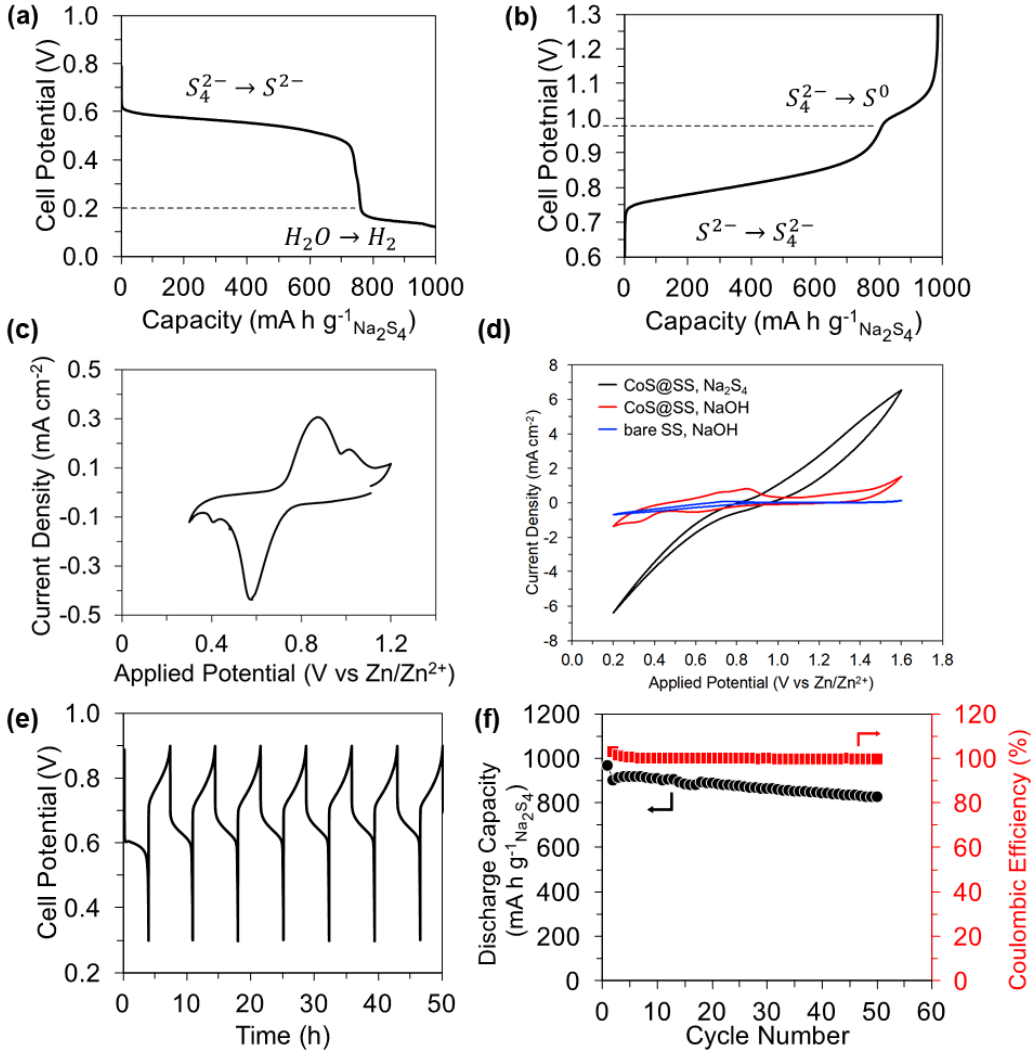

Figure 3.6 (a) Discharge voltage profile to the HER regime and (b) charge voltage profile to precipitate nonvalent sulfur. (c) CV of ZAPS battery at 0.5 mV s^{-1} scan rate, assembled with 0.01 M Na_2S_4 catholyte and CoS@SS electrode. (d) CV of ZAPS battery at 10 mV s^{-1} scan rate assembled with 0.1 M Na_2S_4 + 0.1 M NaOH catholyte and CoS@SS electrode, CoS@SS electrode, and bare SS electrode. (e) Discharge-charge curves of ZAPS battery. (f) Cycling performance of the ZAPS battery, presenting discharge capacity and coulombic efficiency.

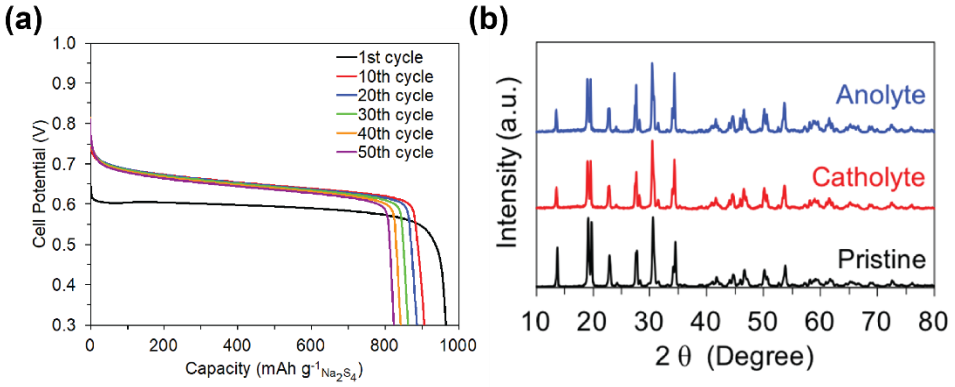

Figure 3.7 (a) Discharge capacity of ZAPS battery during subsequent cycles and (b) XRD patterns of NASICON before cycling (pristine) and after cycling. XRD was performed on the SSE surface facing the ZAPS battery anolyte and on the SSE surface facing the catholyte after cycling. XRD performed on SSE with 800+ total hours and 100+ cycles in multiple batteries.

Figure 3.8 presents the rate and power performances of the ZAPS batteries built with Na^+ and Li^+ mediator ions. The ZAPS batteries with the Na^+ mediator ion (Na-ZAPS) were built as previously described. ZAPS batteries with the Li^+ mediator ion (Li-ZAPS) were assembled with a metallic Zn anode, 0.5 M LiOH anolyte, $Li_{1+x+y}Al_xTi_{2-x}P_{3-y}Si_yO_{12}$ (LATP) SSE, 0.1 M Li_2S_4 + 0.1 M LiOH catholyte, and CoS@SS catalytically active electrode. Each battery was cycled at increasing current densities from 0.1 mA cm^{-2} to 2.5 mA cm^{-2} with a lower voltage limit of 0.2 V imposed to prevent ingression into the HER regime. The Na-ZAPS battery consistently performed better than the Li-ZAPS battery, as shown in Figure 3.8a. The Na-ZAPS battery had a lower overpotential at every current density including the lowest rate of 0.1 mA cm^{-2}. The Li-ZAPS battery showed a degrading charge profile at a current density of 1.5 mA cm^{-2}, and cycling was stopped at 1.75 mA cm^{-2} due to the Li-ZAPS battery reaching the 0.2 V lower voltage limit. The Na-ZAPS battery, on the other hand, was able to cycle to 2.5 mA cm^{-2} without degradation to its voltage profile. The Li-ZAPS battery reached a peak power density of 0.35 mW cm^{-2} as shown in

Figure 3.8b, while the Na-ZAPS battery reached a peak power density of 1.05 mW cm^{-2}, three times that of the Li-ZAPS battery.

To probe the differences between the Na-ZAPS and Li-ZAPS batteries rate and power performances, electrochemical impedance spectroscopy (EIS) was performed on uncycled cells. The EIS spectra show that the Na-ZAPS battery has a lower relative bulk impedance and charge-transfer impedance than the Li-ZAPS battery (Figure 3.8c). The improved performance of the Na-ZAPS over the Li-ZAPS battery may be partly attributed to the higher conductivity of the NASICON membrane (σ = ~1.0 x 10^{-3} S cm^{-1}) compared to that of the LATP membrane (σ = ~1.0 x 10^{-4} S cm^{-1}). To separate the effects of the SSE's conductivities, EIS measurements were taken of the catholyte alone. EIS confirms that the impedance of the Na_2S_4 catholyte is lower than the Li_2S_4 catholyte, with or without the use of a CoS catalyst, as shown in Figure 3.8d and 3.8e. This implies better reaction kinetics for the Na-based catholyte.

At the system level, Na_2S_4 catholyte has a higher capacity than Li_2S_4 due to the higher solubility of Na_2S_4. The solubility limit of Na_2S_4 is estimated to be ~ 2.6 M compared to ~ 2.3 M for Li_2S_4. Li_2S_4 catholyte has a theoretical specific capacity of 1,132 mA h g^{-1} based on the mass of the active material. Na_2S_4 catholyte has a lower specific capacity of 924 mA h g^{-1} due to the added weight from using the Na^+ ion. When the capacity is calculated based on the total weight of the catholyte rather than solely based on the active material, a 2.6 M saturated Na_2S_4 catholyte has a theoretical specific capacity of 288 mA h g^{-1}, or a volumetric capacity of 418 mA h L^{-1}. In comparison, a 2.3 M saturated Li_2S_4 catholyte has a theoretical specific capacity of 279 mA h g^{-1}, or a volumetric capacity of 370 mA h L^{-1}. Thus, despite the lightness of Li_2S_4 compared to Na_2S_4, at a system level, Na_2S_4 catholyte has a higher capacity. Due to the better performance of the Na-ZAPS battery and the higher capacity of Na_2S_4 as discussed above, work in the following chapters

will focus on the development of sodium-based aqueous polysulfide battery systems, with occasional testing of lithium-based systems as appropriate.

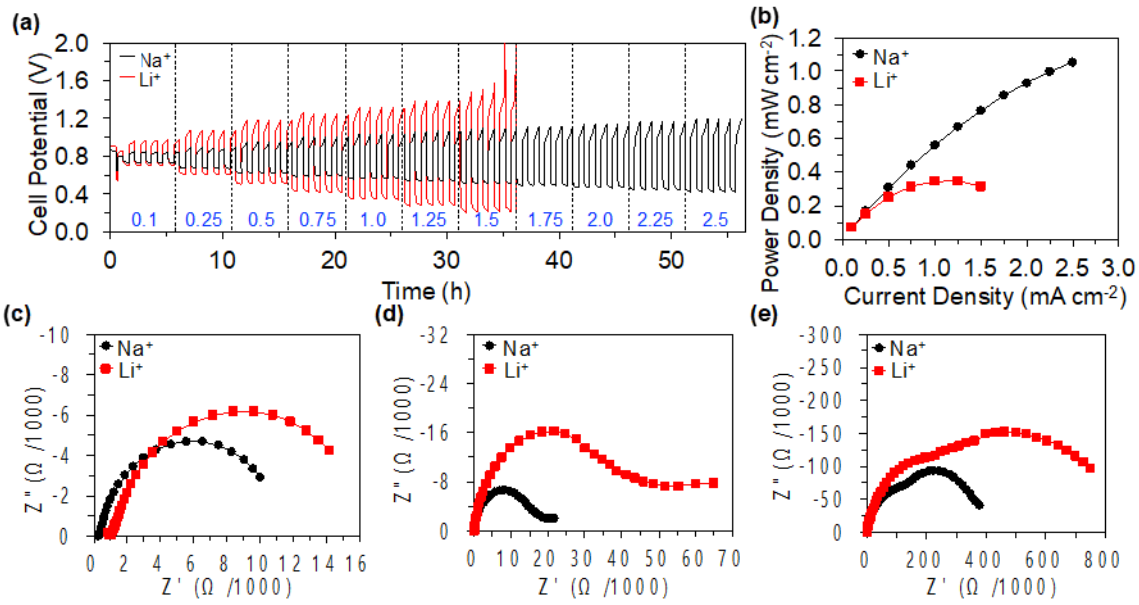

Figure 3.8 Comparison of the Na-ZAPS and Li-ZAPS batteries performances, presenting (a) voltage profiles of the cells at different current densities ranging from 0.1 mA cm^{-2} to 2.5 mA cm^{-2} with the numbers in blue indicating current density in mA cm^{-2}, and (b) polarization curves obtained from an average discharge voltage over 5 cycles. Nyquist plots from the EIS data of (c) uncycled Na-ZAPS and Li-ZAPS batteries, (d) Na_2S_4 and Li_2S_4 catholyte with CoS@SS electrode, and (e) Na_2S_4 and Li_2S_4 catholyte with planar stainless steel electrodes.

3.4 CONCLUSIONS

We demonstrate, for the first time, a rechargeable zinc-aqueous polysulfide battery. This novel battery was achieved by the separation of the zinc anode from the reactive polysulfide catholyte by a mediator-ion solid-state electrolyte. Charge balance is maintained by the mediator alkali metal ions (Na^+ or Li^+) that shuttle through the solid-state electrolyte. This proof-of-concept battery exhibited good performance, maintaining 822 mA h g^{-1} of reversible capacity after 50 cycles with ~ 100% Coulombic efficiency. It

was shown that the ZAPS batteries with a Na^+ mediator ion produced superior rate and power performance over those with a Li^+ mediator ion. Optimization of parameters such as solid-state electrolyte conductivity and catalyst performance could improve battery impedance, which could in turn improve the power density of the cell. Increased concentration of polysulfide in the catholyte could greatly improve the energy density of the system. Overall, the rechargeable ZAPS battery shows promise as a technology that utilizes high energy-density and low-cost electrode materials.

Chapter 4: Aqueous Polysulfide-Air Batteries with a Mediator-ion Solid Electrolyte and a Copper Sulfide Catalyst for Polysulfide Redox*

4.1 INTRODUCTION

Flow batteries are promising systems for grid-scale energy storage in terms of cost, lifetime, and safety but current flow batteries have not reached their theoretical potential.[119] Almost all flow batteries suffer from lower lifetimes than required, due to the use of an ion exchange membrane that fails to prevent active species crossover during cycling.[119-123] The most researched of the different flow batteries, all-vanadium systems, still relies upon expensive materials such as vanadium and Nafion membranes and suffer from chemical crossover.[71, 124] This undercuts the value of developing such systems. As such, different anolytes and catholytes are being explored that use low cost and abundant materials. The development of a "mediator-ion" strategy in which a solid-state Li^+ or Na^+ electrolyte is used as a separator and the corresponding cation is used as an ionic mediator of charge transfer has enabled the exploration of novel liquid battery materials by eliminating chemical crossover.[74, 104-105] Batteries that use redox-active aqueous polysulfide have drawn interest in this regard.

Aqueous polysulfide has historically attracted much attention due to the low cost and environmental benignity of sulfur and the large energy density achievable by saturated polysulfide solutions.[6-7, 24, 71, 92] It fell out of favor when attempts to scale up the most promising system, polysulfide-bromine flow batteries, suffered too much degradation from active-species cross-over through the polymer membrane.[9-11] Recently, aqueous polysulfide has experienced a resurgence in research, having been explored in novel

*M. M. Gross and A. Manthiram "An Aqueous Polysulfide-Air Battery with a Mediator-ion Solid Electrolyte and a Copper Sulfide Catalyst for Polysulfide Redox," *ACS Appl. Energy Mater.*, 2018, **1**, 7230-7236.
M. M. Gross carried out the experimental work. A. Manthiram supervised the project. All participated in the preparation of the manuscript.

configurations that make use of a solid-state electrolyte instead of the polymer membrane to prevent crossover of the polysulfide and other active materials. These include hybrid lithium metal-aqueous lithium polysulfide, lithium polysulfide-air, and zinc-sodium polysulfide batteries.[14, 125-126]

Of these systems, polysulfide-air batteries show great promise due to their high theoretical potential of 1.68 V and use of a benign and theoretically low-cost air cathode. Catalysts, however, are necessary for both the polysulfide anolyte and the air catholyte. Extensive research has been performed on the catalysts for the air catholyte, but less attention has been paid in recent times to catalysts for the polysulfide anolyte. Early research found transition-metal sulfides to have superior catalytic activity towards aqueous polysulfide redox compared to carbon and Pt. Catalyst research has subsequently focused on cobalt, nickel, iron, and molybdenum sulfides.[31-33] Cobalt sulfide shows the highest activity of these catalysts, but it is an expensive and toxic material that is in great demand for both high-performance lithium-ion batteries and other markets.[127-129] Less expensive catalysts, such as nickel and iron sulfide, come at the cost of lower catalytic activity.[32, 43]

Another catalytically active sulfide, copper sulfide, has not been widely explored. Early testing of copper sulfide showed Cu_2S chalcocite phase had high catalytic activity towards polysulfide redox, but it was unstable and quickly broke apart upon prolonged exposure to polysulfide. The addition of zinc to form a brass alloy only slowed the corrosion.[31] However, copper sulfide forms a large number of distinct phases, ranging from the copper rich (Cu_2S, chalcocite) to the sulfur rich (CuS, covellite). These different phases have been tested in quantum dot sensitized solar cells (QDSSCs) as a catalytic counter electrode in which aqueous polysulfide is used as the electrolyte, and it has been found that decreasing the copper content of Cu_xS increased its stability and performance in QDSSCs, with covellite CuS being the best performing phase.[38-39, 130-131] This work indicates that

covellite CuS may be a high activity, stable polysulfide catalyst, but QDSSC operating conditions differ greatly from those of a battery. Direct study is necessary to determine if covellite CuS is stable under cycling conditions in a polysulfide battery, and to date, there has been no such study.

This work presents, for the first time to the best of our knowledge, a study of the long-term cycling performance of sodium polysulfide-air batteries with a covellite CuS polysulfide redox catalyst. Long-term cycling was achieved by means of a decoupled air cathode with standard catalysts in which the charge and discharge electrodes are run on independent channels, and the use of a Na^+ mediator-ion solid-state electrolyte which prevents crossover of the active chemical species. The redox activity of CuS was explored in the intermediate voltage window in a sodium polysulfide-air battery, at pH relevant to that of the polysulfide anolyte. The effect of the copper sulfide redox activity on the catalyst's long-term performance was studied by pre-discharging CuS in LiOH and NaOH electrolyte, before cycling the pre-discharged electrodes in a sodium polysulfide-air battery.

4.2 Experimental Details

4.2.1 Synthesis of CuS

Covellite phase CuS was synthesized by a method previously reported by Yao et al.,[132] in which 30 mL of deionized water containing 2.4 mmol of thioacetamide was added to 40 mL of deionized water containing 2.4 mmol anhydrous cupric chloride ($CuCl_2$). The mixture was allowed to sit without stirring at room temperature for a few minutes until a yellow suspension formed. Then, the mixture was covered and moved to a 60 °C oil bath for 24 h while stirring to form a black precipitate. The mixture was then allowed to cool naturally to room temperature before the precipitate was removed by centrifugation. The

precipitate was cleaned by suspending and centrifuging first in deionized water, then in a water-ethanol mixture (~50 % v/v), and finally in pure ethanol. The precipitate was dried overnight in air at room temperature.

4.2.2 Assembly of Catalyst Electrodes

CuS polysulfide catalyst electrodes were made by suspending 50 mg of CuS in water with 20 % w/w lithiated Nafion binder (LithION, Ion Power Inc.) to make an ink. This ink was then deposited on a Teflon-coated carbon paper substrate (gas diffusion layer, Sigracet 10 BA) to achieve a loading of 1.75 mg cm^{-2}. IrO_2@Ti oxygen evolution reaction (OER) catalyst electrodes were synthesized by anodic electrodeposition of IrO_2 films on Ti mesh, as previously reported by our group.[74] Pt/C@GDL oxygen reduction reaction (ORR) catalyst electrodes were made by mixing commercial Pt/C (40 % w/w Pt) with 20 % w/w LithION binder and depositing on a gas diffusion layer (Sigracet 10 BA) to give a loading of 0.85 mg cm^{-2} of Pt/C. Li-CuS and Na-CuS electrodes were made by discharging pre-fabricated CuS electrodes in, respectively, 0.5 M LiOH or 0.5 M NaOH to 0.95 V versus a zinc anode with an Arbin 2000 battery cycler. CuS electrodes and zinc anodes were separated by a Li-ion or Na-ion solid-state electrolyte to prevent interaction between the zinc anode discharge products and the CuS working electrode.

4.2.3 Synthesis of 1M Na_2S_2 Anolyte

The catholyte was prepared as described in Chapter 2 by mixing NaOH, Na_2S, and S in a 1 : 10 : 10 molar ratio to form a solution of nominally 0.1 M NaOH + 1 M Na_2S_2.

4.2.4 Assembly of Sodium Polysulfide-Air Batteries

Batteries were assembled with parts designed in-house, with a modified anolyte housing as previously described in Chapter 3, and layered decoupled cathode housing as

we have reported for hybrid Li-air batteries.[133] A schematic of the cell assembly is shown in Appendix A. Anodes were assembled with a stainless-steel mesh current collector, CuS, Li-CuS, or Na-CuS electrode, 75 µL of 1 M Na_2S_2 + 0.1 M NaOH anolyte, and sodium-ion solid-state electrolyte (Na-SSE, $Na_3Zr_2Si_2PO_{12}$). Cathodes were assembled with decoupled IrO_2@Ti OER and Pt/C@GDL ORR electrodes before attaching to the anode housing. 0.1 M H_3PO_4 + 1 M NaH_2PO_4 acidic buffer electrolyte was used as a catholyte. A schematic of the sodium polysulfide-air battery is shown in Figure 4.1.

4.2.5 Materials Characterization

High resolution images of CuS morphology and low resolution images of Na-SSE morphology were obtained by SEM and TEM as described in Chapter 2. Phase identification and structural information of the CuS, Li-CuS, and Na-CuS were performed by XRD, WAXS, and Raman as further detailed in Chapter 2.

4.2.6 Electrochemical Characterization

Cyclic voltammetry was performed with a three-electrode setup with a CH Instruments 1040A potentiostat. The reference electrode used was Hg/HgO in 1 M NaOH or LiOH and the counter electrode was platinum foil. For testing of CuS in blank alkaline electrolytes, the working electrode was CuS on the carbon substrate with a titanium wire current collector. For testing catalytic activity in 1 M Na_2S_2 + 0.1 M NaOH anolyte, working electrodes were CuS on a carbon substrate, Sigracet 39 BC, or activated carbon felt (A1600, CeraMaterials) with a stainless-steel mesh current collector. Galvanostatic cycling tests performed on sodium polysulfide-air batteries used two channels to decouple and independently cycle the OER and ORR electrodes. Cycling consisted of a 10 minute rest followed by a 2 h discharge and charge period, at a current density of 0.5 mA cm^{-2}.

Due to evaporation of the catholyte during the long test time, fresh catholyte was periodically added to the cathode chamber during cycling.

4.3 Results & Discussion

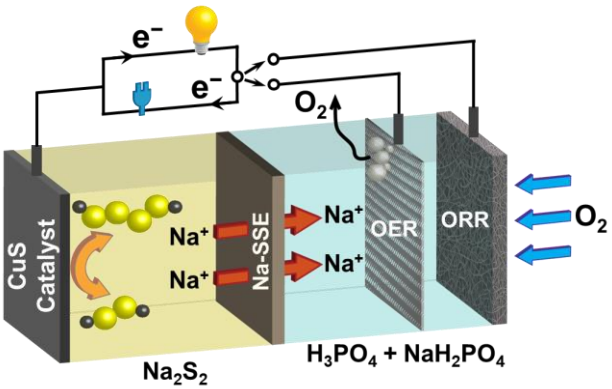

Figure 4.1 Schematic of a sodium polysulfide-air battery, with polysulfide anolyte, Na-ion conducting solid-state electrolyte (Na-SSE), acidic phosphate buffer catholyte, and decoupled OER and ORR electrodes.

CuS was synthesized by a facile, scalable process in which cupric chloride was stirred with thioacetamide in a warm bath overnight. Synthesis resulted in CuS nanoflake agglomerations, in which the nanoflake components are approximately 10 nm in thickness, as shown by scanning electron microscopy (SEM) in Figure 4.2 a – b. X-ray diffraction (XRD) of the particles confirmed covellite phase CuS was formed, with no impurities present, as shown in Figure 4.2c.

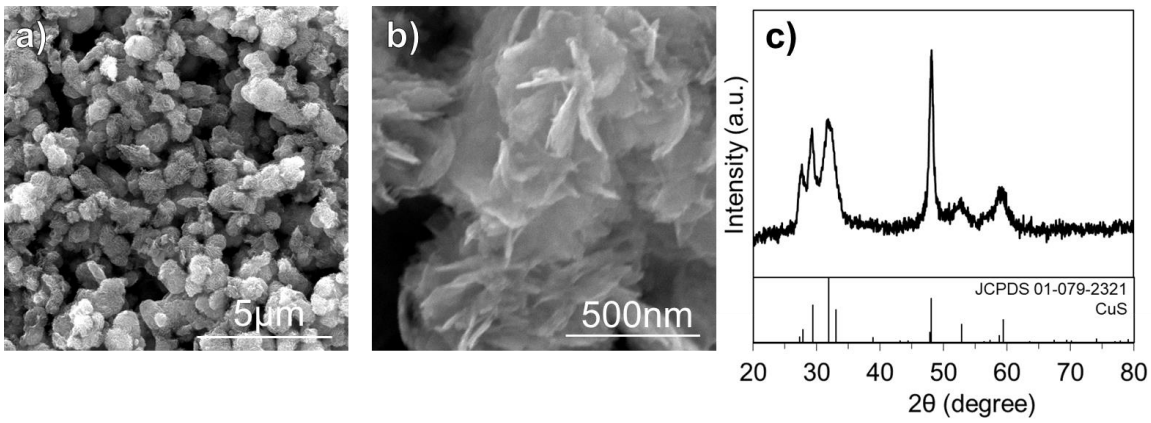

Figure 4.2 (a – b) SEM and (c) XRD of as-synthesized CuS.

CuS is a highly redox-active material that has been used in electrochemical energy storage devices ranging from lithium-ion and sodium-ion battery anodes to supercapacitors. Its behavior depends strongly on the voltages encountered and the electrolytes used. Research on the redox activity of CuS has focused on low-voltage nonaqueous systems, such as intercalation anodes,[134-137] and high-voltage, strongly alkaline systems such as supercapacitors.[138-139] However, there is limited work on the intermediate voltages and pH encountered in an aqueous polysulfide-air battery.

Cyclic voltammetry (CV) was performed in order to determine if CuS displayed redox activity at voltages and electrolyte composition relevant to our system in "blank" alkaline electrolytes, without polysulfide. The behavior of CuS was analyzed in both 0.1 M LiOH and 0.1 M NaOH, as shown in Figure 4.3. Multiple reduction and oxidation peaks are present, indicating many redox reactions. In a single cycle, shown in Figure 4.3a, CuS in LiOH and NaOH behave similarly, with CuS exhibiting more capacitive behavior in NaOH. Peak voltages are shifted slightly negative in LiOH compared to NaOH. After 5 cycles, however, the behavior of CuS in LiOH and NaOH diverges, as shown in Figure 4.3b. CuS in LiOH only exhibits one reduction peak after 5 cycles, while CuS in NaOH

exhibits three. Some of the redox reactions appear to be reversible, indicating possible side reactions may occur during cycling in an aqueous sodium polysulfide-air battery. The evolution of the CV curves over 5 cycles for both LiOH and NaOH are showed in Figure 4.3 c – d. It is clear from the CVs that CuS is highly redox-active within the voltage window of a polysulfide-air battery. Differences between cycling in LiOH and NaOH indicate that

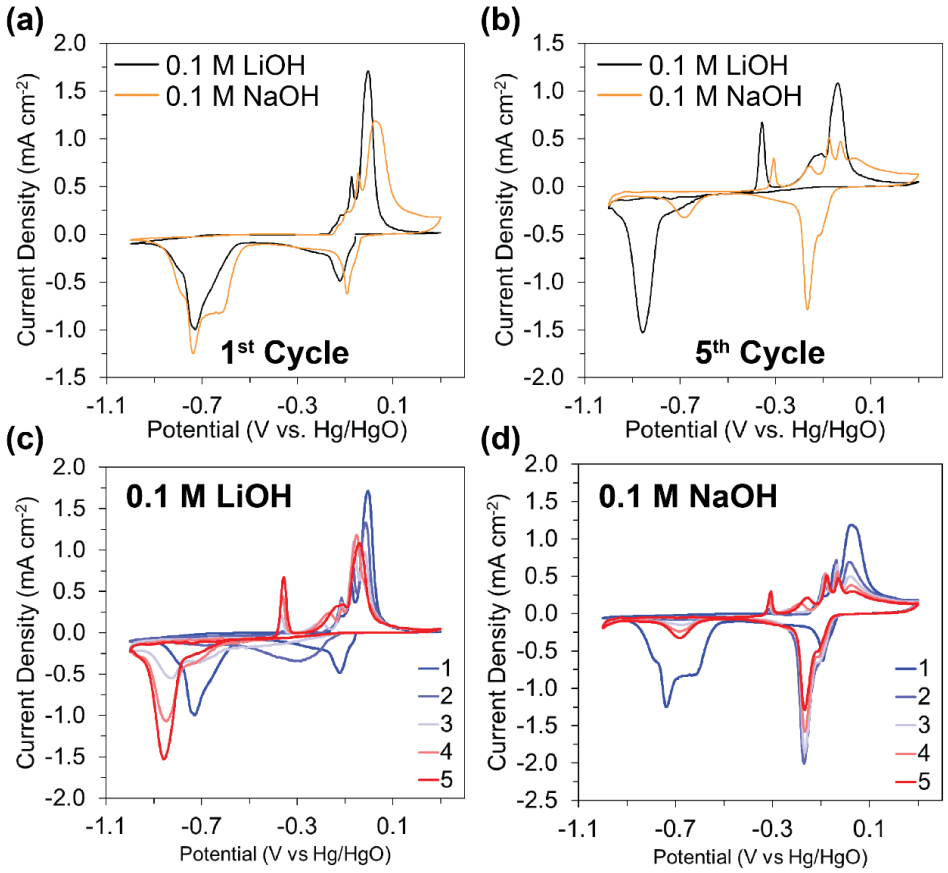

Figure 4.3 CV of CuS in 0.1 M NaOH and 0.1 M LiOH for (a) 1 cycle and (b) 5 cycles at a scan rate of 0.2 mV s^{-1}. CV of CuS in (c) 0.1 M LiOH and (d) 0.1 M NaOH for 5 cycles, with cycle number shown in the chart legend.

the cation present has an effect on its behavior as well. Previous study in aqueous systems have identified formation of CuSOH, CuO, and other Cu-hydroxide phases.[41-42] However,

as these studies have typically taken place at higher voltages in more concentrated alkaline electrolytes, it is unclear if these or similar redox reactions are occurring at the lower voltages studied in this work, and the exact nature of the redox processes is an area worthy of future deep study.

The catalytic activity of the CuS electrodes were verified compared to noncatalytic carbon electrodes in concentrated polysulfide media by cyclic voltammetry. The CuS exhibits superior performance to both 2D and 3D carbon electrodes, as shown in Figure 4.4. Sigracet 39 BC is a 2D non-catalytic electrode composed of a Teflon-coated gas diffusion layer covered with a microporous carbon layer. It was chosen as a carbon-based non-catalytic analogue of the CuS electrode. Activated carbon felt was chosen as a 3D non-catalytic electrode.

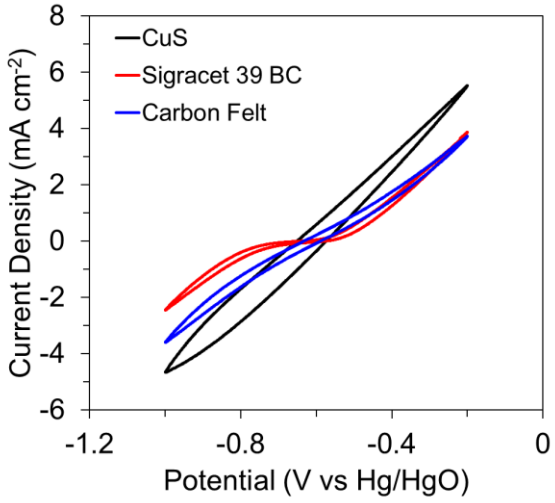

Figure 4.4 CV of CuS, Sigracet 39 BC, and activated carbon felt in 1 M Na_2S_2 + 0.1 M NaOH at 5 mV s^{-1} scan rate.

The long-term performance of sodium polysulfide-air batteries with CuS polysulfide catalyst was tested by cycling batteries for 100 cycles. To determine if the redox activity of CuS had any impact on the stability of the CuS when cycled in aqueous

polysulfide, CuS was pre-discharged in 0.1 M LiOH or 0.1 M NaOH. These samples will be defined as, respectively, Li-CuS and Na-CuS. A representative discharge curve is shown in Figure 4.5.

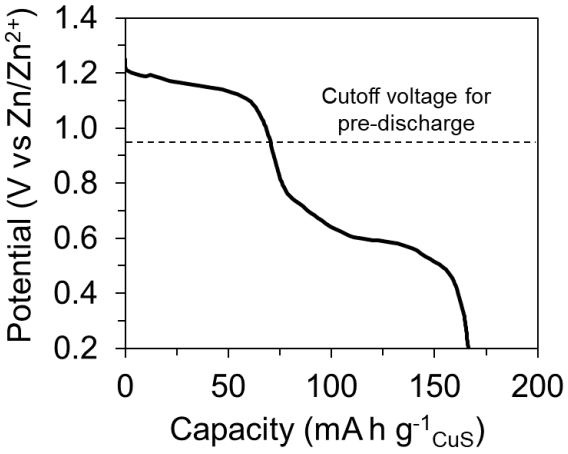

Figure 4.5 Discharge of CuS electrode in 0.5 M NaOH at 0.25 mA cm^{-2} current density.

Batteries were assembled in the charged state with a 1 M Na_2S_2 + 0.1 M NaOH anolyte and 0.1 M H_3PO_4 + 1 M NaH_2PO_4 catholyte, separated by a Na-ion solid-state electrolyte (Na-SSE) as shown in Figure 4.1. Na-SSE has the NASICON crystal structure with a conductivity of ~1.0 x 10^{-3} S cm^{-1}. Decoupled charge and discharge electrodes were used, with standard IrO_2 oxygen evolution reaction (OER) and Pt/C oxygen reduction reaction (ORR) catalysts. During cycling, the battery will undergo the following cell reactions to give a theoretical cell voltage of ~ 1.68V:

$$S_4^{2-} + 2e^- \leftrightarrow 2S_2^{2-} \quad (4.1)$$

$$H_2O \leftrightarrow O_2 + 4H^+ + 4e^- \quad (4.2)$$

Na^+ ions act as a mediator ion, shuttling between the anode and the cathode through the Na-SSE to balance charge. A decoupled charge and discharge setup was used in which the OER and ORR electrodes are cycled independently. This enables long cycle life of the cathode by preventing degradation of the ORR catalyst on charge.

Figure 4.6 shows an expanded view of a single cycle. In Region I, the battery is rested. In Region II, a discharge current is applied to the ORR electrode (solid black line) while the OER electrode (solid red line) is rested. In Region III, a charge current is applied to the OER electrode while the ORR electrode is rested. Overpotential is measured from the highest OER electrode potential measured in the cycle (dashed red line) to the lowest ORR electrode potential measured (dashed black line). Fluctuations observed in the voltage in the resting electrode during battery cycling (OER electrode during discharge, ORR electrode during charge) are due to the electrode experiencing a "semi-equilibrium state" as no current is being passed through the resting electrode but the battery itself is still cycling.

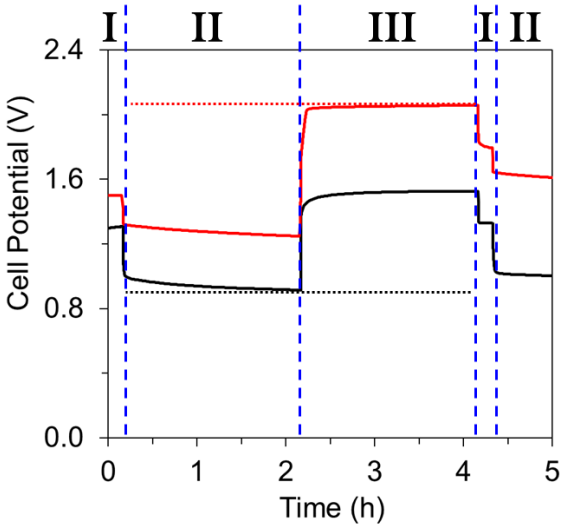

Figure 4.6 Single cycle voltage profile of a polysulfide-air battery with decoupled electrodes.

Cycling profiles of the sodium polysulfide-air batteries with CuS, Li-CuS, and Na-CuS are shown in Figure 4.7. The OER electrode voltage profile is labeled "charge branch" and the ORR electrode voltage profile is labeled "discharge branch." Batteries with CuS

catalyst exhibited a larger overpotential of 1.15 V on the first cycle, which decreases to 1.07 V on the second cycle and afterwards steadily increases back to 1.16 V after 100 cycles. Batteries assembled with Li-CuS exhibits a first cycle overpotential of 1.13 V, which increases to 1.21 V after 100 cycles. Batteries assembled with Na-CuS exhibits a first cycle overpotential of 1.26 V, which increases to 1.39 V after 100 cycles. Overall, the overpotential is the lowest with CuS and the highest with Na-CuS. Batteries assembled with Li-CuS show the greatest stability, exhibiting an increase in overpotential of only 0.08V. Batteries with CuS show an increase of 0.09 V, and those with Na-CuS show an increase of 0.13 V. Additionally, the Na-SSE demonstrated excellent stability with the polysulfide anolyte, displaying no phase or morphology change.

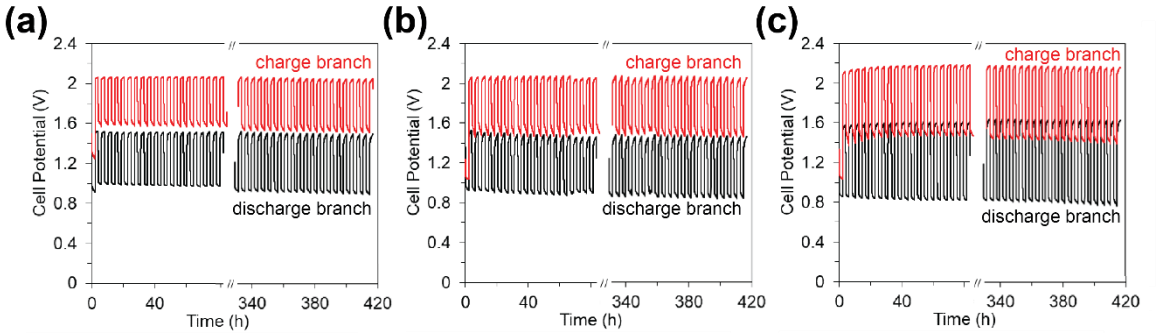

Figure 4.7 Cycling performance of sodium polysulfide-air batteries with (a) CuS, (b), Li-CuS, and (c) Na-CuS catalytic electrodes.

Analysis of the morphology and phase of the catalysts before and after cycling provides some insight into the battery cycling performances. Pre-discharge of CuS in LiOH and NaOH had no effect on the surface morphology of the catalyst before cycling, as shown in Figure 4.8 a – c. Comparison of the surface morphology of the CuS, Li-CuS, and Na-CuS before and after cycling shown in, respectively, Figure 4.8 a – c and Figure 4.8 d – f demonstrates the overall good stability of CuS with and without pre-discharging.

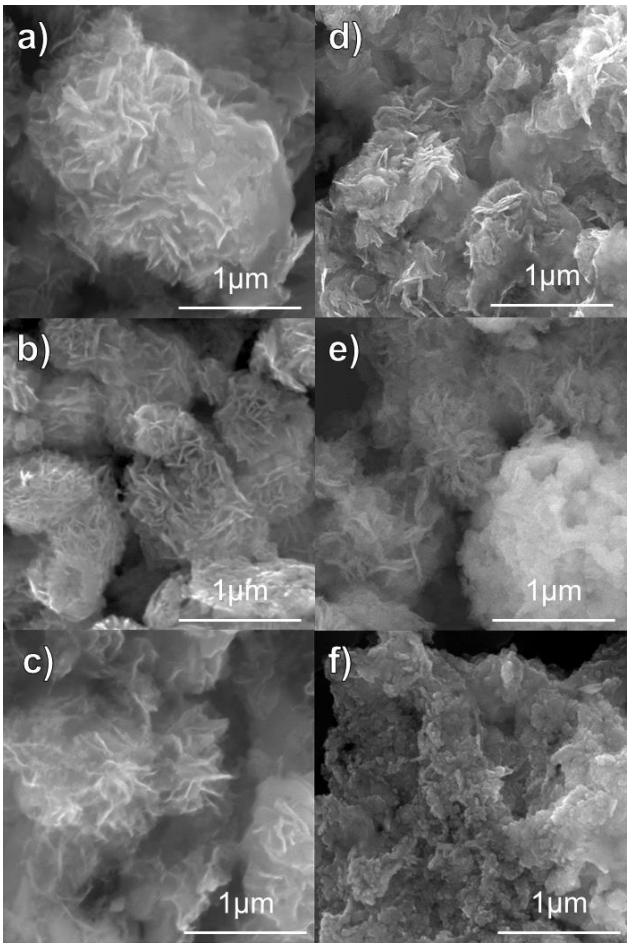

Figure 4.8 SEM of (a) CuS, (b), Li-CuS, (c), Na-CuS before cycling and (d) CuS, (e) Li-CuS, and (f) Na-CuS after cycling in a sodium polysulfide-air battery for 100 cycles.

CuS retains its nanoflake structure but experienced agglomeration of the particles after cycling. Li-CuS shows no morphology change, which may explain the superior performance of polysulfide-air batteries assembled with it. Na-CuS shows both agglomeration and loss of the surface nanoflake structure. This results in a lower exposed surface area, which helps explain the lesser performance of batteries assembled with it compared to those assembled with Li-CuS and CuS.

Transmission electron microscopy (TEM) was used to examine the bulk internal structure of the CuS. The nanoflake agglomeration structure is shown throughout the CuS, with no impact to the structure from pre-discharging as shown in Figure 4.9 a – c. Figure 4.9 d – f shows the internal structure of the catalysts after cycling. CuS, Li-CuS, and

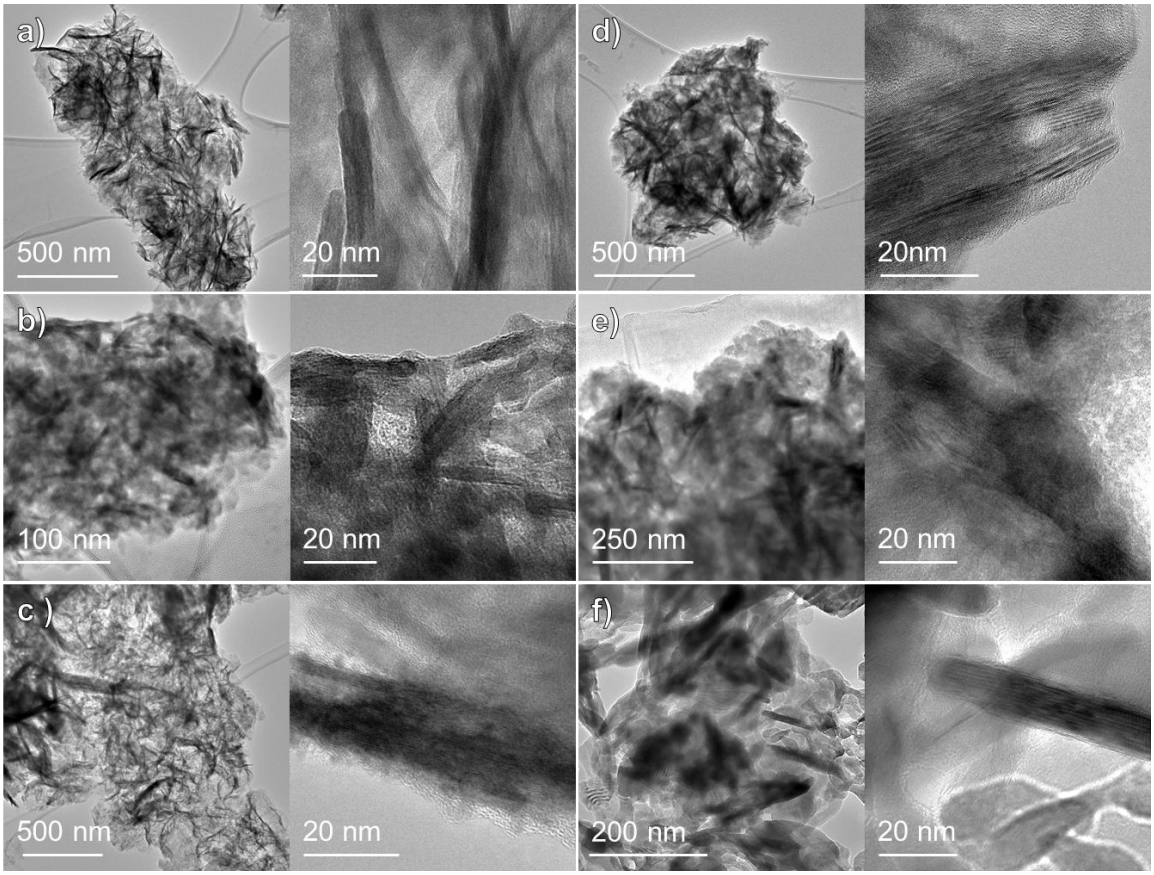

Figure 4.9 TEM of (a) CuS, (b) Li-CuS, and (c) Na-CuS before cycling and (d) CuS, (e) Li-CuS, and (f) Na-CuS after cycling in a sodium polysulfide-air battery for 100 cycles.

Na-CuS all show retention of the internal nanoflake structure after cycling. Na-CuS nanoflakes show some increase in their diameter, but no change is observed in nanoflake thickness.

Due to the low loading of catalyst on electrodes and nanocrystallinity of the CuS, diffraction analysis of CuS, Li-CuS, and Na-CuS was performed using wide angle x-ray scattering (WAXS) on intact electrodes before and after cycling. In addition, small area electron diffraction (SAED) was performed on samples removed from the electrode carbon substrates before cycling. Minor peak shifting is observed by WAXS for Li-CuS and Na-CuS, compared to CuS, as shown in Figure 4.10a.

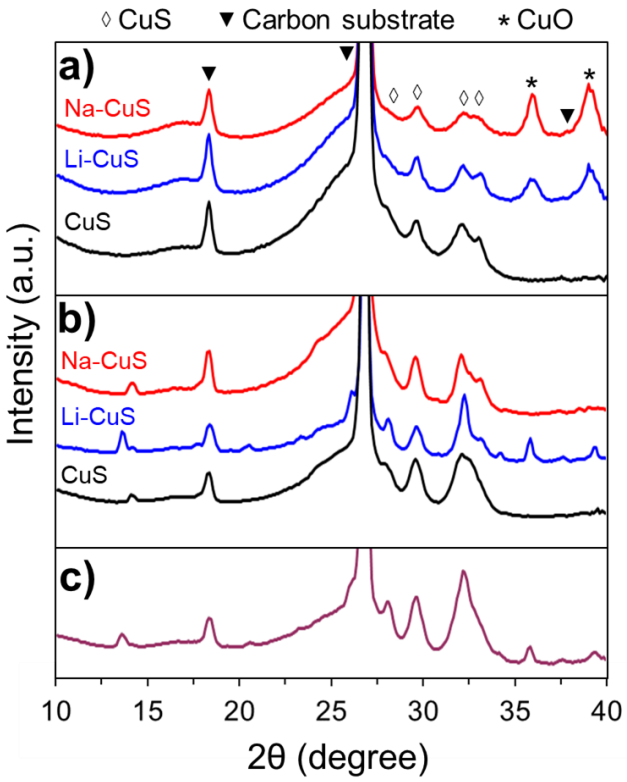

Figure 4.10 WAXS diffraction patterns of CuS electrodes (a) before cycling and (b) after cycling in a sodium polysulfide-air battery and (c) CuS soaked in polysulfide anolyte for 400 h.

Additionally, Li-CuS and Na-CuS show peaks for the formation of CuO, which may provide some insight into the redox processes seen by CV. Peak shifting is more

pronounced when observed by SAED (Figure 4.11), showing a decrease in the d-spacing with pre-discharge in hydroxide electrolyte.

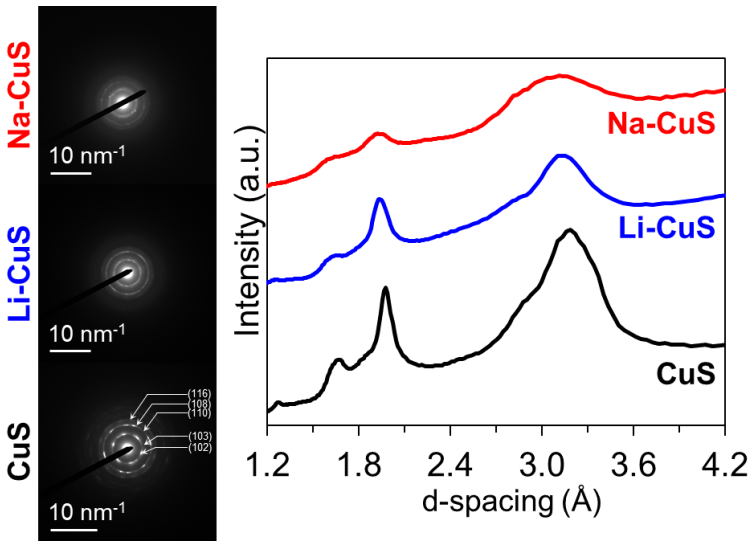

Figure 4.11 SAED pattern of CuS, Li-CuS, and Na-CuS before cycling.

The shift is more pronounced for Na-CuS than Li-CuS. Interestingly, the CuO peaks are not observed by SAED. No peaks for CuO (340 cm^{-1}), Cu_2O (220 cm^{-1}), or $Cu(OH)_2$ (490 cm^{-1}, 288 cm^{-1}) were observed by Raman spectroscopy (Figure 4.12). Only peaks for CuS (473 cm^{-1}, 261 cm^{-1}) can be seen for each material. This potentially indicates the phase is not uniformly distributed over the electrode.

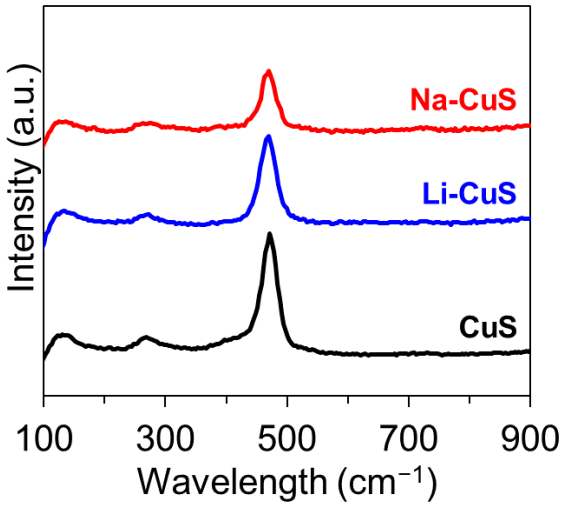

Figure 4.12 Raman spectra of CuS, Li-CuS, and Na-CuS before cycling.

WAXS shows that the electrodes maintain covellite CuS phase after cycling, as shown in Figure 4.10b. CuS and Na-CuS electrodes have matching patterns after cycling, and largely match the patterns of the electrodes before cycling. The CuO peaks in Na-CuS are no longer present after cycling, and both electrodes show a minor impurity peak at 2θ = 14.2°. Li-CuS electrodes retain their CuO peaks after cycling. They show the same impurity peak at 2θ = 14.2°. Additionally, Li-CuS electrodes show a peak at 2θ = 13.6°. This peak also appears in CuS that has been soaked in 1 M Na_2S_2 + 0.1 M NaOH polysulfide anolyte for over 400 h as shown in Figure 4.10c. Overall the CuS, Li-CuS, and Na-CuS do experience some limited change to their phase during the long-cycling but remain relatively stable in their retention of covellite CuS phase.

4.4 Conclusion

This work has demonstrated a long cycle-life sodium polysulfide-air battery with a mediator-ion solid-state electrolyte and CuS polysulfide redox catalyst. Battery

performance was evaluated over 100 cycles and was shown to have only a small increase in overpotential. It was shown that CuS is a redox-active material at voltages and electrolyte compositions relevant to polysulfide-air batteries, but that this redox activity has minimal impact on the battery performance. Pre-discharging CuS in LiOH provides a moderate boost in the battery performance with regard to increasing overpotential, while pre-discharging CuS in NaOH is moderately detrimental to the battery performance. This work was performed with CuS synthesized by a low-cost and scalable method. As such, it shows remarkable promise as a low-cost, high-activity catalyst for use in aqueous polysulfide batteries. Further work to replace IrO_2 and Pt with low-cost OER and ORR catalysts will further reduce the cost of the highly promising sodium polysulfide-air battery system.

Chapter 5: Long–Life Polysulfide–Polyhalide Batteries with a Mediator-ion Solid Electrolyte*

5.1 INTRODUCTION

Grid-scale energy storage requires batteries to have 20 year lifetimes, long storage duration (> 10 h), and very inexpensive levelized cost of storage.[140] To meet these metrics, research needs to focus on development of battery materials that are abundant, geographically widespread, and economically feasible to extract on a terawatt scale.[2, 141-142] Redox flow batteries that make use of such chemistries are particularly attractive, as their ability to decouple their energy and power parameters means they can be deployed for multiple applications ranging from load-leveling operations to bulk power management.[71, 143]

There are, however, a number of unresolved issues with regard to developing redox flow batteries with inexpensive materials. One pressing issue is the separator used in flow batteries.[96, 144] As flow batteries are typically designed specifically for the grid, they must have exceptionally long lifetimes. To achieve long lifetime flow batteries, the separator must have excellent chemical stability and ion selectivity.[97, 145] However current separators that have desirable chemical stability, such as Nafion membranes, typically have poor ion selectivity and a high cost. Furthermore, many membranes allow hydroxide and proton transfer, creating osmotic pressure effects and limiting the use of anolytes and catholytes with different pHs.[15, 96, 146] Batteries with these membranes require periodic rebalancing of their electrolytes for long-term cycling, which adds system-level expenses over the battery lifetime.

---

*M. M. Gross and A. Manthiram "Long–Life Polysulfide–Polyhalide Batteries with a Mediator-ion Solid Electrolyte," submitted, 2019.
M. M. Gross carried out the experimental work. A. Manthiram supervised the project. All participated in the preparation of the manuscript.

These issues with the membrane have led to a resurging interest in novel membranes with improved performances.[97, 144-145] One emerging idea is the use of solid electrolytes. Use of a solid electrolyte as a separator completely prevents cross-contamination and osmotic pressure effects. Improvements in manufacturing is decreasing their cost so they not be prohibitively expensive. The U.S. Department of Energy now forecasts solid electrolyte costs to drop as low as \$10 m^{-2}.[147] There is a drive to develop many novel high ionic conductivity solid electrolytes, but current commercially available solid electrolytes are limited to Li^+ and Na^+ conductors. To overcome this limitation, several systems have recently demonstrated the use of a "mediator-ion" strategy in which the Li^+ or Na^+ cation does not actively participate in the anode and cathode reactions, but instead acts as a passive ionic mediator of charge transfer through the solid electrolyte. This strategy has allowed the development of many novel battery couples, including zinc-air, zinc-ferricyanide, iron-air, and polysulfide-air.[74, 105-106, 125, 148]

In this work, we apply the use of a mediator-ion solid electrolyte to polysulfide-polyhalide battery systems to eliminate chemical crossover and enhance battery cycle life. We demonstrate polysulfide-polybromide batteries with Na^+ and Li^+ mediator ions, and polysulfide-polyiodide batteries with a Na^+ mediator ion. We further discuss the effect of the solid electrolyte on power performance and its stability in the chemically aggressive catholytes.

5.2 Experimental Methods

5.2.1 Synthesis of Polysulfide Anolyte

1 M Na_2S_2 + 0.1 M NaOH and 1 M Li_2S_2 + 0.1 M LiOH polysulfide anolytes were prepared as described in Chapters 2 and 4.

5.2.2 Synthesis of Polyhalide Catholytes

Polybromide catholyte was prepared by first forming a solution of sodium bromide (NaBr) in deionized water, and then mixing in bromine (Br_2) to the desired concentrations. 100 % state of charge (SOC) polybromide catholyte for galvanostatic cycling and soaking tests consisted 1 M Br_2 + 2 M NaBr. 50 % SOC polybromide catholyte for rate testing consisted of 0.5 M Br_2 + 3 M NaBr. Catholyte for Li^+ mediator-ion batteries was synthesized in the same manner, substituting LiBr for NaBr. Polyiodide catholyte was prepared by first forming a solution of sodium iodide (NaI) of the desired concentration in 0.5 M sodium sulfate (Na_2SO_4) solution, and then adding iodine (I_2) as needed. Batteries for galvanostatic cycling tests were assembled with 0 % SOC polyiodide catholyte containing 1.5 M NaI + 0.5 M Na_2SO_4. 50 % SOC polyiodide catholyte for rate testing contained 0.25 M I_2 + 1 M NaI + 0.5 M Na_2SO_4. Concentrated catholyte for soaking tests contained 0.5 M I_2 + 2 M NaI + 0.5 M Na_2SO_4.

5.2.3 Synthesis of Polysulfide Catalytic Electrode

Copper sulfide (CuS) microtubes were synthesized following the method previously described by Yao et al.,[132] in which equimolar amounts of cupric chloride ($CuCl_2$) and thioacetamide were mixed in deionized water and rested without stirring in a 60 °C oil bath for 24 h. The CuS was recovered by vacuum filtration, rinsed with a deionized water/ethanol mixture, and transferred to a 50 °C vacuum oven to dry overnight. Then, 50 mg of CuS was sonicated in deionized water with 20 % w/w lithiated Nafion binder (LithION, Ion Power Inc.) to form an ink, which was then deposited on a Teflon-coated carbon substrate (Sigracet GDL 10 BA) to give a mass loading of 2.5 mg cm^{-2} of CuS.

5.2.4 Assembly of Polysulfide-Polyhalide Batteries

Anodes were assembled using the custom housing described in Chapter 3. Anodes consisted of a stainless steel mesh current collector, CuS electrode, 80 µL of polysulfide anolyte, and a solid electrolyte. Solid electrolytes used were Na^+-ion conductor NASICON or Li^+-ion conductor LATP. A corresponding custom cathode chamber was used, made of Teflon. A schematic of the cell assembly can be found in Appendix A. Battery cells were made by first assembling the anode chamber in an N_2-purged glovebag with attached solid electrolyte. Next, a carbon electrode and Ti mesh current collector were inserted into the cathode chamber. Carbon electrodes consisted of buckypaper unless otherwise noted. The chamber was filled with 60 µL of polyhalide catholyte and sealed to the solid electrolyte by compression with a Viton O-ring.

5.2.5 Materials and Electrochemical Characterization

Morphology and elemental composition were obtained by SEM and EDS as described in Chapter 2. Ceramic electrolytes were soaked in polybromide and polyiodide catholytes for a minimum of 500 h. Carbon electrodes were cleaned by repeated soaking in deionized water to remove absorbed catholyte before analysis. Cyclic voltammetry (CV) was performed with a CH Instruments 1040A potentiostat, saturated calomel reference electrode, carbon foam counter electrode, and glassy carbon working electrode at a scan rate of 5 mV s^{-1}. CV electrolytes consisted of 5 mM NaBr or NaI + 0.5 M NaCl.

Polysulfide-polybromide batteries were assembled with 100 % SOC catholyte for galvanostatic cycling. First discharge of these cells was performed at 0.5 mA cm^{-2} for 30 minutes, then 1 mA cm^{-2} for 10 minutes, and then 1.5 mA cm^{-2} for the remainder of the cycle. All subsequent charge and discharge cycles occurred at 1.5 mA cm^{-2} current density. Polysulfide-polyiodide batteries were assembled with 0 % SOC catholyte for galvanostatic

cycling tests and cycled at 0.5 mA cm^{-2} current density. Polysulfide-polybromide and polysulfide-polyiodide batteries were assembled with their respective 50 % SOC catholytes for rate performance testing. Polarization curves were obtained by charging and discharging each cell for 20 minutes as further described in Chapter 2. Polysulfide-polybromide batteries with a Li^+ mediator ion were cycled for rate performance testing before undergoing galvanostatic cycling without disassembly.

5.3 RESULTS AND DISCUSSION

5.3.1 Polysulfide-Polybromide System

Polysulfide-polybromide (PSB) batteries use as their active material sulfur, a cheap byproduct of oil and gas refining, and bromine, an inexpensive primary product used in a variety of commercial industries.[1] Both sulfur and bromine exhibit high solubility in aqueous systems in the presence of, respectively, sulfide and bromide salts where they complex to form polysulfide and polybromide.[24, 84] They therefore promise a high energy density system at low cost. The polysulfide-polybromide couple consists of the following reactions:

$$2S_2^{2-} \rightarrow S_4^{2-} + 2e^- \qquad \sim -0.5 \text{ V vs SHE} \qquad (5.1)$$

$$Br_3^- + 2e^- \rightarrow 3Br^- \qquad 1.05 \text{ V vs SHE} \qquad (5.2)$$

to give a theoretical cell voltage of ~ 1.55V. The exact potential depends on the concentration and composition of the polysulfide.[26] The polysulfide anolyte is kept at an alkaline pH (9 – 14), which is necessary to suppress H_2S formation and S precipitation, as well as to increase the chemical stability of the polysulfide species, which otherwise thermodynamically favor degradation to thiosulfate as discussed in Section 1.2.2.[19, 25] In contrast, the polybromide catholyte is mildly acidic (pH ~ 3), which necessitates good ionic selectivity against hydroxide and proton migration through the separator.[12] Traditional ion-

exchange membranes (IEMs) and porous membranes fail to prevent crossover of water and redox active species, which results in changing electrolyte pH, sulfate formation, sulfur precipitation and clogging of electrodes, and loss of active material. As the following section will demonstrate, the use of a mediator-ion solid electrolyte eliminates these issues.

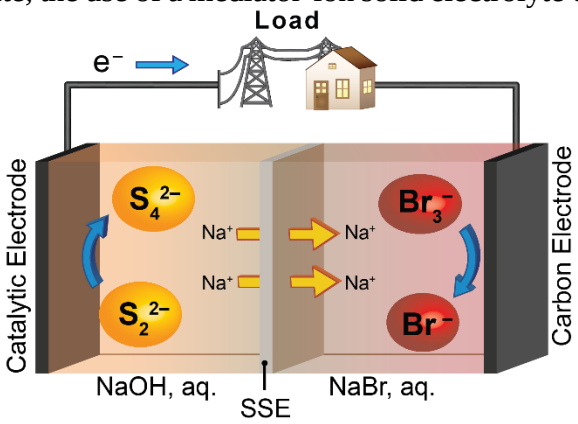

Figure 5.1 Schematic of a polysulfide-polybromide battery with polysulfide anolyte, Na^+ ion solid-state electrolyte (SSE), and polybromide catholyte.

5.3.2 Polysulfide-Polybromide Battery Performance

PSB batteries were assembled with a Na^+ mediator ion in the charge state, as shown in in Figure 5.1. Catholyte consisted of 1 M Br_2 + 2 M NaBr. Excess NaBr was used to ensure solubility of Br_2 in the Br_3^- complex. A NASICON ceramic was used as the solid electrolyte. The first discharge of the cell was performed at 0.5 mA cm^{-2} for 30 minutes before stepping the current to 1.5 mA cm^{-2}, at which all remaining cycling was performed. Cells were charged to 50% state of charge (SOC) and discharged to 0.6 V. PSB batteries exhibited two plateaus in the first cycle as shown in Figure 5.2a. This is reflected in an increase in the efficiencies in the first few cycles (Figure 5.2b). This may be due activation of the carbon electrode, or local trapping of the Br_2 active material. This was seen in PSB batteries assembled with Toray paper carbon electrodes, like that shown in Figure 5.2 a – b, and PSB batteries assembled with buckypaper carbon electrodes, like that shown in the

Figure 5.2 c – d. PSB batteries showed good stability, maintaining a high coulombic efficiency of 98.6 % over 50 cycles. The batteries were disassembled after 50 cycles.

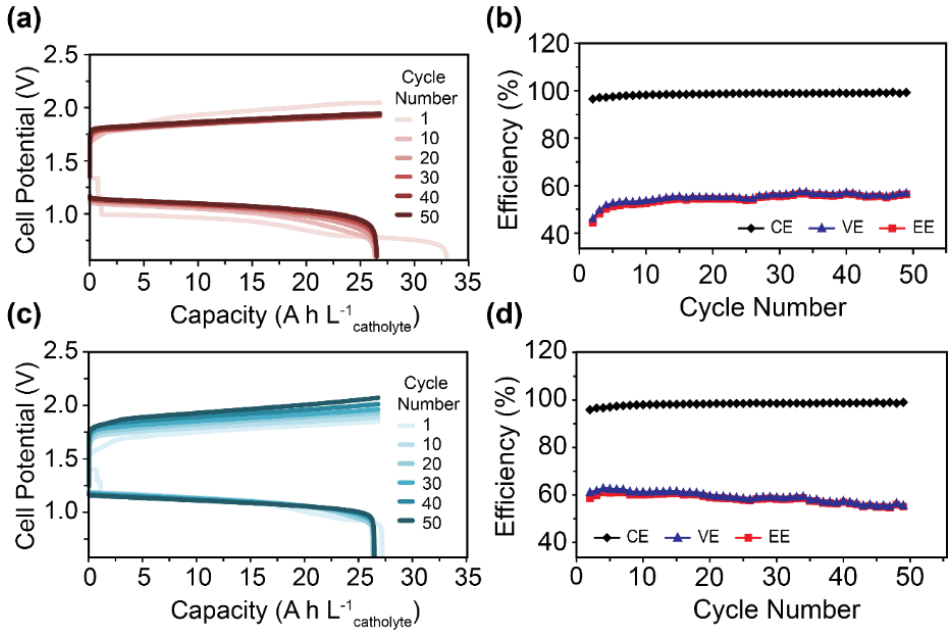

Figure 5.2 Electrochemical performance of a PSB battery at 1.5 mA cm^{-2} and 50% state of charge (SOC) cycling. (a, c) Galvanostatic cycling and (b, d) cycling efficiency including coulombic efficiency (CE), voltage efficiency (VE), and energy efficiency (EE). PSB battery assembled with (a – b) Toray paper, and (c – d) buckypaper carbon electrodes.

Disassembly showed that while the Viton O-ring seal used to assemble our cells was an effective seal for the liquid polybromide catholyte, it failed to contain fumed Br_2 gas which proceeded to react with the cell parts outside of the seal, as shown in Figure 5.3a. This was emphasized in the cells in which excess fuming during assembly and cycling led to a low initial capacity, such as the cell shown in Figure 5.2 c – d. These cells saw an increase in overpotential during cycling, which is likely due to increasing mass transport resistances as Br_3^- concentration dropped. Despite these challenges, the high coulombic efficiency of the cell indicates substantial progress over previous PSB cells, which Zhou et al. reported

to have achieved 97 % coulombic efficiency or lower, by eliminating the electrolyte crossover typical of a polymeric ion-exchange membrane.[149-150] Unlike in PSB batteries that use a Nafion membrane, no sulfur precipitation was observed on the catholyte's carbon electrode, confirming no crossover occurred in the cell, as shown in Figure 5.3c.

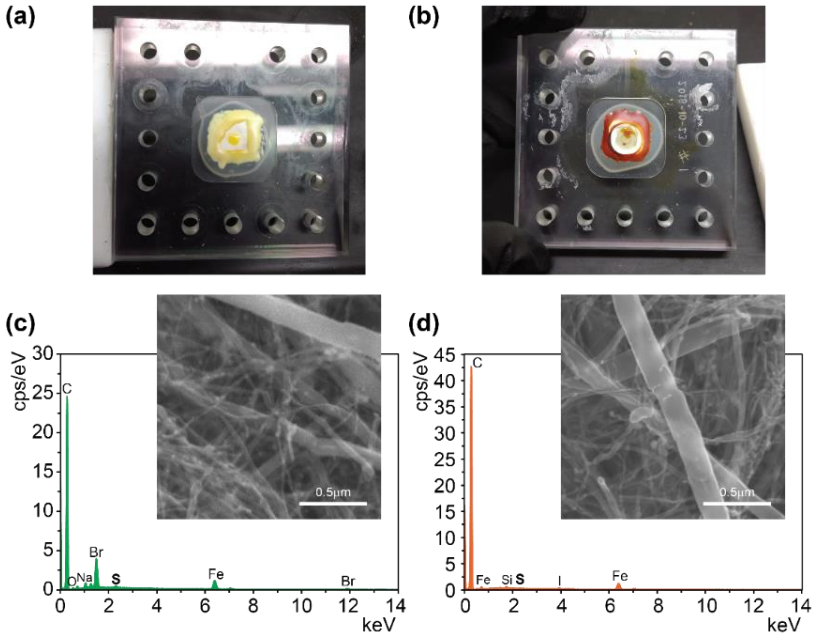

Figure 5.3 Disassembled cells after cycling, showing ceramic and epoxy after O-ring removal in (a) PSB battery and (b) PSI battery. EDS spectra and SEM images of buckypaper carbon electrodes after cycling in (c) PSB battery and (d) PSI battery.

Bromine is a highly corrosive material, and often requires specialized materials and engineering controls to avoid corrosion and to prevent escape of dangerous Br_2 gas and loss of active material. The NASICON ceramic was examined by SEM to determine its stability after exposure to the concentrated polybromide catholyte. The NASICON was studied after cycling in a PSB battery and after long-term soaking in fresh 100% SOC polybromide catholyte, as shown in Figure 5.4 a – f. After 50 cycles in a PSB battery, or ~ 600 h of cycling, the NASICON shows some corrosion of the surface shown in Figure 5.4

c – d, compared to fresh NASICON (Figure 5.4 a – b). Corrosion of the ceramic is most prevalent around the pores in the ceramic. The ceramic soaked in the fresh catholyte, however, showed signs of severe corrosion, as shown in Figure 5.4 e – f. Based on these results, it can be concluded that the complexed Br_3^- or non-complexed Br_2 are the most likely corrosive agents, as the cycled ceramic is exposed to substantially less charge product (Br_3^- or Br_2) over the same period of time compared to the soaked ceramic. This implies that while the NASICON appears to be unstable in the polybromide catholyte, its life can be extended by careful design of cycling parameters, and storage of the battery in the discharge state where only NaBr is present when the battery is not being cycled. Improvements in microstructure by minimizing the number and size of pores may also help to extend battery lifetime. Furthermore, a Li^+-ion conductor, LATP, was also tested for its stability against polybromide catholyte. The LATP, as shown in Figure 5.4 g – h, exhibits substantially higher stability than the NASICON. After soaking in the polybromide catholyte, a slight lengthening of nanometer-sized cracks in the LATP is observed. Otherwise no corrosion is apparent. This represents a substantial improvement over the NASICON and indicates that careful selection of the solid electrolyte material can also improve battery lifetime.

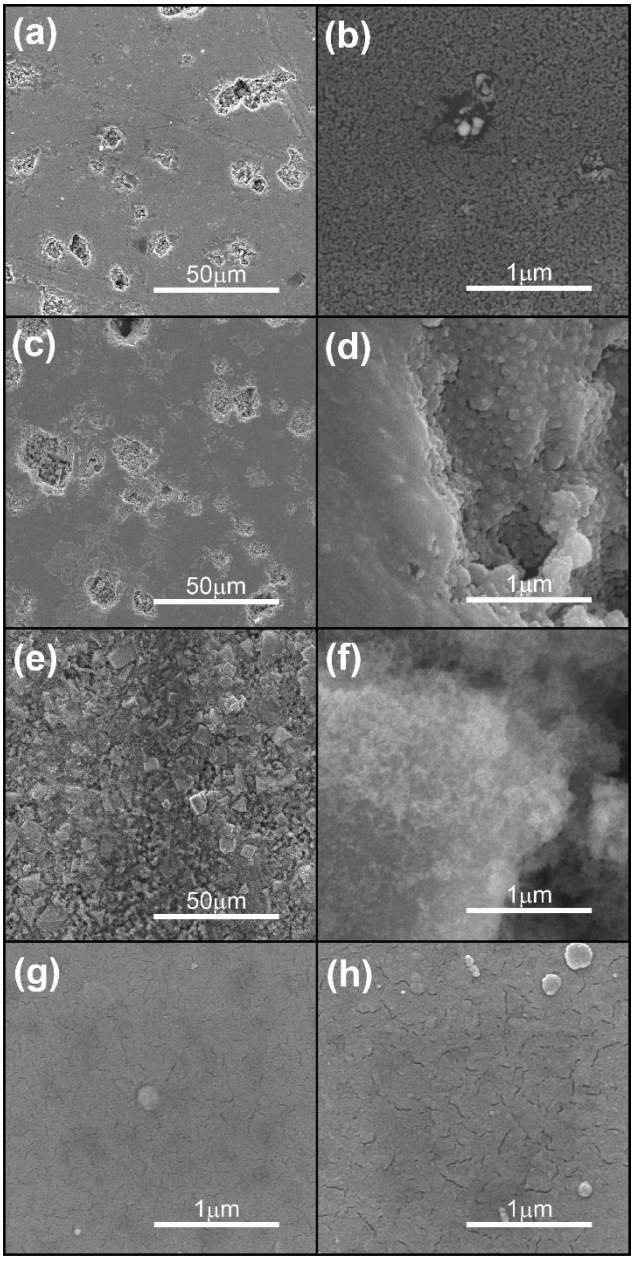

Figure 5.4 SEM of polished NaSICON (a – b) uncycled, (c – d) cycled in a PSB battery, and (e – f) soaked in 1 M Br_2 + 2 M NaBr catholyte. SEM of LATP (g) as-received and (h) soaked in 1 M Br_2 + 2 M NaBr catholyte.

The rate performance of PSB batteries assembled with a Na^+ mediator ion and a Li^+ mediator ion was tested. As Figure 5.5 a – b shows, PSB batteries assembled with a Li^+

mediator ion achieve a substantially lower peak power density (1.6 mW cm^{-2}) compared to PSB batteries assembled with a Na^+ mediator ion (3.9 mW cm^{-2}). This may be due to a variety of reasons. The LATP has a lower ionic conductivity (~ 1.0 x 10^{-4} S cm^{-1}) than the NASICON (~ 1.0 x 10^{-3} S cm^{-1}), which may not be fully made up for by its lower thickness compared to the NASICON. Furthermore, as we have shown in our previous work, both the LiBr and the Li_2S_x redox couples show more sluggish redox kinetics compared to their Na^+ ion counterparts.[105, 126] This is largely attributed to the lower dissociation behavior of the Br^- and S_x^{2-} anions in the presence of Li^+ compared to Na^+ cations. This lower rate performance is reflected in the higher cycling overpotential and lower voltage and energy efficiencies observed in PSB batteries assembled with a Li^+ mediator ion, as shown in Figure 5.5 c – d.

Future work will have to study the optimization of solid electrolyte stability in the presence of Br_3^- to balance cycle life and safety with battery performance. Our cells, being assembled in a static mode and with unoptimized cell components including planar 2D electrodes and a very thick ceramic in the case of Na^+ mediator ion cells, demonstrate a lower power performance compared to PSB batteries that use other separators like Nafion. However, the power and energy densities achieved in this study are substantially higher than the only other PSB system demonstrated with a solid electrolyte by Wang et al. This can largely be attributed to the use of a fully aqueous system and a catalyst for the polysulfide redox reactions, compared to Wang et al.'s use of THF for the polysulfide solvent. The use of high concentration anolyte and catholyte also boosts the power performance by lessening mass transport limitations.[151] Further study of the power performance will require not only optimization of the conductivity and thickness of the ceramic and electrolyte composition, but also optimization of the flow fields and stack

design of the batteries in flow mode, which is an area of future study beyond the scope of this work.

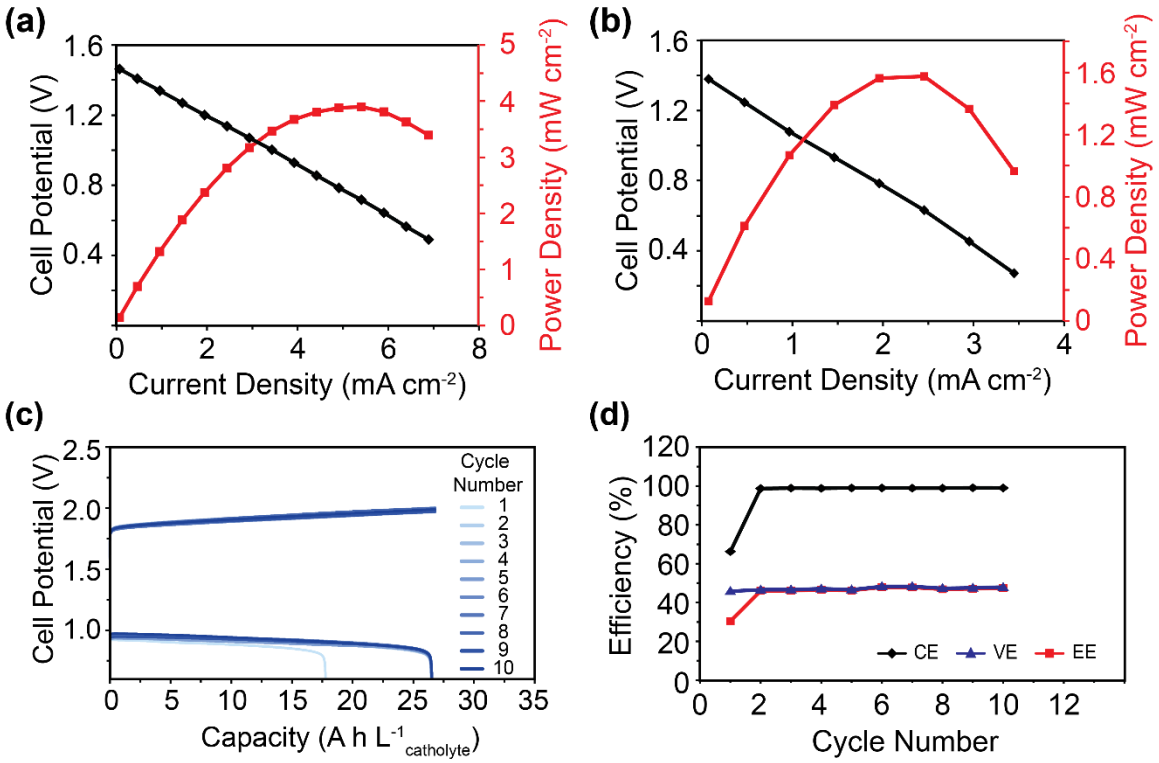

Figure 5.5 Discharge polarization curves of PSB batteries assembled with (a) Na^+ and (b) Li^+ mediator ions. Cycling performance of PSB battery assembled with Li^+ mediator ion, showing (c) galvanostatic cycling and (d) cycling efficiency including coulombic efficiency (CE), voltage efficiency (VE), and energy efficiency (EE).

5.3.3 Polysulfide-Polyiodide System

The corrosive and toxic nature of bromine presents a number of issues, introducing restraints on the types of materials used and vapor management systems to improve systems safety.[92] As our own work in the previous section demonstrates, these limitations can be difficult to overcome. These constraints can introduce higher system-level costs than the low-cost active materials would imply. As a result, iodine has been explored

recently as an alternative material.[87, 93] It is less corrosive than bromine and has a lower vapor pressure. This, however, comes at the cost of a lower cell potential. The reactions in a polysulfide-polyiodide (PSI) battery are as follows:

$$S_2^{2-} + 2e^- \rightarrow 2S^{2-} \qquad \sim -0.51 \text{ V vs SHE} \qquad (5.3)$$

$$3I^- \rightarrow I_3^- + 2e^- \qquad 0.54 \text{ V vs SHE} \qquad (5.4)$$

Giving a total theoretical voltage of 1.05 V. Unlike in the polysulfide-polybromide battery, the lower-order polysulfides are cycled in the PSI battery. This is done to boost the voltage of the cell, as the polyiodide half-cell voltage is so much lower than half-cell voltage of polybromide. A schematic of the PSI battery is shown in Figure 5.6.

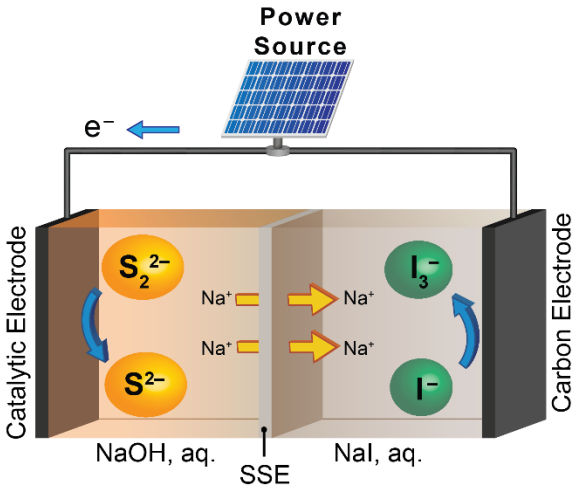

Figure 5.6 Schematic of a polysulfide-polyiodide battery with polysulfide anolyte, Na^+ solid-state electrolyte (SSE), and polyiodide catholyte.

The PSI battery behaves similarly to the PSB battery, requiring the use of iodide salts to achieve a high solubility of I_2 in an aqueous solvent. Like sulfur and bromine, iodine has a high crustal abundance and low cost, being both a byproduct of oil and gas refining and present in nitrate mines, as well as being extractable from seaweed and kelp.[1-2]

5.3.4 Polysulfide-Polyiodide Battery Performance

Polysulfide-polyiodide batteries were assembled with a Na^+ mediator ion in the discharge state with an initial catholyte concentration of 1.5 M NaI + 0.5 M Na_2SO_4. Excess NaI was used to prevent precipitation of insoluble I_2 in the catholyte. Cells were cycled with a 50% SOC upper capacity limit and discharged to 0.3 V at a current density of 0.5 mA cm^{-2}. Cell cycling performance is shown in Figure 5.7. Initial cycles show increasing cell efficiency reflective of electrode activation, though unlike in the polybromide cell, only a single plateau is observed from the first cycle. The PSI battery shows remarkably stable performance, with an average coulombic efficiency of 98.7 % over 100 cycles. In later cycles a small second plateau begins to form at the end of charge. This may be related to loss of active material over time. The PSI cells suffer from the same fuming seen in the PSB cells, as shown in Figure 5.3b. However, as the vapor pressure of I_2 is lower compared to that of Br_2, it is to be expected that the material loss is at a lower rate compared to the PSB cells. Therefore, despite the known leaks in the cathode, the PSI cells as assembled are capable of achieving 100 cycles over 1600+ h.

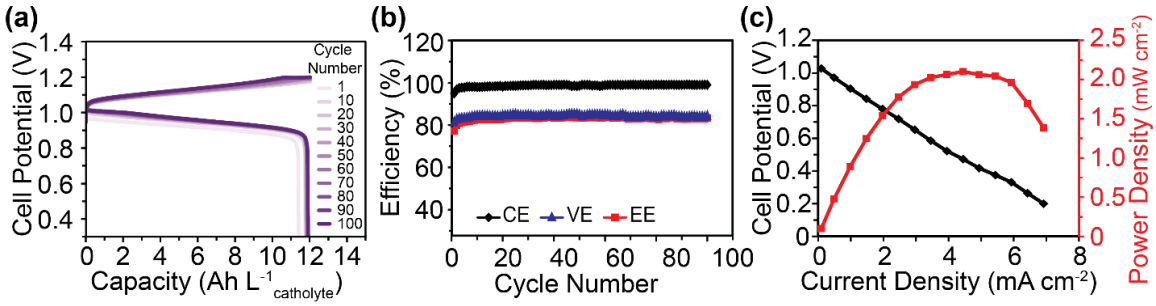

Figure 5.7 Electrochemical performance of PSI battery at 0.5 mA cm^{-2} and 50% state of charge (SOC) cycling. (a) Galvanostatic cycling, (b) cycling efficiency including coulombic efficiency (CE), voltage efficiency (VE), and energy efficiency (EE), and (c) discharge polarization curves.

The rate performance of the PSI battery was tested as well. Li et al. argued that the sluggish kinetics of the polybromide couple would hinder its power performance compared to the polyiodide couple.[93] Cyclic voltammetry confirmed that the polybromide couple does show more sluggish redox kinetics, as shown in Figure 5.8a. However, at the low current densities required by this demonstration system, the lower voltage of the polyiodide couple had a much more profound impact on its power performance. As shown in Figure 5.7c, the peak power density of the PSI battery with a Na^+ mediator ion is 2.8 mW cm^{-2}, compared to the 3.9 mW cm^{-2} of the PSB battery, though it is higher than the PSB battery with a Li^+ mediator ion (1.6 mW cm^{-2}). Furthermore, the overpotential of the PSB battery during rate testing is almost identical to the overpotential of the PSI battery, as shown in Figure 5.8b, and only begins to substantially deviate at higher current densities. This indicates that the conductivity of solid electrolyte is more limiting on the power density than the redox kinetics of the polyhalide couple at low current densities.

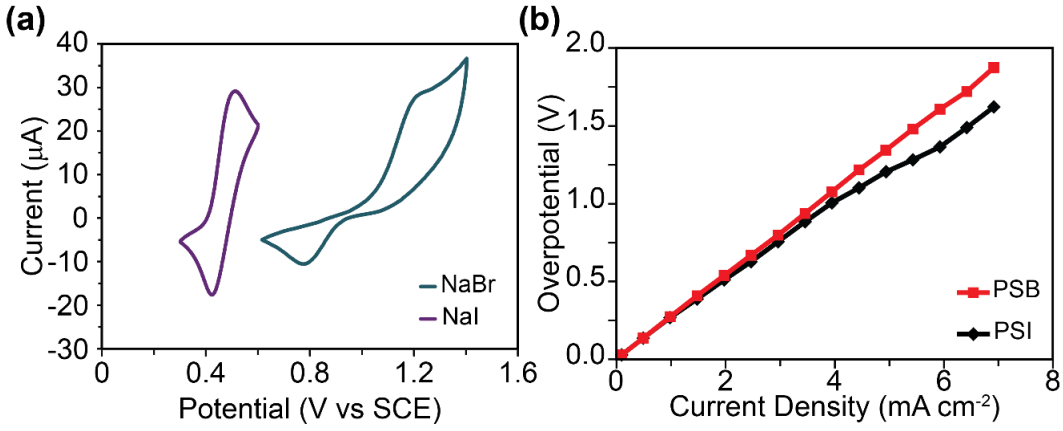

Figure 5.8 (a) Cyclic voltammetry of sodium halide salts and (b) overpotential of PSB and PSI batteries at different current densities.

The NASICON ceramic was analyzed by SEM to further determine its stability in I_2 catholyte. Images of the surface of the NASICON after cycling for more than 1600 h in

a PSI battery show only a slight texturing of the ceramic surface, when compared to polished, uncycled NASICON as shown in Figure 5.9 a – d. Please note that differences in pore sizes between images are due to natural variation between samples of NASICON. Soaking the NASICON in 0.5 M I_2 + 2 M NaI catholyte for over 500 h did reveal some corrosion of the ceramic. This corrosion, however, is substantially less than the corrosion observed in polybromide-soaked NASICON. Additional analysis of LATP, shown in Figure 5.10, reveals that as with the polybromide catholyte, LATP shows very good stability with the polyiodide catholyte.

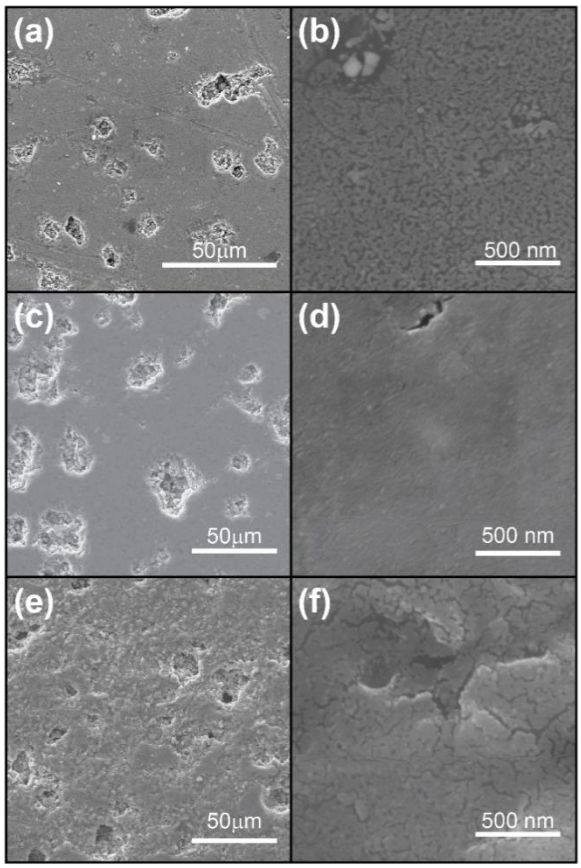

Figure 5.9 SEM of polished NASICON (a – b) uncycled, (c – d) cycled in a PSI battery, and (e – f) soaked in 0.5 M Ir_2 + 2 M NaI catholyte.

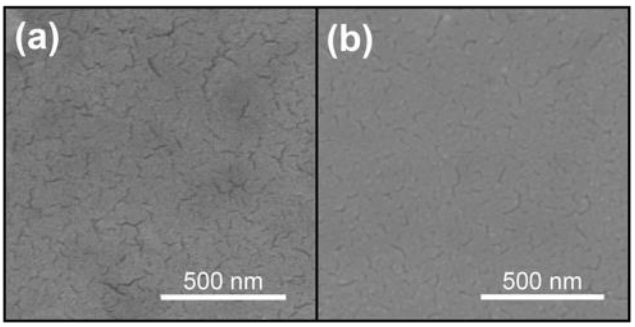

Figure 5.10 SEM images of LATP ceramic (a) as-received, and (b) after soaking in 0.5 M I_2 + 2 M NaI + 0.5 M Na_2SO_4 catholyte.

5.4 CONCLUSION

This work demonstrates two polysulfide-polyhalide battery systems: polysulfide-polybromide (PSB) and polysulfide-polyiodide (PSI), with a mediator ion solid electrolyte to eliminate crossover of redox active species and enable long battery lifetimes. PSB and PSI batteries were demonstrated for, respectively, 50 cycles with an average coulombic efficiency of 98.6 %, and 100 cycles with an average coulombic efficiency of 98.7 %. Na^+ ion-conducting NASICON ceramics show corrosion when soaked in concentrated polybromide and polyiodide catholytes but ceramics from cycled batteries show very little comparative corrosion. Furthermore, Li^+ ion-conducting LATP ceramics show excellent stability against the polybromide and polyiodide catholytes, though its use comes at a cost of lower power density. These results indicate that careful selection of ceramic materials for their stability with polybromide and polyiodide catholytes can enable long-life polysulfide-polyhalide batteries.

Chapter 6: Development of Low-cost Sodium-Aqueous Polysulfide Hybrid Batteries*

6.1 INTRODUCTION

Interest in energy storage is becoming widespread as the world moves towards a sustainable future built on renewable energy generation. To date, energy storage systems beyond pumped hydro have lagged far behind in terms of both development and deployment. [152-153] To compete with traditional energy generation such as fossil fuels and nuclear, energy storage for the electric grid must be ultra-low cost to be competitive.[154-156] The sodium-sulfur system has enjoyed renewed interest in this regard as it makes use of abundant, inexpensive materials. However, traditional sodium-sulfur batteries are operated at temperatures at around 300 °C, leading to concerns regarding their safety and reliability.[54-56, 157] Furthermore, costs over the battery lifetime associated with parasitic losses to maintain battery temperature eat into the levelized cost of storage.[99, 158] To improve the safety and reduce the cost, there has been strong interest in developing room-temperature sodium-sulfur batteries.[52, 159]

The development of room-temperature sodium-sulfur (RT Na-S) batteries is still hindered by a number of issues. As with lithium-sulfur batteries, elemental sulfur and its final discharge products sodium disulfide (Na_2S_2) and sodium sulfide (Na_2S) are inherently highly insulating, requiring a high amount of electrochemically inactive conductive materials, which effectively lowers the system energy density.[160-161] The high solubility of

*M. M. Gross and A. Manthiram "Development of Low-cost Sodium-Aqueous Polysulfide Hybrid Batteries," in preparation, 2019.
M. M. Gross carried out the experimental work. A. Manthiram supervised the project. All participated in the preparation of the manuscript.

intermediate sodium polysulfides in organic electrolytes and the resultant polysulfide shuttling also remain an issue for RT Na-S batteries.[5, 162-164] The free migration of intermediate polysulfides and their reaction with the sodium anode ultimately causes a loss of active material, a lowered energy density, and a decreased cycle life. Furthermore, the Na-metal anode poses the risk of Na dendrite formation, resulting in internal battery shorting and a large safety hazard as a result.[165-166] There has been interest in protecting the Na anode by means of a solid-electrolyte separator to block Na dendrites and prevent polysulfide shuttling. Until recently, however, there has been a lack of commercially-available high-ionic conductivity solid electrolytes. Wenzel et al. demonstrated a RT Na-S battery with a β" alumina solid electrolyte and a simple ball-milled sulfur-carbon electrode that displayed an initial discharge capacity of 475 mA h g^{-1} and a capacity retention of 42% over 40 cycles.[167] Kim et al. also utilized a β" alumina solid electrolyte in a RT Na-S battery, demonstrating improved performance with a activated carbon-sulfur composite electrode and achieving an initial capacity of 855 mA h g^{-1} and a capacity retention of 61% over 104 cycles.[168] However, the capacity loss during cycling demonstrates that the use of a solid electrolyte does not fully solve the many issues associated with the sulfur cathode.

Recently, there have been significant development of several lithium and sodium hybrid battery systems in which an aqueous cathode is used, and the reactive lithium or sodium metal anode is protected by means of a solid electrolyte. This concept has been applied to hybrid lithium-air, sodium-air, and lithium-aqueous polysulfide batteries.[14, 80, 169] However, this concept has not been applied towards the development of a sodium-aqueous polysulfide batteries. We demonstrate here, for the first time, a sodium-aqueous polysulfide (Na-APS) hybrid battery. The Na-APS hybrid battery consists of a Na-metal anode in an organic electrolyte, a solid-electrolyte separator, and a fully liquid aqueous polysulfide catholyte (Figure 6.1). The NASICON solid-electrolyte separator with a high

ionic conductivity (σ = ~ 1 x 10^{-3} S cm^{-1}) protects the Na-metal anode from the aqueous catholyte and blocks Na dendrites from internal shorting and catastrophic battery failure. Furthermore, the use of a solid electrolyte allows independent optimization of the anolyte and catholyte and enables compositional tuning to achieve the desired properties. Additionally, the use of a solid electrolyte completely eliminates crossover of polysulfides. As a result, the cathode of such a system can be optimized for fast redox kinetics, rather than confinement of the polysulfide.

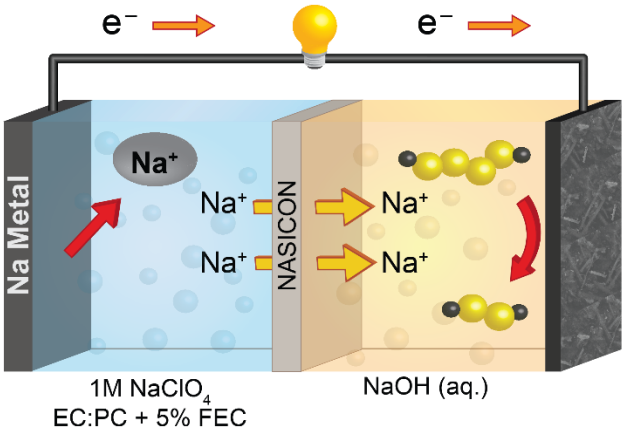

Figure 6.1 Schematic of a sodium-aqueous polysulfide hybrid battery with a sodium-metal anode, organic anolyte, Na^+-ion conducting solid-electrolyte separator, and an alkaline aqueous polysulfide catholyte.

The use of aqueous polysulfide has some distinct advantages over its nonaqueous counterpart. In a traditional sulfur cathode, discharge of the sulfur involves a solid-liquid transition from elemental cyclooctasulfur to Na_2S_8 and then liquid-liquid reactions between the high-order polysulfides (Na_2S_x $4 \leq x \leq 8$) followed by a liquid-solid transition from dissolved Na_2S_4 to solid Na_2S_3, Na_2S_2, or Na_2S and finally a solid-solid reaction between Na_2S_2 and Na_2S.[52] The solid-liquid and solid-solid reactions have particularly slow kinetics resulting in high overpotentials and low capacity retention. Furthermore, the solid-liquid-

solid reactions and differing densities between sulfur and the final discharge product Na_2S cause the active material to undergo a substantial volume change, which must be accommodated by the electrode. In contrast, aqueous polysulfide is cycled entirely within the liquid regime, which allows for fast redox kinetics. Low-order polysulfides (Na_2S_x $1 \leq x \leq 4$) are fully soluble in water to very high concentrations, allowing for high system energy densities.[4, 24] Cycling in the all-liquid regime of the lower order polysulfides avoids the liquid-solid transitions and their associated capacity loss, allowing for enhanced capacity retention. Restricting the capacity to prevent sulfur precipitation does lower the theoretical capacity from 1,675 mA h g^{-1} of sulfur to 1,256 mA h g^{-1}. However, this is still an extremely high capacity.

As aqueous polysulfides are confined by the solid electrolyte, there is no need to further confine the polysulfides at the electrode surface as is typically necessary in nonaqueous RT Na-S batteries. However, the redox kinetics of aqueous polysulfide are still sluggish and benefit from the use of a catalyst.[31, 33] Transition-metal sulfides are typically favored as catalysts for their stability and high catalytic activity.[30, 32, 37] In nonaqueous systems, molybdenum disulfide (MoS_2) is favored for its high adsorption of polysulfides, but in aqueous systems, cobalt sulfide (CoS) is favored for its high activity and stability.[7, 14, 113, 170-171] We demonstrated the good catalytic activity and stability of covellite phase copper sulfide (CuS) towards aqueous polysulfide in Chapter 4.[148] In this work, we present the development of a freestanding electrode made of CuS hollow microtubes and carbon nanotubes (CNTs). The use of a freestanding electrode eliminates the use of binder materials, and the highly porous electrode allows the aqueous polysulfides to have a free access to the catalyst surface. We demonstrate excellent performance with the Na-APS hybrid system over 100 cycles, highlighting how the system differs from traditional RT Na-S batteries and the effect of CuS catalyst on battery rate performance.

6.2 EXPERIMENTAL

6.2.1 Freestanding CuS-CNT Electrode Synthesis

Copper sulfide (CuS) hollow microtubes were synthesized as described in Chapter 5. The resulting black precipitate was recovered by vacuum filtration and dried overnight in a 50 °C vacuum oven. 56 mg of multi-wall carbon nanotubes (CNT, NanoAmor)) + 15 mg of single-wall carbon nanotubes (CNT, TUBALL) were sonicated in ~ 65 mL of ethanol until fully suspended (~ 45 minutes). 24 mg of CuS was added to the mixed CNT suspension and stirred for 10 minutes. The mixture was then vacuum filtrated to form a freestanding electrode with a CuS loading of 1.7 mg cm^{-2}. The resulting freestanding CuS-CNT electrode was dried overnight in a 50 °C vacuum oven. Freestanding CNT electrodes were also prepared in the same manner, without CuS microtubes.

6.2.2 Cell Assembly

Na-APS hybrid batteries were assembled with custom layered housing, as described in our previous work with lithium-air hybrid batteries and in Chapter 3.[126, 172] The batteries consisted of a Ni foam current collector, Na-metal chip, 1 M $NaClO_4$ in ethylene carbonate (EC) : propylene carbonate (PC) (1:1 v/v) + 5 % fluoroethylene carbonate (FEC) additive anolyte, NASICON ceramic electrolyte, aqueous polysulfide catholyte at the specified concentrations, freestanding CuS-CNT catalytic electrode, and stainless steel mesh current collector unless otherwise noted, as further described in Chapter 2. A schematic of the cell assembly can be found in Appendix A. Aqueous polysulfide catholytes were synthesized as described in Chapter 2 by mixing Na_2S and elemental sulfur in a 1 : 3 molar ratio in a sodium hydroxide (NaOH) solution to form a nominal 0.25 M Na_2S_4 + NaOH solution. Catholytes containing 0.1 M NaOH and 1 M NaOH were tested.

6.2.3 Materials Characterization and Electrochemical Measurements

The morphology, composition, and phase of freestanding CuS-CNT electrodes were analyzed by, respectively, SEM, EDS, and XRD as further detailed in Chapter 2. Cyclic voltammetry (CV) was performed on batteries with an Autolab PGSTAT302N potentiostat (Eco Chemie B.V.) at a scan rate of 0.1 mV s^{-1}. Batteries for CVs were assembled with 0.1 M Na_2S_4 + 1mM NaOH catholyte with catalyst-free CNT electrodes. Rate testing was performed as described in Chapter 2 for 20 minute cycles at each current density. Na-APS hybrid batteries for single discharge-charge cycle and for rate testing were assembled with 0.25 M Na_2S_4 + 1 M NaOH catholyte. Na-APS hybrid batteries for galvanostatic cycling were assembled with 0.25 M Na_2S_4 + 0.1 M NaOH unless otherwise noted.

6.3 Results and Discussion

6.3.1 Material Characterization

A schematic of the freestanding CuS-CNT electrode preparation can be seen in Fig. 2a. CuS hollow microtubes were synthesized by mixing equimolar amounts of cupric chloride ($CuCl_2$) and thioacetamide (TAA) [39] to form $Cu_3(TAA)_3Cl_3$ hexagonal prisms. After the prisms begin to form as indicated by the formation of a yellow precipitate, the mixture was transferred to a 60 °C oil bath and allowed to react for 24 h without stirring. The $Cu_3(TAA)_3Cl_3$ acts as a self-sacrificing template, on which spherical CuS nanoparticles grow from the surface. The CuS nanoparticles grow to form nanoflowers which aggregate to form a hollow microtube after fully cannibalizing the $Cu_3(TAA)_3Cl_3$ self-sacrificing hexagonal prism template. A mixture of multi-wall CNTs and single-wall CNTs was fully suspended in ethanol by sonication and then the CuS microtubes were stirred into the CNT mixture. The CuS-CNT mixture was then vacuum-filtrated to form an

electrode and dried overnight. Figure 6.2b shows the morphology and composition of the freestanding CuS-CNT electrode as determined by scanning electron microscopy (SEM) and energy dispersive x-ray spectroscopy (EDS) mapping. Figure 6.2 c – e shows higher resolution SEM images of, respectively, the CuS microtube, the CuS nanoflowers, and the interwoven CNT. Figure 6.2f confirms the electrode to consist of covellite phase CuS and CNT by X-ray diffraction (XRD), matching, respectively, JCPDS references 01-076-2321 and 75-1624.

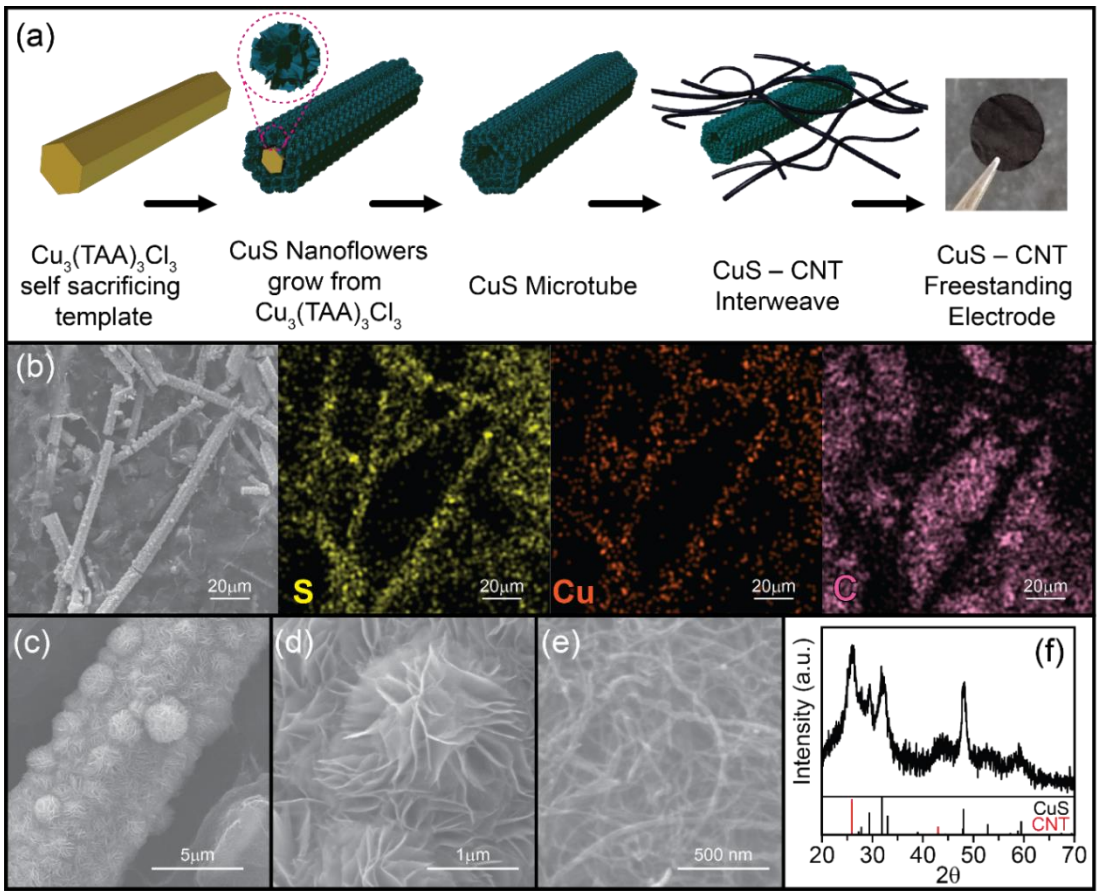

Figure 6.2 Characterization of the freestanding CuS-CNT electrode. (a) Schematic of the CuS-CNT electrode preparation. (b) SEM and EDS maps of the CuS-CNT electrode. High resolution SEM images of the (c) CuS microtube, (d) CuS nanoflowers, and (e) interwoven CNT. (f) XRD pattern of the CuS-CNT electrode.

6.3.2 Electrochemical Behavior

The electrochemical behavior and performance of the Na-APS hybrid battery was probed by cyclic voltammetry and galvanostatic cycling. The Na-APS cells assembled as described in the experimental section were investigated with cyclic voltammetry (CV), as shown in Figure 6.3 a – b. CVs were performed with Na-APS cells with dilute catholyte solutions (0.1 M Na_2S_4 + 1mM NaOH) and non-catalytic CNT electrodes to distinguish individual redox peaks at a scan rate of 0.1 mV s^{-1}. This was due to the fact that redox peaks are not distinguishable in the CVs obtained with concentrated Na_2S_4 catholyte.[14, 24, 31, 126] CVs undertaken in the voltage regime of traditional RT Na-S cells that use all-organic electrolytes immediately show the differences between them and the hybrid Na-APS cell. For RT Na-S batteries, the organic electrolyte used allows for a very wide voltage stability window, permitting the discharge of sulfur to low voltages (1.2 V versus Na/Na^+). In the Na-APS hybrid battery, Figure 6.3a shows that voltages below 1.8 V vs Na/Na^+ are outside the stability window of water, and the catholyte undergoes the hydrogen evolution reaction (HER). However, due to the much better redox kinetics of sodium polysulfide in water, the full discharge of Na_2S_4 to Na_2S occurs above the water splitting potential. Figure 6.3b illustrates the CV between 1.8 and 2.8V, displaying a characteristic profile for aqueous polysulfide redox. These results indicate that the Na-APS hybrid battery shows remarkably low overpotentials associated with Na_2S_4 to Na_2S redox and should, therefore, exhibit a high energy density, but care must be taken not to ingress into the HER regime during cycling.

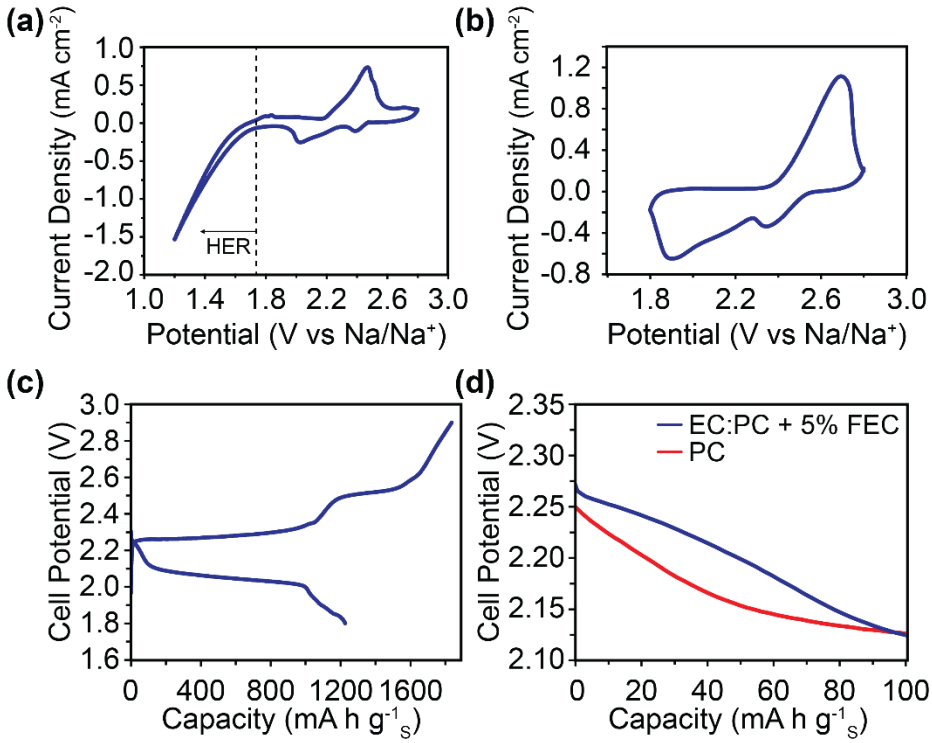

Figure 6.3 Cyclic voltammetry of Na-APS hybrid batteries with 0.1 M Na_2S_4 + 1 mM NaOH catholyte and CNT electrodes at a scan rate of 0.1 mV s^{-1} at (a) 1.2 – 2.8 V and (b) 1.8 – 2.8 V. (c) Single discharge-charge cycle of a Na-APS hybrid battery with 1 M $NaClO_4$ in EC : PC + 5% FEC anolyte, and (d) initial discharge of a Na-APS battery with different anolytes.

The Na-APS hybrid battery was further tested by performing a single deep cycle, in which a cell was discharged to the 1.8 V HER limit, then charged to an upper voltage limit of 2.9 V to fully precipitate sulfur at a current density of 0.5 mA cm^{-2} (Figure 6.3c). The discharge step shows a narrow sloping voltage region until 2.1 V, then a long plateau region before the voltage drops off. This differs from our previous work with zinc-aqueous polysulfide batteries, in which only a single voltage plateau is observed on discharge, as was discussed in Figure 3.6a.[126] Rudola et al. demonstrated with Na metal half-cells that the inclusion of EC in PC-based electrolytes introduces this voltage anomaly.[173] A separate Na-APS cell assembled with 1 M $NaClO_4$ in PC-only electrolyte does not show the initial

sloping voltage region on discharge, as shown in Figure 6.3d. This confirms that anolyte composition has some effect on the voltage profile of the Na-APS cell and may indicate its electrochemical participation during cycling.

The Na-APS hybrid battery performance was evaluated by galvanostatic cycling at different current densities, as shown in Figure 6.4. Batteries were assembled with 1 M $NaClO_4$ in EC : PC + 5% FEC anolyte, and 0.25 M Na_2S_4 + 0.1 M NaOH catholyte. Table 6.1 summarizes the current density, capacity, and energy density of the Na-APS hybrid batteries in the common units used in the reporting of hybrid batteries, sulfur batteries, and flow batteries. Aqueous polysulfide batteries are traditionally cycled between the Na_2S_4 and Na_2S_2 species to achieve good capacity retention, as demonstrated in polysulfide-bromine and polysulfide-air redox flow batteries.[42, 125] Batteries that are deep discharged to Na_2S exhibit linear capacity loss.[14, 126] It was surmised by Demir-Cakan et al. that H_2S gas generation during polysulfide reduction is the main reason for this capacity loss.[15] For this work, Na-APS hybrid batteries were cycled with a capacity limit of 418 mA h g^{-1} of sulfur based on the theoretical capacity of the Na_2S_4 to Na_2S_2 redox reactions to ensure cycling above the redox of Na_2S and below the redox of solid sulfur. Figure 6.4 a – b displays the voltage profile, specific energy, and energy efficiency of a Na-APS hybrid battery cycled at 0.5 mA cm^{-2} current density. Despite only cycling one quarter of the capacity of sulfur, due to the low overpotential associated with the catalyzed aqueous polysulfide redox reactions and the corresponding high voltage of the battery, the Na-APS hybrid battery demonstrated an excellent average specific energy of 910 Wh kg^{-1} over 100 cycles. The voltage profile over that time shows a second plateau on charge and discharge. This is likely caused by the loss of active material during discharge to H_2S formation despite the capacity-limited cycling, which is then compensated for by overcharging the remaining Na_2S_2 to reach the 418 mA h g^{-1} charge capacity in the cycling schedule.

Interestingly, the partial charge and discharge of solid sulfur appears to be relatively efficient in this system, and the energy efficiency of the battery remains steady during cycling. Over 100 cycles, the average energy efficiency was 90%.

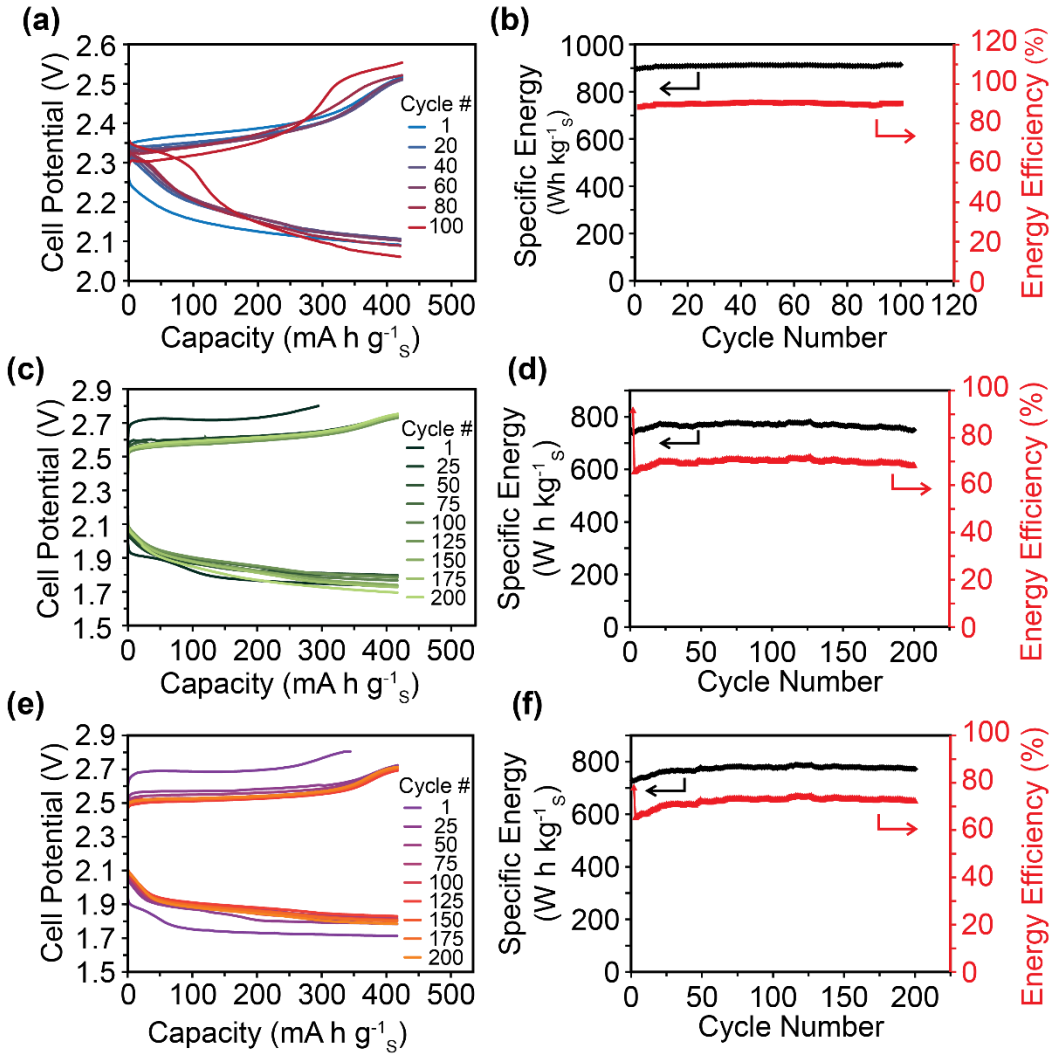

Figure 6.4 Galvanostatic cycling performance of the Na-APS hybrid battery with 0.25 M Na_2S_4 + 0.1M NaOH catholyte: (a) voltage profile, and (b) energy density and energy efficiency at 0.5 mA cm^{-2} current density. (c) Voltage profile and (d) energy density and energy efficiency at 2 mA cm^{-2} current density. (e) Voltage profile, and (f) energy density and energy efficiency of the Na-APS hybrid battery with 0.25 M Na_2S_4 + 1M NaOH catholyte at 2 mA cm^{-2} current density.

Current Density				
2 mA cm^{-2}	=	556 mA g^{-1}_{S}	=	4/3 C
0.5 mA cm^{-2}	=	140 mA g^{-1}_{S}	=	C/3
Capacity				
418 mA h g^{-1}_{S}	=	1.5 mA h cm^{-2}	=	13.4 A h $L^{-1}_{catholyte}$
Energy Density				
910 W h kg^{-1}_{S}	=	29.1 W h $L^{-1}_{catholyte}$		
775 W h kg^{-1}_{S}	=	24.8 W h $L^{-1}_{catholyte}$		

Table 6.1 Na-APS hybrid battery performance data reported in common units.

Accelerated cycling of Na-APS hybrid batteries was also performed at 2 mA cm^{-2} current density with the capacity limits of 418 mA h g^{-1}. Voltage limits of 1.65 V and 2.8 V (versus Na/Na^{+}) were also imposed to avoid water splitting. The lower voltage limit was tolerated due to the higher overpotential associated with HER at the high current density. As Figure 6.4c shows, the first cycle of the Na-APS hybrid battery displayed two plateaus on discharge, and prematurely hit the voltage limit on charge due to a large overpotential. Subsequent cycles saw the first plateau turn into a sloped voltage feature seen previously in Figure 6.3c and Figure 6.4a. The overpotential decreased for 10 cycles until it became steady. This is reflected in the initially increasing energy efficiency of the battery, as shown in Figure 6.4d. Overall, the Na-APS hybrid battery under a high current density exhibits remarkable stability. The capacity profile highlights that unlike at low current density, the Na-APS hybrid battery demonstrates no development of a second plateau at 2 mA cm^{-2} during cycling. The Na-APS hybrid battery is able to maintain a specific energy of 765 Wh kg^{-1} with energy efficiency of 70 % over 200 cycles. The effect of increasing the NaOH

concentration in the catholyte in an effort to reduce H_2S gas generation was also tested, but it was shown to have a negligible effect on the Na-APS hybrid battery performance. Data for a Na-APS hybrid battery with 0.25 M Na_2S_4 + 1 M NaOH is shown in Figure 6.4 e – f.

The rate capability of the Na-APS hybrid battery was also tested with and without the use of the CuS catalyst in the freestanding electrode to verify its catalytic activity. Rate testing was performed by discharging and charging the Na-APS hybrid batteries for 20 minutes at each current density. As can be seen in Figure 6.5 a – b, the rate performance of the Na-APS hybrid battery is substantially better when the CuS catalyst is used. Na-APS hybrid batteries with CuS-CNT electrodes achieved a power density of 5.2 mW cm^{-2}, while catalyst-free Na-APS hybrid batteries with CNT electrodes only achieved a power density of only 2.2 mW cm^{-2}. Half-cells were assembled to compare the catalytic activity of CuS-CNT to the CoS@SS and CuS catalytic electrodes developed in, respectively, Chapters 3 and 5. Figure 6.6 shows that the rate performance of the CuS-CNT electrode exceeds that of both CoS@SS and CuS. Closer analysis of the discharge profiles at each current density in the Na-APS hybrid battery with CuS-CNT electrode shows that as the current density is increased, the voltage feature seen in Figure 6.3d appears and becomes more pronounced. This is in good agreement with the work from Rudola et al.[173] that discussed the rate-dependence of the voltage feature in addition to its electrolyte dependence. This also matches the results seen in the voltage profile of the first cycle of the Na-APS hybrid battery cycled at 2 mA cm^{-2} current density (Figure 6.4c), compared to the first cycle of the Na-APS hybrid battery cycled at 0.5 mA cm^{-2} (Figure 6.4a). This further highlights the electrochemical participation of the anolyte at the Na metal anode and it is an area of interest for future work.

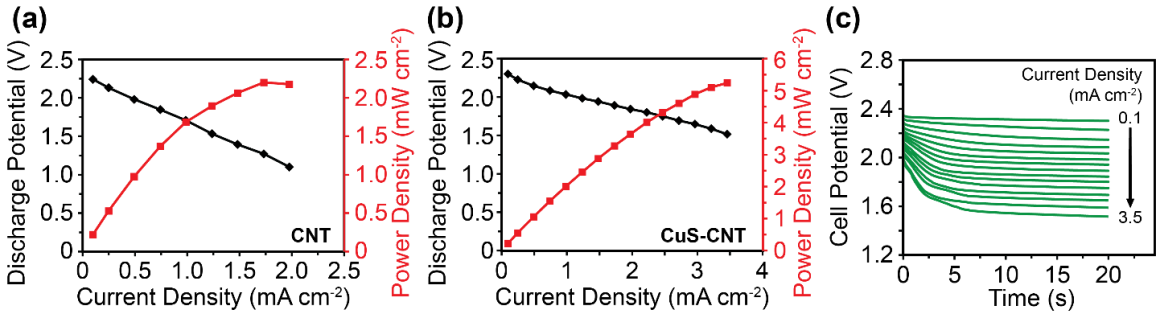

Figure 6.5 Rate performance of the Na-APS hybrid battery (a) with CNT electrode and (b) with CuS-CNT electrode. (c) Evolution of the Na-APS hybrid battery discharge curves with increasing current density.

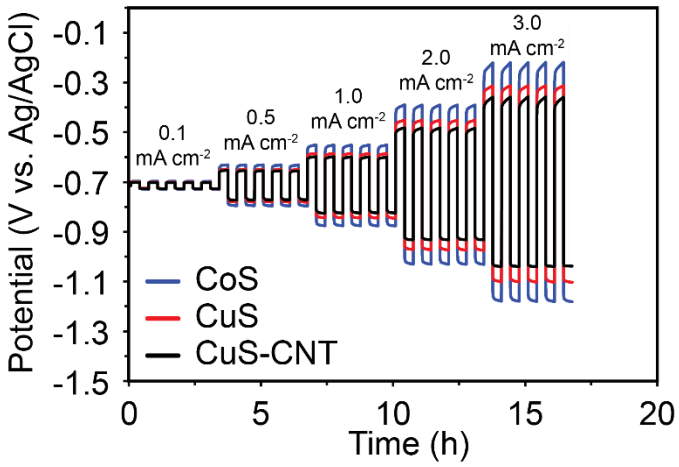

Figure 6.6 Rate performance of CuS-CNT electrodes (CuS loading: 1.7 mg cm^{-2}) compared to CoS@SS electrodes developed in Chapter 3, and CuS electrodes developed in Chapter 5 (CuS loading: 2.0 mg cm^{-2}).

6.4 Conclusions

In summary, this work demonstrates, for the first time, a sodium-aqueous polysulfide (Na-APS) hybrid battery, in which a sodium-metal anode and the organic anolyte are protected from an aqueous polysulfide catholyte by means of a high ionic conductivity Na^+ ion solid electrolyte. The Na-APS hybrid battery displays good

cyclability with the use of a freestanding CuS-CNT catalytic membrane that allows for cycling at high current densities with good rate performance. This work also demonstrates that unlike in a traditional room-temperature sodium-sulfur battery, care must be taken by appropriate choice of cycling parameters to avoid hydrogen evolution reaction and generation of H_2S gas in the aqueous catholyte. Overall the Na-APS hybrid battery shows promise as a room-temperature sodium-sulfur battery system with long cycle life and high energy density.

Chapter 7: Summary

Aqueous polysulfide shows great promise as a low-cost, high-energy density battery material for large-scale energy storage. The objective of this work has been to expand the number of potential redox couples in novel battery systems with aqueous polysulfide, as well as the improvement of battery cycle lifetimes by means of a solid electrolyte. This dissertation has focused on low-cost active materials and worked to improve battery performance by the development of high activity polysulfide catalysts. The findings of this work can be summarized as follows:

- *Polysulfide Battery Systems*: This work demonstrated novel polysulfide battery systems by means of a solid electrolyte including (i) a rechargeable zinc-aqueous polysulfide battery and (ii) a sodium-aqueous polysulfide hybrid battery. This work also demonstrated improvement of polysulfide battery systems by the utilization of a solid electrolyte and improved polysulfide catalysts, including (i) a polysulfide-air battery, (ii) a polysulfide-polybromide battery, and (iii) a polysulfide-polyiodide battery. The use of a solid electrolyte effectively confines the aqueous polysulfide, protecting high activity anodes and blocking dendrites. The solid electrolyte also prevents crossover of redox active species and osmotic pressure effects, allowing for pH differentials between anolytes and catholytes and substantially improving battery cycle life.

- *Polysulfide Electrocatalyst*: Rational design of the polysulfide electrocatalyst has demonstrated the superior catalytic activity of CoS and CuS. Furthermore, the effect of the catalyst substrate stability on the battery performance and capacity retention is demonstrated. CuS was demonstrated to be stable for long-term cycling despite its

redox activity in the intermediate voltage range of a polysulfide-air battery and shown to have a catalytic activity exceeding that of CoS@SS.

- *Solid Electrolyte*: The use of a solid electrolyte has a substantial effect on the performance of the battery, negatively affecting the power density and energy efficiency compared to batteries that utilize traditional separators. However, its use substantially increases the lifetime of the different aqueous battery systems.

- *Mediator Ion*: This work consistently demonstrates that the redox kinetics of the Li-based systems are inferior to that of the Na-based systems. The impact of the choice of mediator ion is demonstrated in both the zinc-aqueous polysulfide battery and the polysulfide-polybromide battery. However, differences in composition, microstructure, and conductivity in the different commercially available solid electrolytes mean that other factors such as electrolyte stability must be taken into account in the development of batteries with a mediator-ion system.

This work demonstrated the usefulness of the solid electrolyte in enabling long lifetime aqueous polysulfide battery systems, as well as developing novel high activity catalysts for polysulfide redox. Looking towards future development, this work has also identified areas of research that would prove fruitful for further aqueous polysulfide battery systems improvements. Primarily, the conductivity of the solid electrolyte needs to be increased to allow for higher battery power density and energy efficiency. In the case of NASICON, the ceramic density should also be increased to reduce pore size and improve microstructure for improving the electrolyte stability in corrosive electrolytes. Finally, polysulfide-air, polysulfide-polyhalide, and hybrid sodium-aqueous polysulfide batteries were demonstrated with either excess polysulfide anolyte or restricted polysulfide capacity

cycling to prevent capacity fade, as was shown in the deep-cycling of the zinc-aqueous polysulfide system. However, the degradation mechanism for aqueous polysulfide under active cycling conditions is poorly understood. Efforts to unlock the remaining capacity of aqueous polysulfide and improve the battery cycle life should focus on determining this mechanism.

Appendices

APPENDIX A: CELL HOUSING SCHEMATICS

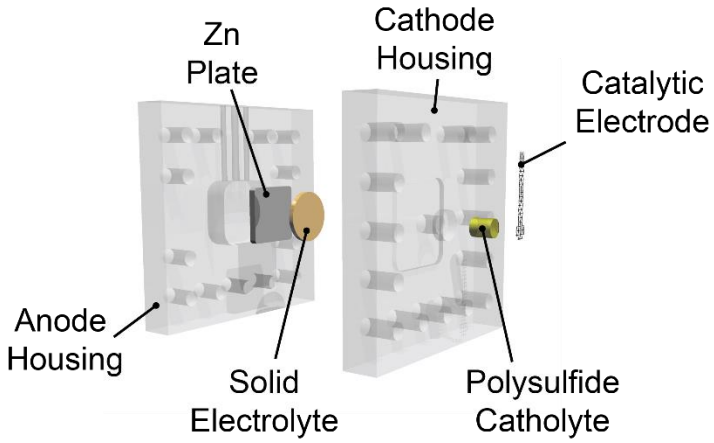

Figure A.1 Schematic of a Zinc-Aqueous Polysulfide battery

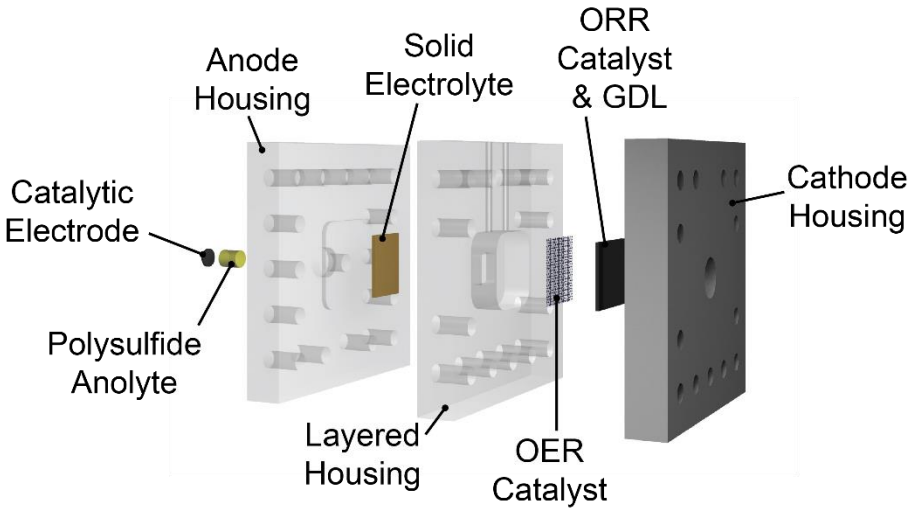

Figure A.2 Schematic of a Polysulfide-Air battery

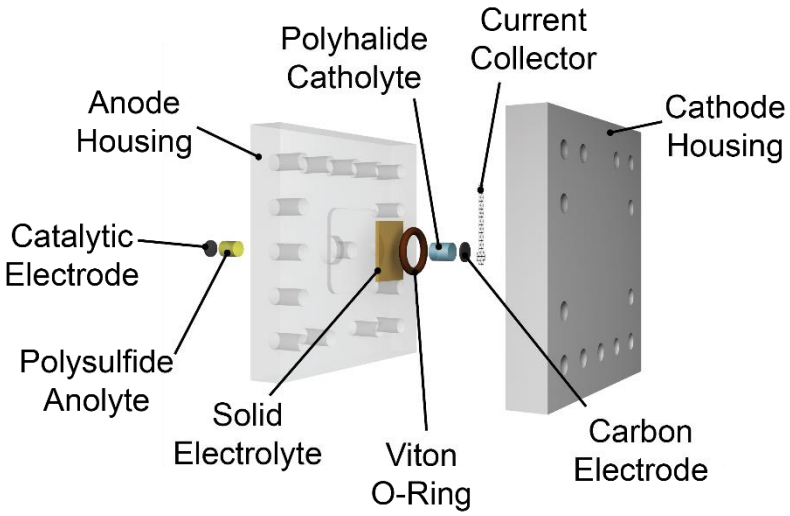

Figure A.3 Schematic of a Polysulfide-Polyhalide battery

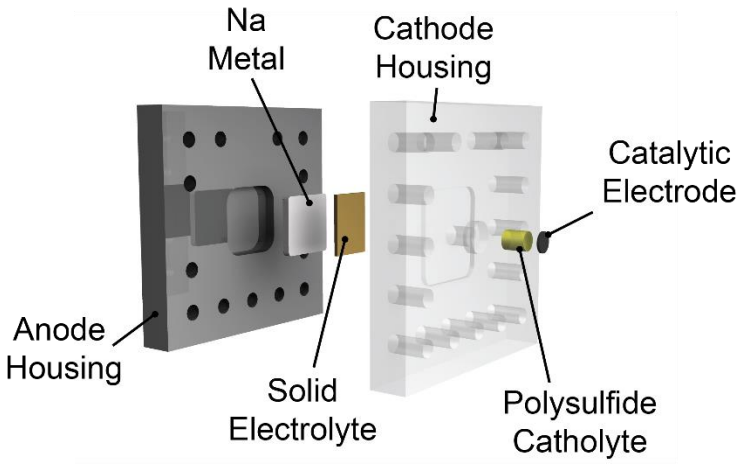

Figure A.4 Schematic of a Sodium-Aqueous Polysulfide battery

APPENDIX B: LIST OF PUBLICATIONS

1. M. M. Gross and A. Manthiram "Rechargeable Zinc-Aqueous Polysulfide Battery with a Mediator-Ion Solid Electrolyte," *ACS Appl. Mater. Interfaces*, 2018, **10**, 10612-10617.

2. M. M. Gross and A. Manthiram "An Aqueous Polysulfide-Air Battery with a Mediator-ion Solid Electrolyte and a Copper Sulfide Catalyst for Polysulfide Redox," *ACS Appl. Energy Mater.*, 2018, **1**, 7230-7236.

3. M. M. Gross and A. Manthiram, "Long–Life Polysulfide–Polyhalide Batteries with a Mediator-ion Solid Electrolyte," submitted, 2019.

4. M. M. Gross and A. Manthiram, "Development of Low-cost Sodium-Aqueous Polysulfide Hybrid Batteries," submitted, 2019.

References

1. U.S. Geological Survey, *Mineral Commodity Summaries 2018*; U.S. Department of the Interior: Reston, Virginia, 2018; p 200.

2. Vesborg, P. C. K., Jaramillo, T. F., *RSC Advances* **2012,** *2*, 7933-7947.

3. Manthiram, A., Fu, Y., Chung, S.-H., Zu, C., Su, Y.-S., *Chemical Reviews* **2014,** *114*, 11751-11787.

4. Licht, S., *Journal of The Electrochemical Society* **1988,** *135*, 2971-2975.

5. Rauh, R. D., Shuker, F. S., Marston, J. M., Brummer, S. B., *Journal of Inorganic and Nuclear Chemistry* **1977,** *39*, 1761-1766.

6. Licht, S., Peramunage, D., *Journal of The Electrochemical Society* **1993,** *140*, L4-L6.

7. Bendikov, T. A., Yarnitsky, C., Licht, S., *Journal of Materials Chemistry B* **2002,** *106*, 2989-2995.

8. Bendikov, T. Novel Aqueous Zinc Sulfur Battery. Technion - Israel Institute of Technology, Haifa, Israel, 2001.

9. Scamman, D. P., Reade, G. W., Roberts, E. P. L., *Journal of Power Sources* **2009,** *189*, 1220-1230.

10. Scamman, D. P., Reade, G. W., Roberts, E. P. L., *Journal of Power Sources* **2009,** *189*, 1231-1239.

11. Skyllas-Kazacos, M., Chakrabarti, M. H., Hajimolana, S. A., Mjalli, F. S., Saleem, M., *Journal of The Electrochemical Society* **2011,** *158*, R55-R79.

12. Zhang, H., Polysulfide-bromine flow batteries (PBBs) for medium- and large-scale energy storage. In *Advances in Batteries for Medium- and Large-scale Energy Storage: Types and Applications*, Menictas, C.; Skyllas-Kazacos, M.; Lim, T. M., Eds. Elsevier Science: 2015; pp 317-327.

13. Visco, S. J., Nimon, Y. S., Katz, B. D., De Jonghe, L. C., Goncharenko, N., Loginova, V. Aqueous Electrolyte Lithium Sulfur Batteries. US 20130122334A1, 2013.

14. Li, N., Weng, Z., Wang, Y., Li, F., Cheng, H.-M., Zhou, H., *Energy and Environmental Science* **2014,** *7*, 3307-3312.

15. Demir-Cakan, R., Morcrette, M., Tarascon, J.-M., *Journal of Materials Chemistry A* **2015,** *3*, 2869-2875.

16. Boulegue, J., *Phosphorus and Sulfur and the Related Elements* **1978,** *5*, 127-128.

17. Hartler, N., Libert, J., Teder, A., *Industrial & Engineering Chemistry Process Design and Development* **1967,** *6*, 398-406.

18. Giggenbach, W., *Inorganic Chemistry* **1972,** *11*, 1201-1207.

19. Giggenbach, W. F., *Inorganic Chemistry* **1974,** *13*, 1730-1733.

20. Licht, S., Hodes, G., Manassen, J., *Inorganic Chemistry* **1986,** *25*, 2486-2489.

21. Gun, J., Modestov, A. D., Kamyshny, A., Ryzkov, D., Gitis, V., Goifman, A., Lev, O., Hultsch, V., Grischek, T., Worch, E., *Microchimica Acta* **2004,** *146*, 229-237.

22. Kamyshny Jr., A., Goifman, A., Gun, J., Rizkov, D., Lev, O., *Environmental Science & Technology* **2004,** *38*, 6633-6644.

23. Licht, S., Davis, J., *Journal of Materials Chemistry B* **1997,** *101*, 2540-2545.

24. Licht, S., *Journal of The Electrochemical Society* **1987,** *134*, 2137-2141.

25. Teder, A., *Acta Chemica Scandinavica* **1971,** *25*, 1722-1728.

26. Lessner, P. M., McLarnon, F. R., Winnick, J., Cairns, E. J., *Journal of The Electrochemical Society* **1993,** *140*, 1847-1849.

27. Steudel, R., Holdt, G., Nagorka, R., *Zeitschrift für Naturforschung* **1986,** *41b*, 1519-1522.

28. Mao, Z., Anani, A., White, R. E., Srinivasan, S., Appleby, A. J., *Journal of The Electrochemical Society* **1991,** *138*, 1299-1303.

29. Maronny, G., *Electrochimica Acta* **1959,** *1*, 58-69.

30. Hodes, G., Manassen, J., Cahen, D., *Journal of Applied Electrochemistry* **1977,** *7*, 181-182.

31. Hodes, G., Manassen, J., *Journal of The Electrochemical Society* **1980,** *127*, 544-549.

32. Faber, M. S., Lukowski, M. A., Ding, Q., Kaiser, N. S., Jin, S., *Journal of Physical Chemistry C* **2014,** *118*, 21347-21356.

33. Lessner, P. M., McLarnon, F. R., Winnick, J., Cairns, E. J., *Journal of Applied Electrochemistry* **1992,** *22*, 927-934.

34. Stephens, I. E. L., Ducati, C., Fray, D. J., *Journal of The Electrochemical Society* **2013,** *160*, A757-A768.

35. Cunha, I. T., Teixeira, I. F., Albuquerque, A. S., Ardisson, J. D., Macedo, W. A. A., Oliveira, H. S., Tristão, J. C., Sapag, K., Lago, R. M., *Catalysis Today* **2016,** *259*, 222-227.

36. Barrera, D., de Mendonça, F. G., de Castro, A. H., de Mesquita, J. P., Lago, R. M., Sapag, K., *New Journal of Chemistry* **2018,** *42*, 11708-11714.

37. Faber, M. S., Jin, S., *Energy & Environmental Science* **2014,** *7*, 3519-3542.

38. Ye, M., Gao, X., Hong, X., Lui, Q., He, C., Liu, X., Lin, C., *Sustainable Energy & Fuels* **2017,** *1*, 1217-1231.

39. Hwang, I., Yong, K., *ChemElectroChem* **2015,** *2*, 634-653.

40. Lefers, J. B., Koetsier, W. T., Van Swaaij, W. P. M., *The Chemical Engineering Journal* **1978,** *15*, 111-120.

41. Lemos, B. R. S., Teixeira, I. F., de Mesquita, J. P., Ribeiro, R. R., Donnici, C. L., Lago, R. M., *Carbon* **2012,** *50*, 1386-1393.

42. Ge, S. H., Yi, B., Zhang, H., *Journal of Applied Electrochemistry* **2004,** *34*, 181-185.

43. Zhao, P., Zhang, H., Zhou, H., Yi, B., *Electrochimica Acta* **2005,** *51*, 1091-1098.

44. Su, L., Kowalski, J. A., Carroll, K. J., Brushett, F. R., Recent Developments and Trends in Redox Flow Batteries. In *Rechargeable Batteries: Materials, Technologies and New Trends*, Zhang, Z.; Zhang, S. S., Eds. Springer International Publishing: Cham, 2015; pp 673-712.

45. Caramia, V., Bozzini, B., *Materials for Renewable and Sustainable Energy* **2014,** *3*, 28.

46. Yu, T., Cai, R., Chen, Z., Zn–Air Batteries. In *Metal-Air Batteries*, 2018.

47. Gilligan, G. E., Qu, D., Chapter 12 - Zinc-air and other types of metal-air batteries. In *Advances in Batteries for Medium and Large-Scale Energy Storage*, Menictas, C.; Skyllas-Kazacos, M.; Lim, T. M., Eds. Woodhead Publishing: 2015; pp 441-461.

48. Sun, K. E. K., Hoang, T. K. A., Doan, T. N. L., Yu, Y., Zhu, X., Tian, Y., Chen, P., *ACS Applied Materials & Interfaces* **2017,** *9*, 9681-9687.

49. Li, Y., Dai, H., *Chemical Society Reviews* **2014,** *43*, 5257-5275.

50. Banik, S. J., Akolkar, R., *Journal of The Electrochemical Society* **2013,** *160*, D519-D523.

51. Rampel, G. Dendrite-Inhibiting Additive for Battery Cell having Zinc Electrode. US3660170, 1972.

52. Kumar, D., Kuhar, S. B., Kanchan, D. K., *Journal of Energy Storage* **2018,** *18*, 133-148.

53. Gur, T. M., *Energy & Environmental Science* **2018,** *11*, 2696-2767.

54. Kumar, D., Rajouria, S. K., Kuhar, S. B., Kanchan, D. K., *Solid State Ionics* **2017,** *312*, 8-16.

55. Kim, H., Jeong, G., Kim, Y.-U., Kim, J.-H., Park, C.-M., Sohn, H.-J., *Chemical Society Reviews* **2013,** *42*, 9011-9034.

56. Wen, Z., Cao, J., Gu, Z., Xu, X., Zhang, F., Lin, Z., *Solid State Ionics* **2008,** *179*, 1697-1701.

57. Bayley, P. M., Trease, N. M., Grey, C. P., *Journal of the American Chemical Society* **2016,** *138*, 1955-1961.

58. Iermakova, D. I., Dugas, R., Palacín, M. R., Ponrouch, A., *Journal of The Electrochemical Society* **2015,** *162*, A7060-A7066.

59. Ponrouch, A., Monti, D., Boschin, A., Steen, B., Johansson, P., Palacín, M. R., *Journal of Materials Chemistry A* **2015,** *3*, 22-42.

60. Peled, E., Menkin, S., *Journal of The Electrochemical Society* **2017,** *164*, A1703-A1719.

61. Dugas, R., Ponrouch, A., Gachot, G., David, R., Palacin, M. R., Tarascon, J. M., *Journal of The Electrochemical Society* **2016,** *163*, A2333-A2339.

62. Seh, Z. W., Sun, J., Sun, Y., Cui, Y., *ACS Central Science* **2015,** *1*, 449-455.

63. Cao, R., Mishra, K., Li, X., Qian, J., Engelhard, M. H., Bowden, M. E., Han, K. S., Mueller, K. T., Henderson, W. A., Zhang, J.-G., *Nano Energy* **2016,** *30*, 825-830.

64. Zheng, J., Chen, S., Zhao, W., Song, J., Engelhard, M. H., Zhang, J.-G., *ACS Energy Letters* **2018,** *3*, 315-321.

65. Luo, W., Lin, C.-F., Zhao, O., Noked, M., Zhang, Y., Rubloff, G. W., Hu, L., *Advanced Energy Materials* **2017,** *7*, 1601526.

66. Zhao, Y., Goncharova, L. V., Lushington, A., Sun, Q., Yadegari, H., Wang, B., Xiao, W., Li, R., Sun, X., *Advanced Materials* **2017,** *29*, 1606663.

67. Zhao, Y., Goncharova, L. V., Zhang, Q., Kaghazchi, P., Sun, Q., Lushington, A., Wang, B., Li, R., Sun, X., *Nano Letters* **2017,** *17*, 5653-5659.

68. Liu, S., Tang, S., Zhang, X., Wang, A., Yang, Q.-H., Luo, J., *Nano Letters* **2017,** *17*, 5862-5868.

69. Sun, B., Li, P., Zhang, J., Wang, D., Munroe, P., Wang, C., Notten, P. H. L., Wang, G., *Advanced Materials* **2018,** *30*, 1801334.

70. Soloveichik, G. L., *Chemical Reviews* **2015,** *115*, 11533-11558.

71. Wang, W., Luo, Q., Li, B., Wei, X., Li, L., Yang, Z., *Advanced Functional Materials* **2013,** *23*, 970-986.

72. Lee, J.-S., Tai Kim, S., Cao, R., Choi, N.-S., Liu, M., Lee, K. T., Cho, J., *Advanced Energy Materials* **2011,** *1*, 34-50.

73. R. Mainar, A., Leonet, O., Bengoechea, M., Boyano, I., de Meatza, I., Kvasha, A., Guerfi, A., Alberto Blázquez, J., *International Journal of Energy Research* **2016,** *40*, 1032-1049.

74. Li, L., Manthiram, A., *Advanced Energy Materials* **2015**, 1502054.

75. Han, B., Risch, M., Belden, S., Lee, S., Bayer, D., Mutoro, E., Shao-Horn, Y., *Journal of The Electrochemical Society* **2018,** *165*, F813-F820.

76. Suen, N.-T., Hung, S.-F., Quan, Q., Zhang, N., Xu, Y.-J., Chen, H. M., *Chemical Society Reviews* **2017,** *46*, 337-365.

77. Kim, J. S., Kim, B., Kim, H., Kang, K., *Advanced Energy Materials* **2018,** *8*, 1702774.

78. Shao, M., Chang, Q., Dodelet, J.-P., Chenitz, R., *Chemical Reviews* **2016,** *116*, 3594-3657.

79. Oh, H.-S., Nong, H. N., Reier, T., Bergmann, A., Gliech, M., Ferreira de Araújo, J., Willinger, E., Schlögl, R., Teschner, D., Strasser, P., *Journal of the American Chemical Society* **2016,** *138*, 12552-12563.

80. Li, L., Manthiram, A., *Nano Energy* **2014,** *9*, 94-100.

81. Greatbatch, W., Holmes, C. F., *Pacing and Clinical Electrophysiology* **1992,** *15*, 2034-2036.

82. Kim, J.-K., Lee, E., Kim, H., Johnson, C., Cho, J., Kim, Y., *ChemElectroChem* **2015,** *2*, 328-332.

83. Price, A., Bartley, S., Male, S., Cooley, G., *Power Engineering Journal* **1999**, 122-129.

84. Adanuvor, P. K., White, R. E., Lorimer, S. E., *Journal of The Electrochemical Society* **1987,** *134*, 1450-1454.

85. Ensync Energy Systems, Product Data Sheet: Agile Flow Battery. https://www.ensync.com/agile-flow-battery (accessed 2/13/19).

86. Lotspeich, C. In *A Comparative Assessment of Flow Battery Technologies*, EESAT, San Francisco, CA, April 15, 2002; San Francisco, CA, 2002.

87. Su, L., Badel, A. F., Cao, C., Hinricher, J. J., Brushett, F. R., *Industrial & Engineering Chemistry Research* **2017,** *56*, 9783-9792.

88. Li, B., Nie, Z., Vijayakumar, M., Li, G., Liu, J., Sprenkle, V., Wang, W., *Nature Communications* **2015,** *6*, 6303.

89. Weng, G.-M., Li, Z., Cong, G., Zhou, Y., Lu, Y.-C., *Energy & Environmental Science* **2017,** *10*, 735-741.

90. ThermoFisher Scientific, Safety Data Sheet - Iodine (CAS 7553-56-2). 2018.

91. ThermoFisher Scientific, Safety Data Sheet - Bromine (CAS 7726-95-6). 2018.

92. Tennessee Valley Authority, *Environmental Assessment for the 20-MW Windfarm and Associated Energy Storage System Facility*; 2002.

93. Li, Z., Weng, G., Zou, Q., Cong, G., Lu, Y.-C., *Nano Energy* **2016,** *30*, 283-292.

94. Honig, R. E., *RCA Reviews* **1962,** *23*, 567-586.

95. Arora, P., Zhang, Z., *Chemical Reviews* **2004,** *104*, 4419-4462.

96. Yuan, Z., Zhang, H., Li, X., *Chemical Communications* **2018,** *54*, 7570-7588.

97. Lu, W., Yuan, Z., Zhao, Y., Zhang, H., Zhang, H., Li, X., *Chemical Society Reviews* **2017,** *46*, 2199-2236.

98. Deng, N., Kang, W., Liu, Y., Ju, J., Wu, D., Li, L., Hassan, B. S., Cheng, B., *Journal of Power Sources* **2016,** *331*, 132-155.

99. Hueso, K. B., Armand, M., Rojo, T., *Energy & Environmental Science* **2013,** *6*, 734-749.

100. Francisco, B. E., Stoldt, C. R., *Journal of Physical Chemistry C* **2015,** *119*, 16432-16442.

101. Viallet, V., Fleutot, B., Solid Ionic Conductors. In *Inorganic Massive Batteries*, ISTE Ltd. John Wiley & Sons, Inc.: 2018; Vol. 4, pp 13-46.

102. Nakajima, K., Katoh, T., Inda, Y., Hoffman, B. In *Lithium Ion Conductive Glass Ceramics: Properties and Application in Lithium Metal Batteries*, Symposium on Energy Storage Beyond Lithium Ion; Materials Perspective, Oak Ridge National Laboratory, Oak Ridge National Laboratory, October 7-8, 2010.

103. www.421energy.com (accessed 2/25/2016).

104. Manthiram, A., Yu, X., Wang, S., *Nature Reviews Materials* **2017,** *2*.

105. Yu, X., Gross, M. M., Wang, S., Manthiram, A., *Advanced Energy Materials* **2017,** *1602454*.

106. Yu, X., Manthiram, A., *ACS Energy Letters* **2017,** *2*, 1050-1055.

107. Lochala, J., Liu, D., Wu, B., Robinson, C., Xiao, J., *ACS Applied Materials & Interfaces* **2017,** *9*, 24407-24421.

108. Manthiram, A., Chung, S.-H., Zu, C., *Advanced Materials* **2015,** *27*, 1980-2006.

109. Visco, S. J., Nimon, Y. S., Katz, B. D., De Jonghe, L. C., Goncharenko, N., Loginova, V. Electrode Structures for Aqueous Electrolyte Lithium Sulfur Batteries. US8828573B2, 2014.

110. Demir-Cakan, R., Morcrette, M., Leriche, J.-B., Tarascon, J.-M., *Journal of Materials Chemistry A* **2014,** *2*, 9025.

111. Tekin, B., Sevinc, S., Morcrette, M., Demir-Cakan, R., *Energy Technology* **2017,** *5*, 1-8.

112. Sun, K. E. K., Hoang, T. K. A., Doan, T. N. L., Yu, Y., Zhu, X., Tian, Y., Chen, P., *ACS Applied Materials & Interfaces* **2017,** *9*, 9681-9687.

113. Peramunage, D., Licht, S., *Science* **1993,** *261*, 1029-1032.

114. Kohler, J., Imanaka, N., Adachi, G.-y., *Chemistry of Materials* **1998,** *10*, 3790-3812.

115. Ikeda, S., Kanbayashi, Y., Nomura, K., Kasai, A., Ito, K., *Solid State Ionics* **1990,** *40*, 79-82.

116. Premlatha, S., Sivasakthi, P., Ramesh Bapu, G. N. K., *RSC Advances* **2015,** *5*, 74374-74380.

117. Ahn, S., Yang, J., Lim, H., Shin, H. S., *Nano Convergence* **2016,** *3*.

118. Tao, F., Zhao, Y.-Q., Zhang, G.-Q., Li, H.-L., *Electrochemistry Communications* **2007,** *9*, 1282-1287.

119. Yang, Z., Zhang, J., Kintner-Meyer, M. C. W., Lu, X., Choi, D., Lemmon, J. P., Liu, J., *Chemical Reviews* **2011,** *111*, 3577-3613.

120. Won, S., Oh, K., Ju, H., *Electrochimica Acta* **2015,** *177*, 310-320.

121. Allcorn, E., Nagasubramanian, G., Pratt III, H. D., Spoerke, E., Ingersoll, D., *Journal of Power Sources* **2018,** *378*, 353-361.

122. Darling, R. M., Weber, A. Z., Tucker, M. C., Perry, M. L., *Journal of The Electrochemical Society* **2016,** *163*, A5014-A5022.

123. Jiang, B., Yu, L., Wu, L., Mu, D., Liu, L., Xi, J., Qiu, X., *ACS Applied Materials & Interfaces* **2016,** *8*, 12228-12238.

124. Kear, G., Shah, A. A., Walsh, F. C., *International Journal of Energy Research* **2012,** *36*, 1105-1120.

125. Li, Z., Sam Pan, M., Su, L., Tsai, P.-C., Badel, A. F., Valle, J. M., Eiler, S. L., Xiang, K., Brushett, F. R., Chiang, Y.-M., *Joule* **2017,** *1*, 306-327.

126. Gross, M. M., Manthiram, A., *ACS Applied Materials & Interfaces* **2018,** *10*, 10612-10617.

127. Wang, X., Gaustad, G., Babbit, C. W., Richa, K., *Resources, Conservation and Recycling* **2014,** *83*, 53-62.

128. Shedd, K. B., McCullough, E. A., Bleiwas, D. I., *Mining Engineering* **2017,** *69*, 37-42.

129. Tisserant, A., Pauliuk, S., *Journal of Economic Structures* **2016,** *5*, 1-19.

130. Akhtar, M., Alghamdi, Y., Akhtar, J., Aslam, Z., Revaprasadu, N., Malik, M. A., *Materials Chemistry and Physics* **2016,** *180*, 404-412.

131. Kim, C. S., Choi, S. H., Bang, J. H., *ACS Applied Materials & Interfaces* **2014,** *6*, 22078-22087.

132. Yao, Z., Zhu, X., Wu, C., Zhang, X., Xie, Y., *Crystal Growth & Design* **2007,** *7*, 1256-1261.

133. Li, L., Liu, S., Manthiram, A., *Nano Energy* **2015,** *12*, 852-860.

134. Park, J. Y., Kim, S. J., Chang, J. H., Seo, H. K., Lee, J. Y., Yuk, J. M., *Nature Communications* **2018,** *9*.

135. Ren, Y., Wei, H., Yang, B., Wang, J., Ding, J., *Electrochimica Acta* **2014,** *145*, 193-200.

136. He, K., Yao, Z., Hwang, S., Li, N., Sun, K., Gan, H., Du, Y., Zhang, H., Wolverton, C., Su, D., *Nano Letters* **2017,** *17*.

137. Feng, C., Zhang, L., Yang, M., Song, X., Zhao, H., Jia, Z., Sun, K., Liu, G., *ACS Applied Materials & Interfaces* **2015,** *7*, 15726-15734.

138. Xu, W., Liang, Y., Su, Y., Zhu, S., Cui, Z., *Electrochimica Acta* **2016,** *211*, 891-899.

139. Zhang, J., Feng, H., Yang, J., Qin, Q., Fan, H., Wei, C., Zheng, W., *ACS Applied Materials & Interfaces* **2015,** *7*, 21735-21744.

140. U.S. Department of Energy, Duration Addition to electricitY Storage (DAYS) Overview. 2018.

141. Alonso, E., Gregory, J., Field, F., Kirchain, R., *Environmental Science & Technology* **2007,** *41*, 6649-6656.

142. Sarkar, E. M., Sarkar, T., Bharadwaj, M. D., *Current Science* **2018,** *114*, 2453-2458.

143. Liu, W., Lu, W., Zhang, H., Li, X., *Chemistry – A European Journal* **2018,** *24*.

144. Doan, T. N. L., Hoang, T. K. A., Chen, P., *RSC Advances* **2015,** *5*, 72805-72815.

145. Varcoe, J. R., Atanassov, P., Dekel, D. R., Herring, A. M., Hickner, M. A., Kohl, P. A., Kucernak, A. R., Mustain, W. E., Nijmeijer, K., Scott, K., Xu, T., Zhuang, L., *Energy & Environmental Science* **2014,** *7*, 3135-3191.

146. Khataee, A., Wedege, K., Dražević, E., Bentien, A., *Journal of Materials Chemistry A* **2017,** *5*, 21875-21882.

147. U.S. Department of Energy, *ARPA-E Funding Opportunity Announcement: Integration and Optimization of Novel Ion Conducting Solids (IONICS)*; DE-FOA-0001478; 2016.

148. Gross, M. M., Manthiram, A., *ACS Applied Energy Materials* **2018**.

149. Zhou, H., Zhang, H., Zhao, P., Yi, B., *Electrochimica Acta* **2006,** *51*, 6304-6312.

150. Zhou, H., Zhang, H., Zhao, P., Yi, B., *Electrochemistry Communications* **2006,** *74*, 296-298.

151. Wang, L., Wang, X., Liu, J., Yang, H., Fu, C., Xia, Y., Liu, T., *Journal of Materials Chemistry A* **2018,** *6*, 20737-20745.

152. Beaudin, M., Zareipour, H., Schellenberglabe, A., Rosehart, W., *Energy for Sustainable Development* **2010,** *14*, 302-314.

153. Chatzivasileiadi, A., Ampatzi, E., Knight, I., *Renewable and Sustainable Energy Reviews* **2013,** *25*, 814-830.

154. Goodenough, J. B., *Energy & Environmental Science* **2014,** *7*, 14-18.

155. Dresselhaus, M. S., Thomas, I. L., *Nature* **2001,** *414*, 332.

156. Denholm, P., Hand, M., *Energy Policy* **2011,** *39*, 1817-1830.

157. Min, J. K., Stackpool, M., Shin, C. H., Lee, C.-H., *Journal of Power Sources* **2015,** *293*, 835-845.

158. Min, J. K., Lee, C.-H., *Journal of Power Sources* **2012,** *210*, 101-109.

159. Manthiram, A., Yu, X., *Small* **2015,** *11*, 2108-2114.

160. Yu, X., Manthiram, A., *The Journal of Physical Chemistry C* **2014,** *118*, 22952-22959.

161. Ren, Y. X., Jiang, H. R., Zhao, T. S., Zeng, L., Xiong, C., *Journal of Power Sources* **2018,** *396*, 304-313.

162. Qiang, Z., Chen, Y.-M., Xia, Y., Liang, W., Zhu, Y., Vogt, B. D., *Nano Energy* **2017,** *32*, 59-66.

163. Kumar, A., Ghosh, A., Roy, A., Panda, M. R., Forsyth, M., MacFarlane, D. R., Mitra, S., *Energy Storage Materials* **2018**.

164. Lu, Q., Wang, X., Cao, J., Chen, C., Chen, K., Zhao, Z., Niu, Z., Chen, J., *Energy Storage Materials* **2017,** *8*, 77-84.

165. Schafzahl, L., Hanzu, I., Wilkening, M., Freunberger, S. A., *ChemSusChem* **2017,** *10*, 401-408.

166. Lee, J., Lee, Y., Lee, J., Lee, S.-M., Choi, J.-H., Kim, H., Kwon, M.-S., Kang, K., Lee, K. T., Choi, N.-S., *ACS Applied Materials & Interfaces* **2017,** *9*, 3723-3732.

167. Wenzel, S., Metelmann, H., Raiss, C., Durr, A. K., Janek, J., Adelhelm, P., *Journal of Power Sources* **2013,** *243*, 758-765.

168. Kim, I., Park, J.-Y., Kim, C. H., Park, J.-W., Ahn, J.-P., Ahn, J.-H., Kim, K.-W., Ahn, H.-J., *Journal of Power Sources* **2016,** *301*, 332-337.

169. Hwang, S. M., Go, W., Yu, H., Kim, Y., *Journal of Materials Chemistry A* **2017,** *5*, 11592-11600.

170. Han, P., Chung, S.-H., Manthiram, A., *ACS Applied Materials & Interfaces* **2018,** *10*, 23122-23130.

171. Dirlam, P. T., Park, J., Simmonds, A. G., Domanik, K., Arrington, C. B., Schaefer, J. L., Oleshko, V. P., Kleine, T. S., Char, K., Glass, R. S., Soles, C. L., Kim, C., Pinna, N., Sung, Y.-E., Pyun, J., *ACS Applied Materials & Interfaces* **2016,** *8*, 13437-13448.

172. Li, L., Zhao, X., Manthiram, A., *Electrochemistry Communications* **2012,** *14*, 78-81.

173. Rudola, A., Aurbach, D., Balaya, P., *Electrochemistry Communications* **2014,** *46*, 56-59.